IDENTIFICATION OF THE MOLECULAR DETERMINANTS FOR REGULATION OF MICROTUBULE SEVERING BY KATANIN

Kyle David Grode

A dissertation submitted to the faculty of the University of North Carolina at Chapel Hill in partial fulfillment of the requirements for the degree of Doctor of Philosophy in the Department of Biology in the College of Arts and Sciences.

Chapel Hill
2015

Approved by:

Stephen Rogers

Richard Cheney

Mark Peifer

Bob Goldstein

Kevin Slep

ABSTRACT

Kyle David Grode: IDENTIFICATION OF THE MOLECULAR DETERMINANTS FOR REGULATION OF MICROTUBULE SEVERING BY KATANIN
(Under the direction of Stephen Rogers)

Microtubules are dynamic cytoskeletal polymers that form complex and highly organized arrays essential for cell motility, morphogenesis, and division. Microtubule severing is a reaction that generates an internal break in the microtubule polymer and catalysis of microtubule severing is important for the proper organization and function of microtubule-based arrays in a wide range of eukaryotic cells. Katanin is a conserved heterodimeric ATPase that severs and disassembles stable microtubules, but the molecular and cellular mechanisms underlying microtubule severing by katanin are poorly understood. Using cultured *Drosophila* cells as our model system, we conducted two independent studies to investigate 1) whether katanin plays a role in cell migration and 2) how the structural domains of katanin regulate microtubule severing. In our first study, we discovered that *Drosophila* katanin functions as a negative regulator of cell motility by suppressing fast and persistent migration. In our second study, we identified the non-catalytic domains of *Drosophila* katanin as the major determinants for regulation of its abundance and microtubule-disassembly activity. Taken together, our work contributes to a basic understanding about how cells regulate microtubule severing to build and remodel microtubule-based arrays necessary for normal cellular function.

I would like to dedicate my work to Rita Grode and Jan Markiewicz, both of whom greatly shaped my perspective on life and left us too soon.

ACKNOWLEDGEMENTS

First, I would like to thank my advisor Stephen Rogers for providing me with the freedom and support to pursue my own research interests, without which I would not have strengthened my ability to think creatively and independently. I am particularly grateful for his patience and understanding, both of which allowed me to take advantage of meaningful opportunities to further my own personal and professional development. Next, I would like to thank the members of my thesis committee for their intellectual contributions to and constructive feedback on my work. I am indebted to Richard Cheney, whose sincere guidance and mentorship helped me become the open-minded and resourceful scientist that I am today. I am also very appreciative of Mark Peifer for his valuable input on my research and generous support. Finally, I would like to thank my best friend and partner Blaire Steinwand for her continuous love and encouragement throughout the course of my graduate studies. Words cannot express how truly grateful I am to have made this challenging and rewarding journey together.

PREFACE

Chapter 2 is a published manuscript describing work done in collaboration with the laboratories of David Sharp (Albert Einstein College of Medicine), Ao Ma (Albert Einstein College of Medicine), Jennifer Ross (University of Massachusetts - Amherst), and Hernando Sosa (Albert Einstein College of Medicine). This work was published in *Nature Cell Biology* in April of 2011[1]. I performed and analyzed all experiments with the migratory *Drosophila* D17 cell line, generated several figures, and contributed to the writing of the manuscript.

Chapter 3 is a published manuscript describing work that was a collaborative effort between Stephen Rogers and myself. This work was published in *PLoS One* in April of 2015[2]. I designed, performed, and analyzed all experiments. In addition, I generated all of the figures and wrote the manuscript.

[1]Zhang D, Grode KD, Stewman SF, Diaz-Valencia JD, Liebling E, Rath U, et al. Drosophila katanin is a microtubule depolymerase that regulates cortical-microtubule plus-end interactions and cell migration. Nat Cell Biol. 2011; 13:361–9.

[2]Grode KD, Rogers SL. The non-catalytic domains of Drosophila katanin regulate its abundance and microtubule-disassembly activity. PLoS One. 2015; 10:e0123912.

TABLE OF CONTENTS

LIST OF FIGURES

LIST OF TABLES

LIST OF ABBREVIATIONS

AAA	ATPases associated with various cellular activities
AMPPNP	5′-adenylyl-β-γ-imididodiphosphate
ATP	Adenosine triphosphate
BDGP	Berkeley Drosophila Genome Project
C	Carboxy
CBB	Cell blocking buffer
cDNA	Complementary deoxyribonucleic acid
CDS	Coding sequence
CTD	Carboxy- or COOH-terminal domain
Dm	Drosophila melanogaster
DMSO	Dimethyl sulfoxide
DNA	Deoxyribonucleic acid
dsRNA	Double-stranded ribonucleic acid
GFP	Green fluorescent protein
GST	Glutathione S-transferase
GTPase	Guanosine triphosphatase
h	Hour
His	Histidine
HRP	Horseradish peroxidase
IgG	Immunoglobulin G
IQR	Interquartile range
kD	Kilo Dalton

kV	Kilo volt
min	Minute
MIT	Microtubule interacting and trafficking
MT	Microtubule
NA	Numerical aperture
PAGE	Polyacrylamide gel electrophoresis
PBS	Phosphate buffered saline
PCR	Polymerase chain reaction
r	Recombinant
RFP	Red fluorescent protein
RNA	Ribonucleic acid
RNAi	RNA interference
RT	Room temperature
SD	Standard deviation
SDS	Sodium dodecyl sulfate
SEM	Standard error of the mean
TIRF	Total internal reflection fluorescence
UTR	Untranslated region

CHAPTER 1: BACKGROUND AND SIGNIFICANCE

Microtubules are protein polymers composed of stable α/β-tubulin heterodimers arranged head-to-tail into protofilaments that associate laterally to form hollow tubes (Nogales, 2000). Due to this structural asymmetry, microtubules are polarized with two distinct ends – a fast-growing plus end and a slow-growing minus end (Desai and Mitchison, 1997; Nogales, 2000). Uniquely among the three major cytoskeletal polymers, microtubules undergo spontaneous growth and shrinkage at their ends and this behavior, termed dynamic instability, is the fundamental mechanism of microtubule assembly and disassembly (Mitchison and Kirschner, 1984; Desai and Mitchison, 1997). In living cells, microtubule dynamic instability is tightly controlled to regulate the structure and function of the microtubule cytoskeleton (Kirschner and Mitchison, 1986). During the cell cycle, microtubules are organized into diverse arrays, also termed microtubule superstructures in this dissertation, with specific cellular functions. Microtubules during interphase, for example, form complex arrangements such as the axonemal structures of cilia and flagella, the cortical arrays of plant cells, and the radial networks of animal cells. Microtubule-based scaffolds such as these are required, respectively, for ciliary and flagellar motility, directional cell expansion and growth, and the establishment and maintenance of cytoplasmic polarity (Ehrhardt and Shaw, 2005; Siegrist and Doe, 2007; Satir and Christensen, 2007). Microtubules during cell division, by contrast, create a single higher-order structure called a bipolar spindle that is required for the segregation of genetic material within the germline and somatic tissues

of multi-cellular organisms (Wittman et al., 2001; Müller-Reichert et al., 2010). Thus, microtubule superstructures play specialized and essential roles in a variety of processes including cell motility, morphogenesis, and division.

Despite their diversity of formations and functions, microtubule superstructures are built and remodeled by many of the same conserved stabilizing and destabilizing cellular factors. Microtubule-associated proteins that either increase or decrease the stability of microtubules perform a wide range of functions with respect to microtubule dynamics and organization. Microtubule-stabilizing proteins, for example, may regulate microtubule dynamics by enhancing polymer growth rates, suppressing shortening rates, or promoting paused states (Desai and Mitchison, 1997; Howard and Hyman, 2003; Akhmanova and Steinmetz, 2008). These regulatory functions are dependent on the direct binding of microtubule-stabilizing proteins to microtubule ends or to the microtubule wall, also termed the microtubule lattice. Loss or inhibition of these proteins compromises microtubule assembly and stability and can lead to highly disorganized and defective microtubule-based arrays (Whittington et al., 2001; Rogers et al., 2002; Brittle and Ohkura, 2005; Applewhite et al., 2010). Other microtubule-associated proteins promote disassembly either by binding and sequestering tubulin heterodimers, which shifts the equilibrium toward the unpolymerized state, or by actively depolymerizing microtubules from their ends (Desai and Mitchison, 1997; Howard and Hyman, 2003). Decreased expression or activity of these proteins increases microtubule stability and such changes in microtubule behavior often result in abnormal microtubule-based arrays with impaired function (Wittman et al., 2003; Rogers et al., 2004; Hedrick et al., 2008). Thus, both microtubule-stabilizing and destabilizing proteins contribute to

microtubule dynamics and are necessary for the proper assembly and disassembly of microtubule superstructures.

In contrast to the majority of microtubule-destabilizing proteins that function at microtubule ends, one class of proteins binds to the microtubule lattice and catalyzes a break in the microtubule wall to promote microtubule depolymerization. These proteins, termed microtubule-severing enzymes, are hexameric ring-shaped ATPases of the AAA (ATPases associated with various cellular activities) superfamily and they are widely distributed in eukaryotes (Vale, 2000; Frickey and Lupas, 2004; Roll-Mecak and McNally, 2010). Members of this superfamily are functionally diverse and have been implicated in a variety of fundamental cellular processes (Lupas and Martin, 2002). Despite their diversity of functions, however, they share a common mechanism in which they use the energy from ATP hydrolysis to denature, remodel, or transport large macromolecular complexes in the cell (Vale, 2000; Lupas and Martin, 2002; Erzberger and Berger, 2006). Thus, AAA proteins are often referred to as 'molecular motors' or 'ATP-fueled machines'. Microtubule-severing enzymes, for example, require ATP hydrolysis to partially unfold tubulin or locally destabilize tubulin-tubulin interactions in the microtubule lattice to sever and disassemble microtubules (Roll-Mecak and McNally, 2010). Unlike microtubule end depolymerization, which can occur spontaneously, loss of tubulin subunits from the microtubule wall is energetically unfavorable and is predicted to occur infrequently (Dye et al., 1992). Therefore, when microtubule severing is observed in cells, it is due to the catalytic activities of microtubule-severing enzymes. To date, three microtubule-severing enzymes have been identified – katanin, spastin, and fidgetin – and each contains a single catalytic AAA ATPase domain that is highly

conserved between these enzymes (Frickey and Lupas, 2004; Roll-Mecak and McNally, 2010;). Each of these enzymes also exhibits a characteristic multi-domain protein structure that can be divided into an AAA motor module, a microtubule-binding domain, and an intervening linker region. This domain organization suggests that these molecular machines have co-opted the ATPase activity of the AAA domain to catalyze the assembly and disassembly of microtubule superstructures in a variety of cell types. This hypothesis is supported by a number of functional studies that have uncovered diverse biological roles for the microtubule-severing enzyme family and established the importance of microtubule severing in the development and function of many different eukaryotic cells (Mains et al., 1990; Buster et al., 2002; Clark-Maguire and Mains, 1994; Lohret et al., 1998; McNally and Thomas, 1998; Sryako et al., 2000; Dymek et al., 2004; Sherwood et al., 2004; Trotta et al., 2004; McNally et al., 2006; Sryako et al., 2006; Wood et al., 2006; Yang et al., 2006; Sharma et al., 2007; Zhang et al., 2007; Yu et al., 2008; Nakamura and Hasimoto, 2009; Rasi et al., 2009; Nakamura et al., 2010; McNally and McNally, 2011; Zhang et al., 2011).

The best characterized of the microtubule-severing enzymes with regard to biological function is katanin, which was identified based on its ATP-dependent microtubule-severing activity in sea urchin eggs and named after the Japanese word for sword (McNally and Vale, 1993). Functional analyses in many different organisms have since revealed important roles for katanin in building and remodeling microtubule superstructures in a wide variety of cellular processes. One of the most conserved roles for katanin is likely in the assembly and disassembly of the axonemal structures of cilia and flagella. Loss-of-function mutations in katanin result in axonemal structures without

a central microtubule pair in both *Chlamydomonas* and *Tetrahymena* – two distantly related unicellular organisms (Dymek et al., 2004; Sharma et al., 2007). In addition, depletion of katanin in *Chlamydomonas* prevents disassembly of the axoneme during resorption of the flagellar machinery (Rasi et al., 2009). Another pivotal role for katanin during interphase is in establishing and maintaining the organization of cytoplasmic microtubule-based arrays. In *Arabidopsis*, for instance, loss-of-function mutations in katanin cause defects in the microtubule nucleation-and-release cycle that is essential for proper microtubule incorporation and orientation within the cortical array (Nakamura and Hasimoto, 2009; Nakamura et al., 2010). Similarly, depletion of katanin in cultured *Drosophila* cells results in microtubules that are unusually stable at the cell cortex, which perturbs the spatial organization of the radial network (Zhang et al., 2011). Among the more established roles for katanin during the cell cycle is the regulation of bipolar spindle assembly and maintenance during cell division. In *C. elegans* oocytes, for example, complete loss-of-function mutations in katanin result in failure to form a bipolar spindle whereas partial loss-of-function mutants fail to maintain a stable bipolar spindle (Mains et al., 1990; Clark Maguire and Mains, 1994; Sryako et al., 2000; McNally et al., 2006; Sryako et al., 2006; McNally and McNally, 2011;). Similar bipolar spindle defects are observed in other animal cell types during mitosis upon depletion or inhibition of katanin (Buster et al., 2002; McNally et al., 2006; Zhang et al., 2007).

Given the importance of katanin in the formation and function of microtubule superstructures in these diverse biological contexts, it is likely that catalysis of microtubule severing by katanin is tightly controlled by cells to coordinate microtubule-severing with the normal cellular program. Furthermore, it is conceivable that the

principle regulatory mechanisms controlling microtubule severing by katanin will be highly conserved among microtubule-severing enzyme family members across many different organisms due to their sequence and structural similarity. Thus, determining the molecular regulation of microtubule severing by katanin is critical for understanding how these ATP-fueled machines operate in a wide range of eukaryotic cells.

REFERENCES

Akhmanova A, Steinmetz MO. Tracking the ends: a dynamic protein network controls the fate of microtubule tips. Nat Rev Mol Cell Biol. 2008; 9:309–22.

Applewhite DA, Grode KD, Keller D, Zadeh AD, Slep KC. The spectraplakin Short stop is an actin-microtubule cross-linker that contributes to organization of the microtubule network. Mol Biol Cell. 2010; 21:1714–24.

Brittle AL, Ohkura H. Mini spindles, the XMAP215 homologue, suppresses pausing of interphase microtubules in Drosophila. EMBO J. 2005; 24:1387–96.

Buster D, McNally K, McNally FJ. Katanin inhibition prevents the redistribution of gamma-tubulin at mitosis. J Cell Sci. 2002; 115:1083–92.

Clark-Maguire S, Mains PE. Mei-1, a gene required for meiotic spindle formation in Caenorhabditis elegans, is a member of a family of ATPases. Genetics. 1994; 136:533–46.

Desai A, Mitchison T. Microtubule polymerization dynamics. Annu Rev Cell Dev Biol. 1997; 13:83–117.

Dye RB, Flicker PF, Lien DY, Williams RC. End-stabilized microtubules observed in vitro: stability, subunit interchange, and breakage. Cell Motil Cytoskeleton. 1992; 21:171–86.

Dymek EE, Lefebvre PA, Smith EF. PF15p is the Chlamydomonas homologue of the Katanin p80 subunit and is required for assembly of flagellar central microtubules. Eukaryotic Cell. 2004; 3:870–9.

Ehrhardt DW, Shaw SL. Microtubule dynamics and organization in the plant cortical array. Annu Rev Plant Biol. 2006; 57:859–75.

Erzberger JP, Berger JM. Evolutionary relationships and structural mechanisms of AAA+ proteins. Annu Rev Biophys Biomol Struct. 2006; 35:93–114.

Frickey T, Lupas AN. Phylogenetic analysis of AAA proteins. J Struct Biol. 2004; 146:2–10.

Hedrick DG, Stout JR, Walczak CE. Effects of anti-microtubule agents on microtubule organization in cells lacking the kinesin-13 MCAK. Cell Cycle. 2008; 7:2146–56.

Howard J, Hyman AA. Dynamics and mechanics of the microtubule plus end. Nature. 2003; 422:753-8.

Kirschner M, Mitchison T. Beyond self-assembly: from microtubules to morphogenesis. Cell. 1986; 45:329–42.

Lohret TA, McNally FJ, Quarmby LM. A role for katanin-mediated axonemal severing during Chlamydomonas deflagellation. Mol Biol Cell. 1998; 9:1195–207.

Lupas A, Martin J. AAA proteins. Curr Opin Struct Biol. 2002; 12:746–53.

Mains PE, Kemphues KJ, Sprunger SA, Sulston IA, Wood WB. Mutations affecting the meiotic and mitotic divisions of the early Caenorhabditis elegans embryo. Genetics. 1990; 126:593–605.

McNally FJ, Thomas S. Katanin is responsible for the M-phase microtubule-severing activity in Xenopus eggs. Mol Biol Cell. 1998; 9:1847–61.

McNally FJ, Vale RD. Identification of katanin, an ATPase that severs and disassembles stable microtubules. Cell. 1993; 75:419–29.

McNally KP, McNally FJ. The spindle assembly function of C. elegans katanin does not require microtubule-severing activity. Mol Biol Cell. 2011; 22:1550-60.

McNally K, Audhya A, Oegema K, McNally FJ. Katanin controls mitotic and meiotic spindle length. J Cell Biol. 2006; 175:881–91.

Mitchison T, Kirschner M. Microtubule assembly nucleated by isolated centrosomes. Nature. 1984; 312:232–7.

Müller-Reichert T, Greenan G, O'Toole E, Srayko M. The elegans of spindle assembly. Cell Mol Life Sci. 2010; 67:2195–213.

Nakamura M, Hashimoto T. A mutation in the Arabidopsis gamma-tubulin-containing complex causes helical growth and abnormal microtubule branching. J Cell Sci. 2009; 122:2208–17.

Nakamura M, Ehrhardt DW, Hashimoto T. Microtubule and katanin-dependent dynamics of microtubule nucleation complexes in the acentrosomal Arabidopsis cortical array. Nat Cell Biol. 2010; 12:1064–70.

Nogales E. Structural insights into microtubule function. Annu Rev Biochem. 2000; 69:277–302.

Rasi MQ, Parker JDK, Feldman JL, Marshall WF, Quarmby LM. Katanin knockdown supports a role for microtubule severing in release of basal bodies before mitosis in Chlamydomonas. Mol Biol Cell. 2009; 20:379–88.

Rogers GC, Rogers SL, Schwimmer TA, Ems-McClung SC, Walczak CE, Vale RD, et al. Two mitotic kinesins cooperate to drive sister chromatid separation during anaphase. Nature. 2004; 427:364–70.

Rogers SL, Rogers GC, Sharp DJ, Vale RD. Drosophila EB1 is important for proper

assembly, dynamics, and positioning of the mitotic spindle. J Cell Biol. 2002; 158:873–84.

Roll-Mecak A, McNally FJ. Microtubule-severing enzymes. Curr Opin Cell Biol. 2010; 22:96–103.

Satir P, Christensen ST. Overview of structure and function of mammalian cilia. Annu Rev Physiol. 2007; 69:377–400.

Sharma N, Bryant J, Wloga D, Donaldson R, Davis RC, Jerka-Dziadosz M, et al. Katanin regulates dynamics of microtubules and biogenesis of motile cilia. J Cell Biol. 2007; 178:1065–79.

Sherwood NT, Sun Q, Xue M, Zhang B, Zinn K. Drosophila spastin regulates synaptic microtubule networks and is required for normal motor function. PLoS Biol. 2004; 2:2094-111.

Siegrist SE, Doe CQ. Microtubule-induced cortical cell polarity. Genes Dev. 2007; 21:483–96.

Srayko M, Buster DW, Bazirgan OA, McNally FJ, Mains PE. MEI-1/MEI-2 katanin-like microtubule severing activity is required for Caenorhabditis elegans meiosis. Genes Dev. 2000; 14:1072–84.

Srayko M, O'Toole ET, Hyman AA, Müller-Reichert T. Katanin disrupts the microtubule lattice and increases polymer number in C. elegans meiosis. Curr Biol. 2006; 16:1944–9.

Trotta N, Orso G, Rossetto MG, Daga A, Broadie K. The hereditary spastic paraplegia gene, spastin, regulates microtubule stability to modulate synaptic structure and function. Curr Biol. 2004; 14:1135–47.

Vale RD. AAA proteins: lords of the ring. J Cell Biol. 2000; 150:F13-9.

Whittington AT, Vugrek O, Wei KJ, Hasenbein NG, Sugimoto K, Rashbrooke MC, et al. MOR1 is essential for organizing cortical microtubules in plants. Nature. 2001; 411:610–3.

Wittmann T, Bokoch GM, Waterman-Storer CM. Regulation of microtubule destabilizing activity of Op18/Stathmin downstream of Rac1. J Biol Chem. 2003; 279:6196–203.

Wittmann T, Hyman A, Desai A. The spindle: a dynamic assembly of microtubules and motors. Nat Cell Biol. 2001; 3:E28-34.

Wood JD, Landers JA, Bingley M, McDermott CJ, Thomas-McArthur V, Gleadall LJ, et al. The microtubule-severing protein Spastin is essential for axon outgrowth in the zebrafish embryo. Hum Mol Genet. 2006; 15:2763–71.

Yang Y, Mahaffey CL, Bérubé N, Franel WN. Interaction between Fidgetin and protein kinase A-anchoring protein AKAP95 Is critical for palatogenesis in the mouse. J Biol Chem. 2006; 281:22352–9.

Yu W, Qiang L, Solowska JM, Karabay A, Korulu S, Baas PW. The microtubule-severing proteins spastin and katanin participate differently in the formation of axonal branches. Mol Biol Cell. 2008; 19:1485–98.

Zhang D, Grode KD, Stewman SF, Diaz-Valencia JD, Liebling E, Rath U, et al. Drosophila katanin is a microtubule depolymerase that regulates cortical-microtubule plus-end interactions and cell migration. Nat Cell Biol. 2011; 13:361–9.

Zhang D, Rogers GC, Buster DW, Sharp DJ. Three microtubule severing enzymes contribute to the “Pacman-flux” machinery that moves chromosomes. J Cell Biol. 2007; 177:231–42.

CHAPTER 2: *DROSOPHILA* KATANIN IS A MICROTUBULE DEPOLYMERASE THAT REGULATES CORTICAL-MICROTUBULE PLUS-END INTERACTIONS AND CELL MIGRATION[1]

Summary

Regulation of microtubule dynamics at the cell cortex is important for cell motility, morphogenesis and division. Here we show that the *Drosophila* katanin Dm-Kat60 functions to generate a dynamic cortical-microtubule interface in interphase cells. Dm-Kat60 concentrates at the cell cortex of S2 *Drosophila* cells during interphase, where it suppresses the polymerization of microtubule plus-ends, thereby preventing the formation of aberrantly dense cortical arrays. Dm-Kat60 also localizes at the leading edge of migratory D17 *Drosophila* cells and negatively regulates multiple parameters of their motility. Finally, *in vitro*, Dm-Kat60 severs and depolymerizes microtubules from their ends. On the basis of these data, we propose that Dm-Kat60 removes tubulin from microtubule lattice or microtubule ends that contact specific cortical sites to prevent stable and/or lateral attachments. The asymmetric distribution of such an activity could help generate regional variations in microtubule behaviors involved in cell migration.

[1]Zhang D, Grode KD, Stewman SF, Diaz-Valencia JD, Liebling E, Rath U, et al. Drosophila katanin is a microtubule depolymerase that regulates cortical-microtubule plus-end interactions and cell migration. Nat Cell Biol. 2011; 13:361–9.

Introduction

Microtubules form complex and dynamic arrays with pivotal roles in the development and function of eukaryotic cells. Although microtubules are intrinsically dynamic, their cellular behaviors are tightly regulated by a host of other factors (Jaworski et al., 2008; van der Vaart et al., 2009). Thus, the microtubule cytoskeleton is responsive to a variety of cues and can locally adapt its dynamic properties accordingly. These regulatory inputs seem to be particularly relevant at the cell cortex, where localized alterations in microtubule dynamics and organization are central to cell migration, polarization, morphogenesis and division (Watanabe et al., 2005; Siegrist and Doe, 2007; Martin, 2009; Siller and Doe, 2009).

Katanin is a phylogenetically conserved enzyme that uses the energy of ATP hydrolysis to generate microtubule breakage *in vitro* (Roll-Mecak and McNally, 2010). Katanin was originally purified from sea urchin eggs as a heterodimer of p60, a catalytic subunit of relative molecular mass 60,000 (M_r 60,K) and p80, a targeting and regulatory subunit M_r (K) 80 (McNally and Vale, 1993). Katanin p60 and p80 homologues have now been identified in evolutionarily diverse systems and many organisms contain several genes encoding distinct p60 and/or p80 proteins. Functional analyses reveal diverse roles for katanin in mitosis and meiosis (Buster et al., 2002; McNally et al., 2006; Sryako et al., 2006; Zhang et al., 2007), in neuronal morphogenesis (Karabay et al., 2004; Yu et al., 2008) and in the assembly and disassembly of cilia and flagella (Quarmby, 2000; Sharma et al., 2007; Casanova et al., 2009; Rasi et al., 2009;). In addition, a katanin in higher plants has been shown to regulate the assembly of cortical microtubule arrays, which, in turn, determine the directional deposition of cellulose and thus impact cell morphogenesis (Burk et al., 2001; Stoppin-Mellet et al., 2006; Burk et al., 2007;

Stoppin-Mellet et al., 2007). In this context, katanin releases new microtubules nucleated from the walls of pre-existing microtubules (Nakamura et al., 2010; Roll-Mecak and McNally, 2010).

We previously found that the *Drosophila* katanin p60, Dm-Kat60, associates with mitotic chromosomes and stimulates the depolymerization of kinetochore-associated microtubule plus-ends during anaphase A (Zhang et al., 2007). In the present study, we tested the hypothesis that Dm-Kat60 also functions to regulate microtubule dynamics during interphase – a topic that has not been addressed in any other animal system.

Results

Dm-Kat60 localizes at the interphase cell cortex

We first probed the localization of Dm-Kat60 in cultured interphase S2 cells using immunofluorescence. Dm-Kat60 immunostaining was found to be strongly enriched within a 0.5–3-μm-thick band extending around the entire cell boundary (Figure 2.1A). This cortical staining pattern was reduced or abolished by Dm-Kat60 RNA interference (RNAi), supporting its specificity (Figure 2.S1A). Ectopically expressed Dm-Kat60 fused to green fluorescent protein (GFP) also acquired a cortical localization (Figure 2.S2 A and B).

Although Dm-Kat60 showed little co-localization with microtubules in the interphase cell interior, numerous microtubule plus-ends were observed to extend into and terminate within the Dm-Kat60-rich cortical zone (Figure 2.1 B and C). Dm-Kat60 also generally co-localized with cortical actin (Figure 2.1D). Cortical localization of Dm-Kat60 occurs independently of microtubules, as it persists following microtubule depolymerization with colchicine. However, it is nearly completely abolished when cells are treated with cytochalasin D, indicating a strong reliance on actin (Figure 2.S3). On the other hand, Dm-Kat60 RNAi did not prevent the cortical accumulation of actin (Figure 2.S1B).

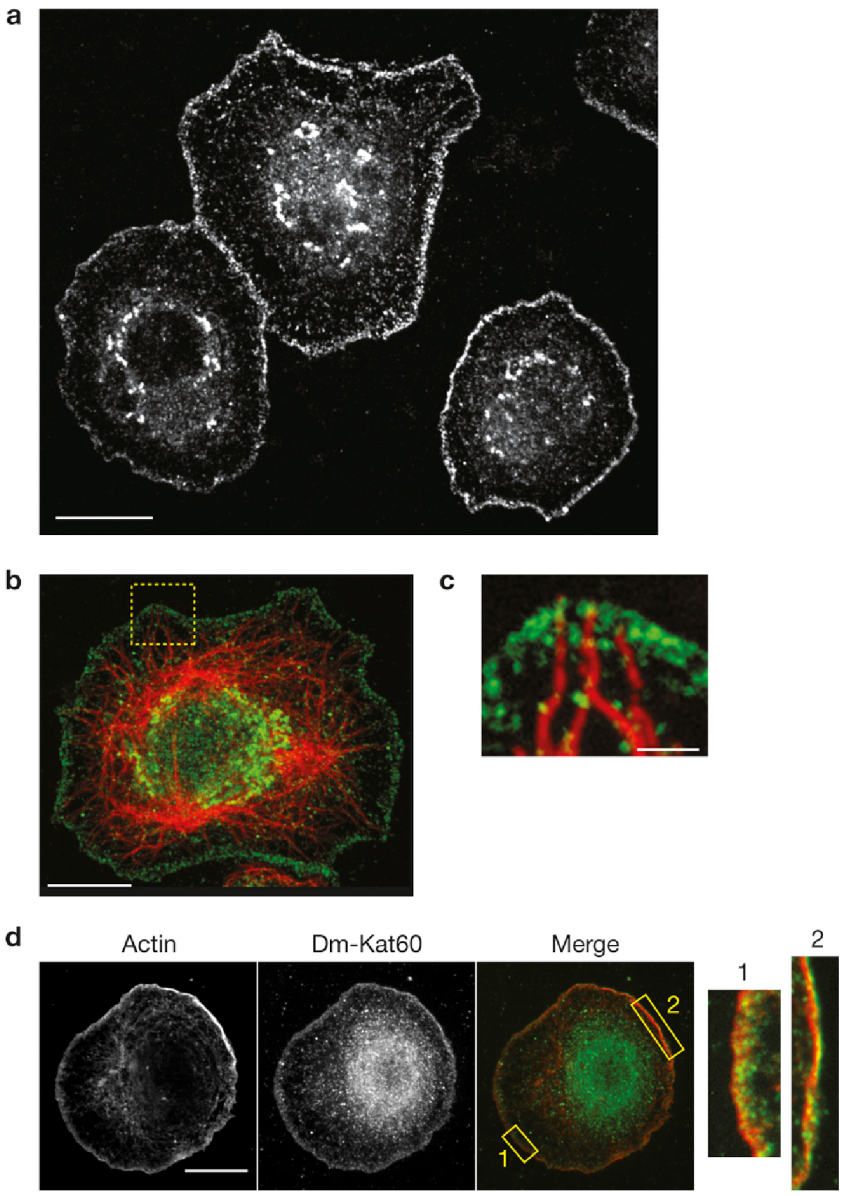

Figure 2.1. Dm-Kat60 targets the cell cortex of interphase cells. (A) Immunofluorescence micrograph showing the localization of Dm-Kat60 in interphase S2 cells (antibody characterized in Zhang et al., 2007). (B) Immunofluorescence micrograph of an interphase S2 cell double labeled for microtubules (anti-α-tubulin; red) and Dm-Kat60 (green). (C) High magnification of the region outlined in B. (D) Immunofluorescence of an interphase S2 cell double labeled for actin (red) and Dm-Kat60 (green) and a higher magnification of the two regions outlined in the 'merge' panel. Scale bars, 10 μm (A, B, and D) and 2 μm (C).

Dm-Kat60 regulates interphase microtubules

We then carried out live analyses of microtubule dynamics in control and Dm-Kat60 RNA-treated S2 cells expressing GFP–α-tubulin. In control cells, microtubules generally grew perpendicularly to the cortex, briefly paused on contacting the cortex and then underwent catastrophe (transition from growth to shrinkage) into the cell interior (Figure 2.2A; Mennella et al., 2005). More than 90% of plus-end catastrophes (78 out of 84 observed in nine cells) occurred within 3 μm of the cell edge, indicating that the Dm-Kat60-rich cortical zone is a potential 'hotspot' for the induction of microtubule depolymerization.

Interestingly, some microtubules were also observed to break very near their ends on contacting the cortex. The newly formed plus-ends of these 'severed' microtubules initiated catastrophe immediately thereafter (Figure 2.2B). Although such events were rarely observed when cells were imaged at 5 s intervals (our standard for longer time series), they appeared much more frequently when images were acquired at subsecond intervals (0.2–0.8 images per second). Under these conditions, putative severing events near microtubule tips preceded ~30% of observed catastrophes (20 out of 63 microtubule catastrophes observed in seven cells).

In stark contrast to controls, microtubules in most Dm-Kat60-depleted cells were noticeably curled beneath the cortex and often formed dense parallel arrays ringing the cell periphery (Figure 2.2C). This phenotype was largely reversed by the induced expression of an RNAi-resistant Dm-Kat60-GFP construct (Figure 2.S2 C and D). Although we were unable to observe the formation of these cortical arrays *de novo*, examination of the few clearly visible individual microtubules present at the onset of

imaging provided insights into their genesis. Similarly to controls, these microtubules often contacted the cortex with their plus-end. However, instead of rapidly initiating catastrophe, they continued to grow along the cortex until they came into proximity with the underlying ring of microtubules, into which they were ultimately incorporated (Figure 2.2D).

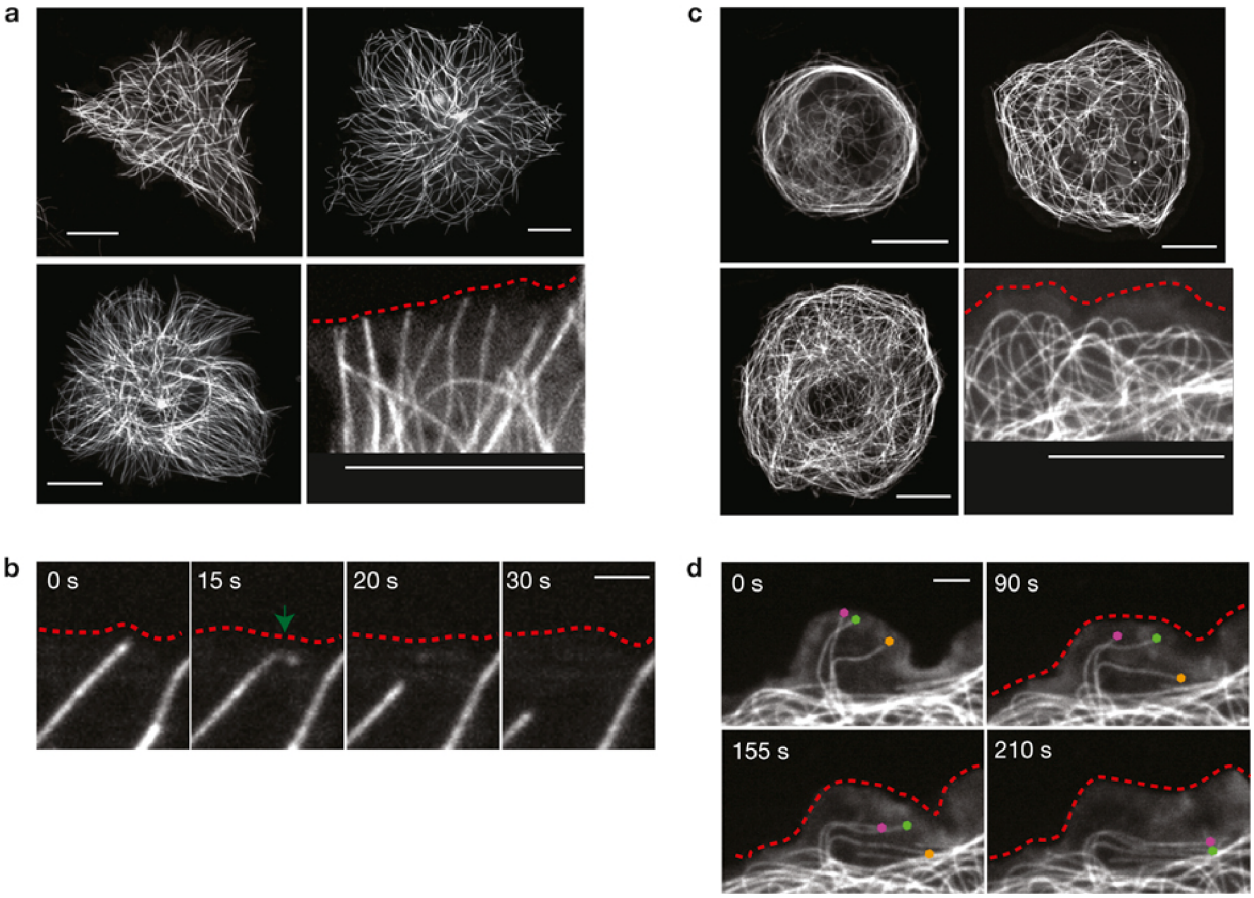

Figure 2.2. Depletion of Dm-Kat60 causes significant microtubule curling and bundling beneath the cortex. (A) Confocal images of live GFP–α-tubulin-expressing S2 cells treated with control RNA. The cell border is marked with a dashed red line in the higher-magnification image shown on the bottom right. (B) Time series of a putative microtubule-severing event at the cortex. The green arrow marks the site of microtubule breakage and the dashed red line marks the cell border. (C) Images of live GFP–α-tubulin-expressing S2 cells treated with Dm-Kat60 RNA. As in A, the cell border is marked with a dashed red line in the higher-magnification image shown in the bottom right of this panel. (D) Time series of images obtained from a Dm-Kat60 RNA-treated cell showing lateral growth of microtubule ends along the cortex and their subsequent incorporation into the underlying microtubule array. Individual ends are indicated by colored circles and time (s) is labeled in each image. Scale bars, 10 μm (A and C), 1 μm (B), and 2 μm (D).

A unique role for Dm-Kat60 in microtubule dynamic instability

Approximately a quarter of the Dm-Kat60 RNA-treated interphase S2 cells imaged contained at least some cortical domains with numerous unambiguously identifiable microtubule plus-ends. The dynamics of these were analyzed in detail. To measure large numbers of plus-end dynamics, we developed an automated tracking algorithm that could accurately follow the position of microtubule ends over time (Figure 2.3A). The validity of this approach was confirmed by comparing a subset of microtubule trajectories generated automatically with those generated by hand (Figure 2.S4).

Consistent with our visual inspection of the data, control cells, most microtubule plus-end growth/shrinkage trajectories occurred along largely straight paths oriented perpendicular to the cortex (Figure 2.3B). In contrast, Dm-Kat60 RNAi cells exhibited numerous plus-end trajectory paths parallel to the cortex (Figure 2.3C). Moreover, on average, microtubule plus-ends in Dm-Kat60 RNAi cells spent significantly more time in growth (as opposed to shrinkage) parallel to the cortex and were positioned significantly closer to the cell edge (Figure 2.3 D and E).

We then analyzed the life-history plots of the tracked microtubule plus-ends to specify the impact of Dm-Kat60 on dynamic instability (Table 2.1). As expected, Dm-Kat60 RNAi significantly suppressed plus-end catastrophes by more than twofold. Thus, Dm-Kat60 is normally a potent catastrophe promoter. Dm-Kat60 depletion also increased transitions from pause to growth; paused plus-ends were almost twice as likely to proceed to the growth state. Surprisingly, the frequency of the reverse transition (a growing plus-end stalling into pause) also increased after Dm-Kat60 RNAi, but by a

more modest 20%. Finally, we measured a slight (~20%), but significant, increase in microtubule growth rate in Dm-Kat60 RNAi cells. On the other hand, depletion of Dm-Kat60 did not significantly impact the frequency of transitions out of the shrinkage state, nor did it alter the average rate of shrinkage.

The *Drosophila* kinesin-13 protein, kinesin-like protein 10A (KLP10A), has also been found to promote catastrophes at the cortex of interphase S2 cells (Mennella et al., 2005). To better understand the functional inter-relationship of Dm-Kat60 with this protein, we reassessed the influence of KLP10A on microtubule dynamics using our present methodologies (Table 2.1). As with Dm-Kat60 RNAi, the depletion of KLP10A significantly reduced the frequency of microtubule catastrophes. However, KLP10A RNAi also increased the frequency of transitions into pause, whereas Kat60 RNAi had the opposite effect. Also unlike Dm-Kat60 RNAi, KLP10A RNAi had no influence on microtubule growth rate, but strongly suppressed the rate of shrinkage.

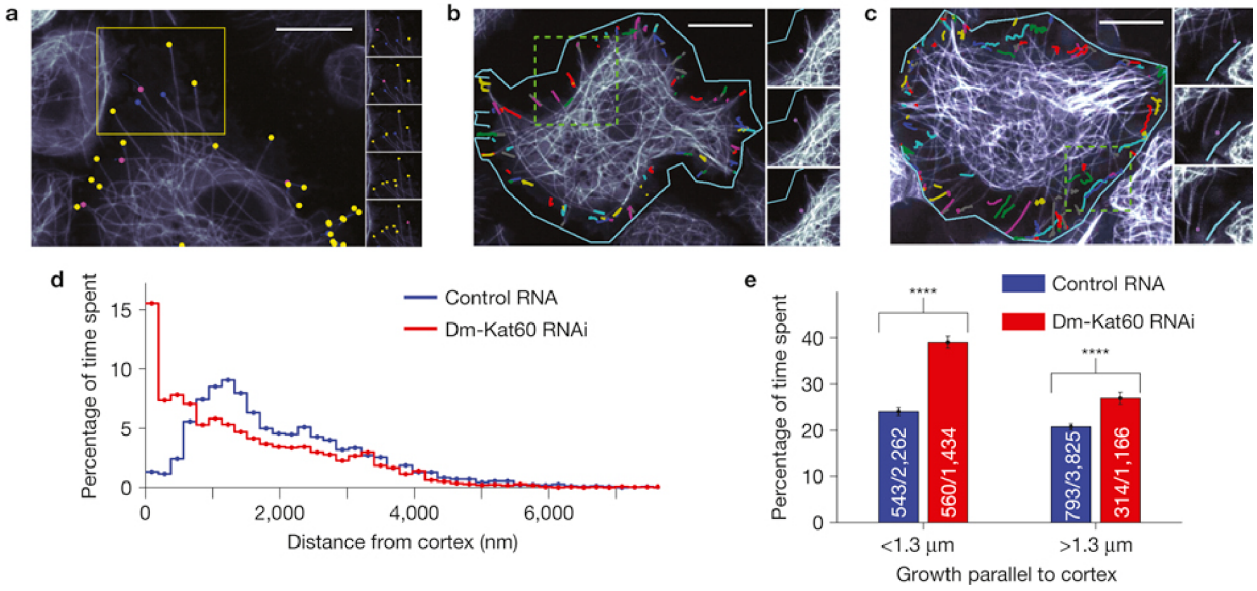

Figure 2.3. Automated tracking and quantitative analysis of microtubule plus-end organization and dynamics in control and Dm-Kat60 RNAi-treated cells. (A) Ends of GFP-labeled microtubules were tracked with an automated tracking algorithm. Each tracked microtubule end is marked with a colored dot: growing ends in blue, pausing ends in yellow and shrinking ends in pink. The stack of panels on the right is a time series of the outlined region. (B) Trajectories of microtubule ends tracked in a control RNA-treated cell. Individual microtubule trajectory paths are indicated by colored lines. (C) Trajectories of microtubule ends tracked in a Dm-Kat60 RNAi cell. Again, individual trajectory paths are indicated by colored lines. Relative to controls, significantly more microtubules continue to grow after reaching the cortex, and so microtubules are frequently observed to bend and grow parallel to the cortex. (D) The microtubule ends in Dm-Kat60 RNAi cells (five cells, 494 microtubules, 6,087 distances) spent significantly (P<0.0001) more time in the vicinity of the cortex, compared with control cells (seven cells, 257 microtubules, 2,600 distances). Microtubule ends within the cell interior could not be identified and thus were not analyzed. (E) Cortical microtubules spend more time growing after Dm-Kat60 knockdown. The change in dynamic behavior is most prominent in microtubule ends very near the cell margin (<1.3 µm), but is still significant (P<0.0001) for ends further away (>1.3 µm). Numbers within bars indicate the number of frames in which microtubules grew parallel to the cortex/total number of frames observed. Error bars, SEM. Scale bars, 10 µm (all image panels).

State to state	Control RNA	Dm-Kat60 RNAi	KLP10A RNAi
G→S	0.0106 (34)[*]	0.0041 (7)	0.0028 (4)
	0.0072–0.0144 [†]	0.0017–0.0081	0.0007–0.0073
		P=0.0249[‡]	*P*=0.0004[***]
G→P	0.0479 (167)	0.0576(75)[*]	0.0958 (116)
	0.0432–0.0522	0.0501–0.0645	0.0809–0.1053
		P=0.0225[*]	*P*=0.0181[*]
S→G	0.0098 (21)	0.0110 (10)	0.0045 (2)
	0.0063–0.0146	0.0056–0.0195	N/A
		P=0.7687	N/A
S→P	0.0521 (109)	0.0590 (42)	0.1113 (47)
	0.0466–0.0575	0.0477–0.0678	0.0972–0.1242
		P=0.2084	*P*=0.0035[**]
P→G	0.0291 (72)	0.0481 (47)	0.0641 (60)
	0.0223–0.0369	0.0360–0.0627	0.0461–0.0817
		P=0.0145[*]	*P*=0.1778
P→S	0.0216 (77)	0.0156 (22)	0.0119 (14)
	0.0166–0.0275	0.0080–0.0263	0.0059–0.0237
		P=0.2657	*P*=0.0031[**]
Growth	52.79 (1,083)	62.13 (580)	58.68 (530)
	1.25 [§]	1.97	1.73
		P<0.0001[****]	*P*=0.033[*]
Shrinkage	84.88 (819)	81.96 (316)	58.43 (179)
	2.81	4.61	3.63
		P=0.8380	*P*=0.0001[***]

Table 2.1. Comparison of state-to-state frequency (no. s^{-1}) and growth/shrinkage rate (nm s^{-1}) between control, Dm-Kat60 RNAi and KLP10A RNAi cells. [*]Numbers in parentheses indicate the event count in control RNA (five cells), Dm-Kat60 RNAi (seven cells) or KLP10A RNAi (five cells) treatment. [†]Intervals indicated are 95% confidence intervals calculated using a bootstrapping procedure with 1,000 resamples, and bias corrected and accelerated (BCa) correction. [‡]Indicates statistically different from control if $P<0.05$ (P values are shown). [**] $P<0.01$, [***] $P<0.001$, [****] $P<0.0001$. Statistical significance determined using a simulated two-tailed permutation test with 1,000 resamples. [§]SEM.

Dm-Kat60 localizes at the leading edge of D17 cells and regulates their migration

The influence of Dm-Kat60 on microtubule dynamics at the cell cortex indicated a role in cell migration (Ozon et al., 2002; Lee et al., 2004; Borghese et al., 2006; Jankovics et al., 2006). As S2 cells are immotile, we examined this possibility in migratory D17 cells. D17 cells were originally isolated from cultures of dissected imaginal discs (Ui et al., 1987); despite their epithelial origin, D17 cells exhibit a gene-expression profile that is consistent with that of *Drosophila* hemocytes. Similarly to hemocytes (Kurtti and Brooks, 1970; Merchant et al., 2008; Stramer et al., 2010), D17 cells spontaneously polarize in culture, assemble an exaggerated leading edge and exhibit robust cell motility. Immunofluorescence revealed that Dm-Kat60 accumulates at the leading edge of polarized D17 cells, where it extensively co-localizes with actin (Figure 2.4A). The other microtubule-severing enzymes in *Drosophila*, spastin and fidgetin (Roll-Mecak and Vale, 2005; Zhang et al., 2007), showed no such cortical enrichment, nor did their depletion obviously alter D17 cell migration (Figure 2.S5).

The influence of Dm-Kat60 on D17-cell migration was first examined in a wound-healing assay. D17-cell cultures were treated with Dm-Kat60 or control double-stranded RNA for 10 days, the confluent monolayers were wounded with a pipette tip and the resulting ‘wounds’ were imaged immediately or 24 h later. Unexpectedly, we measured a significant 1.4-fold increase in the rate of wound closure following Dm-Kat60 RNAi treatment (Figure 2.4 C and D). To specify the basis of this difference, we then assessed the intrinsic motility properties of single cells using time-lapse microscopy (Figure 2.5A). Dm-Kat60 RNAi-treated cells moved significantly faster than controls, with a striking increase in the number of high-velocity movements (Figure 2.5 B and C).

They also exhibited an increase in total migration distance (Figure 2.5D). Although control D17 cells do not exhibit directional motility in this assay, we did observe a slight, but significant, decrease in directionally persistent migration (Figure 2.5E), indicating that the increased migration of Dm-Kat60 depleted cells in wound healing assays does not result from increased directionality. Finally, we measured a notable difference in persistent migration following Dm-Kat60 RNAi treatment. Whereas migrating control cells spent ~63% of their time moving, cells depleted of Dm-Kat60 spent ~73% of their time migrating (Figure 2.5F). Taken together, these data indicate that Dm-Kat60 normally serves as a negative regulator of cell motility by suppressing fast and persistent migration.

We also examined whether Katanin carried out a similar function in human cells. Although conventional human p60 had no apparent impact on cell movement, the p60-like protein KATNA1 (Torres et al., 2009; Sonbuchner et al., 2010) localizes at the leading edge of migratory cells, regulates microtubule growth and negatively affects cell movement (Figure 2.S6). Thus, human KATNA1 is potentially the functional orthologue of Dm-Kat60, at least during interphase.

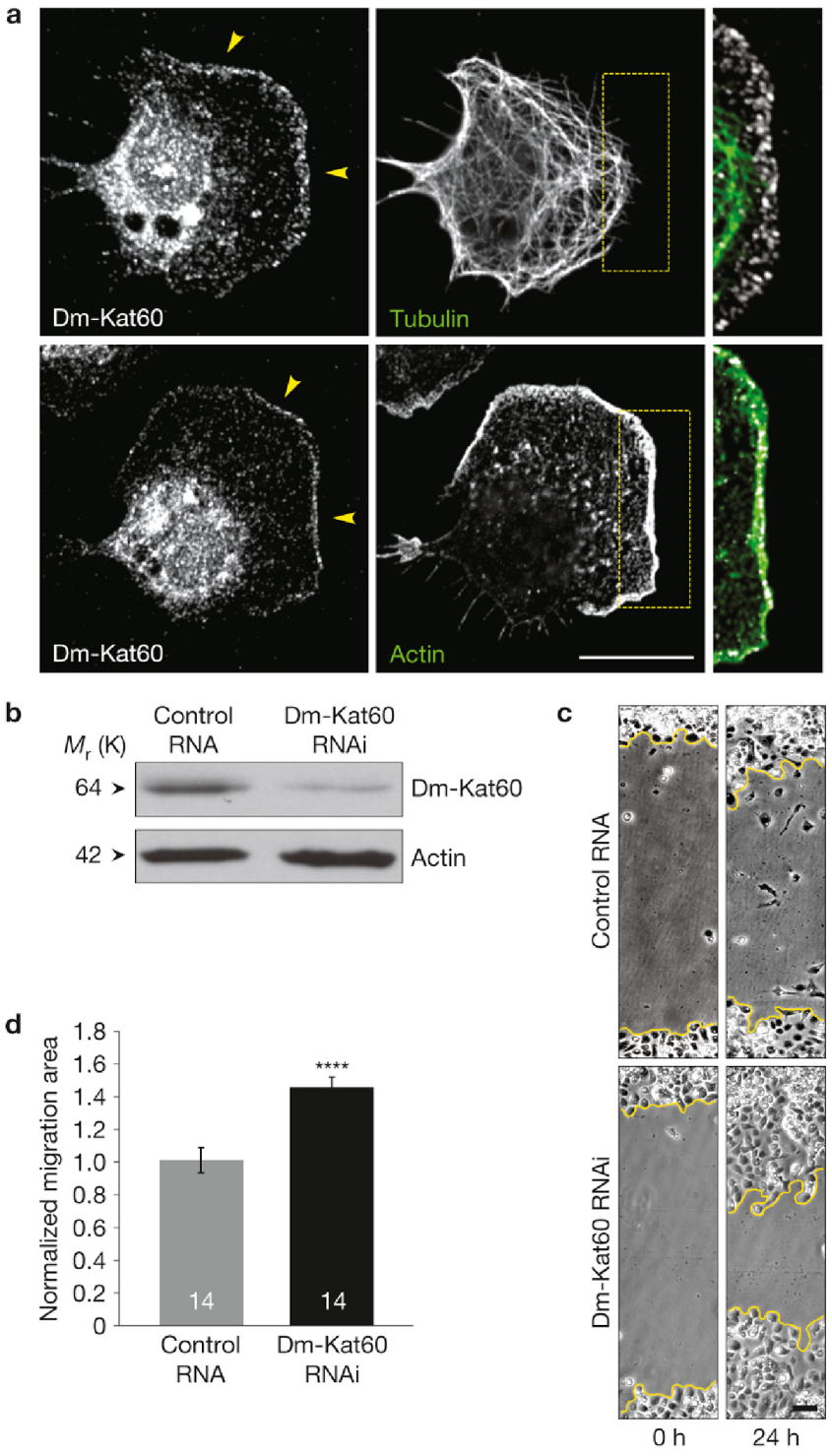

Figure 2.4. Dm-Kat60 targets to the leading edge of motile D17 cells and negatively regulates their migration. (A) Immunolocalization of Dm-Kat60, tubulin and actin in polarized *Drosophila* D17 cells. The arrowheads indicate enrichment of Dm-Kat60 at the leading edge; the outlined areas are magnified in the far right panels. (B) Western blot showing the depletion of Dm-Kat60 in D17 cells using RNAi.

(C) Representative phase-contrast images of scratch-wounds at 0 and 24 h after wounding. (D) Quantification of migration during wound closure for control and Dm-Kat60 RNAi-treated D17 cells. Migration area was calculated by subtracting the total wound area at 24 h from the total wound area at 0 h after wounding and then normalized to control RNA. $P=8.5\times10^{-5}$. Data represent mean values ± SEM from four independent experiments. Numbers in bars are sample sizes. Scale bars, 10 µm (A) and 50 µm (C).

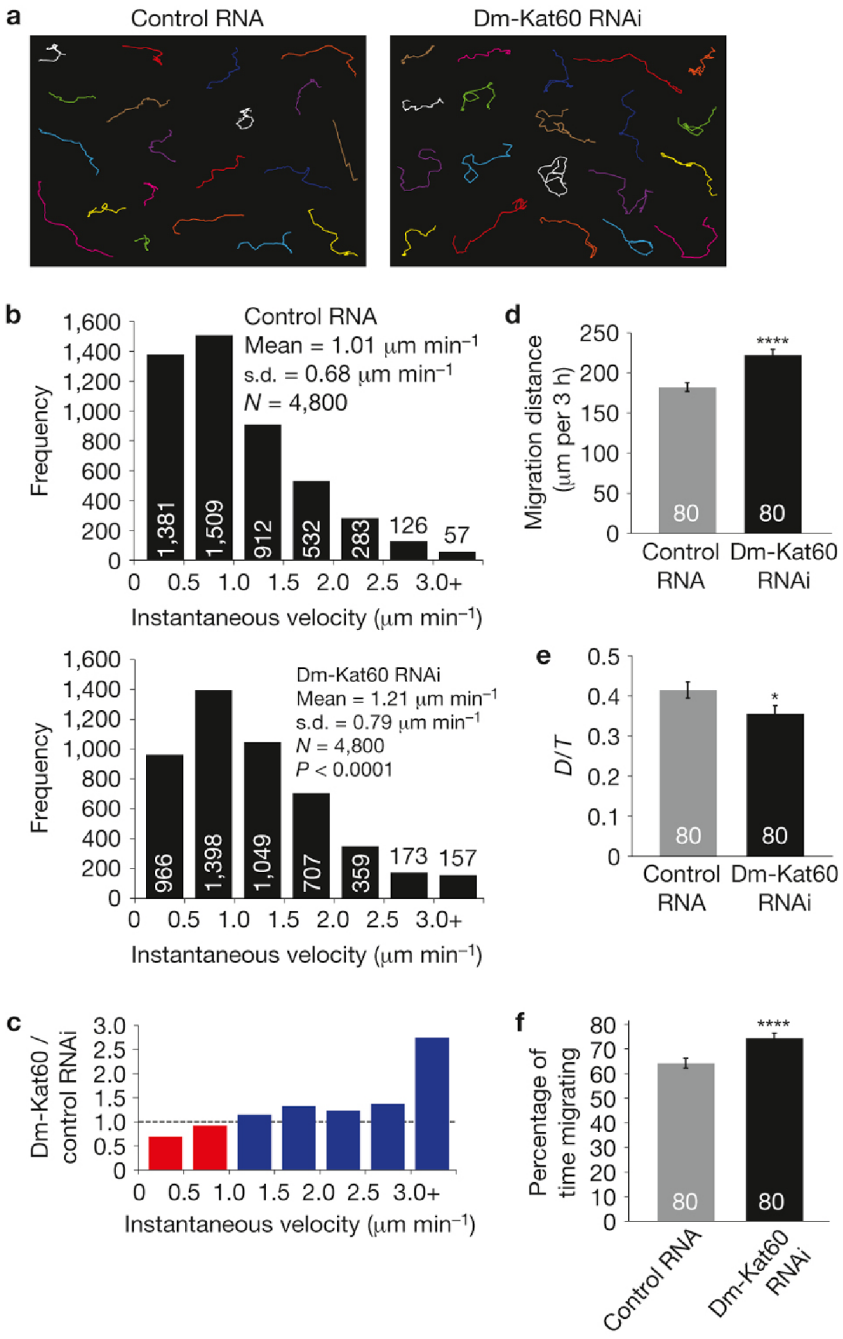

Figure 2.5. Dm-Kat60 negatively regulates multiple parameters of D17-cell motility. (A) Representative migration tracks of 20 cells for each treatment group (control and Dm-Kat60 RNAi). (B) Frequency distributions of instantaneous cell velocities from time-lapse imaging of individual D17-cell movements. P=8.2×10^{-40}. (C) Quantification of the ratio of velocity frequencies between Dm-Kat60 and control RNAi treatments. The Dm-Kat60/control RNAi ratio was calculated by dividing the number of movements for Dm-Kat60 RNAi-treated cells by the number of movements for control RNA-treated cells for a given range of velocities from the graphs in B. A ratio less than one (red) represents a decreased number of movements for Dm-Kat60 RNAi

relative to control RNA, and a ratio greater than one (blue) represents an increased number of movements for Dm-Kat60 RNAi relative to control RNA. Relative to control, Dm-Kat60 depletion decreases the frequency of cells migrating at low rates while increasing the frequency of high migration rates. (D) Quantification of total migration distance over a 3 h time period. $P=1.5\times10^{-5}$. (E) Quantification of intrinsic cell directionality. Directionally persistent migration (D/T) was calculated as a ratio of the direct distance between start and end points (D) to the total migration distance (T). $P=3.6\times10^{-2}$. (F) Quantification of persistent migration. The percentage of time that cells spent migrating was calculated by subtracting those movements between frames that were less than 2 μm (considered to be migratory pauses) from the total number of movements and then dividing by the total number of movements. $P=3.7\times10^{-5}$. Data represent mean values ± SEM from four separate double-stranded RNA treatments. Numbers in bars are sample sizes.

Dm-Kat60 inhibits actin protrusions at the cell edge

Microtubules are believed to impact cell movement largely through the regulation of actin-based structures, such as lamellae (Waterman-Storer and Salmon, 1997; Waterman-Storer et al., 1999; Waterman-Storer et al., 2000; Watanabe et al., 2005A; Watanabe et al., 2005B). Unfortunately, technical limitations precluded us from testing these cytoskeletal interactions in D17 cells. However, this could be studied in S2 cells co-expressing GFP–α-tubulin and mCherry–actin. Although Dm-Kat60 RNAi did not significantly impact on the accumulation of actin at the cortex or the rate of actin retrograde flow, it did strongly influence the cycles of lamellipodium protrusion and retraction (Figure 2.6A). Specifically, Dm-Kat60 RNAi-treated cells showed a significant approximately threefold increase in the frequency of protrusions and a more than twofold increase in the average displacement per protrusion (Figure 2.6 B and C). The increased cell-migration rates observed following Dm-Kat60 RNAi treatment could conceivably be due to a localized increase in the protrusion–retraction cycle at the leading edge.

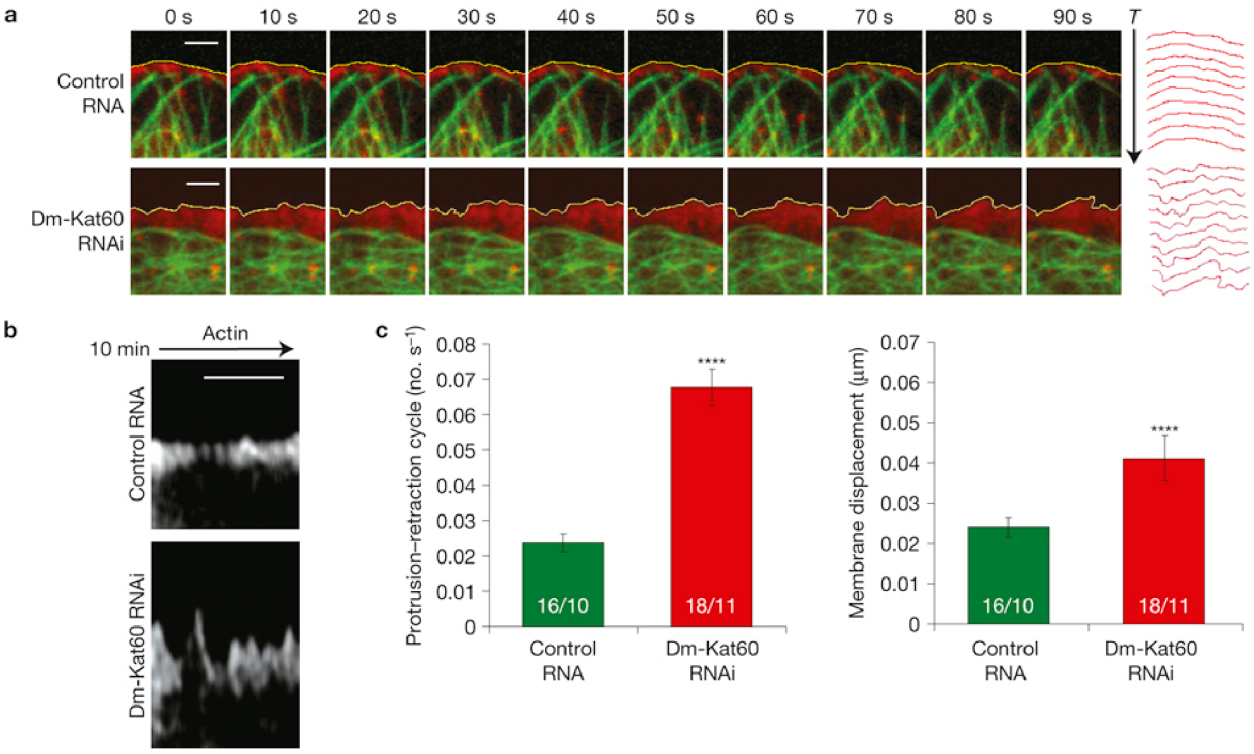

Figure 2.6. Dm-Kat60 negatively regulates actin protrusions at the cell edge. (A) Time-lapse images showing the cortical dynamics of control and Dm-Kat60 RNAi-treated S2 cells expressing GFP–α-tubulin and mCherry–actin. Yellow lines outline the edges of the cortical actin arrays in each image. These lines are stacked vertically (and shown in red) on the far right to illustrate the time-dependent alterations in the morphology of the cell edge (protrusions) in each condition (*T* labels the time axis). (B) Representative kymographs of mCherry–actin-labeled cortical regions from a control and Dm-Kat60 RNAi-treated cell. (C) Dm-Kat60 RNAi significantly increases both the frequency (left) and average displacement (right) of actin-based membrane protrusions ($P<0.0001$ for both). Data represent mean ± SEM and numbers in the columns indicate regions/cells analyzed. Scale bars, 2 µm for A and B.

Dm-Kat60 is a microtubule-severing enzyme and a microtubule end depolymerase

Finally, we examined the *in vitro* mechanism of action of Dm-Kat60 using purified, baculovirus-expressed, recombinant GFP–Dm-Kat60 (rDm-Kat60). Taxol-stabilized, rhodamine-labeled microtubules were immobilized on coverslips (McNally and Thomas, 1998), incubated with 50 nM rDm-Kat60 (Figure 2.7A) and imaged over time using total-internal-reflection microscopy (TIRF). rDm-Kat60 robustly severed taxol-stabilized microtubules in the presence of ATP (Figure 2.7 B and C), and this reaction was inhibited when ATP was depleted with hexokinase and glucose or replaced with the non-hydrolysable ATP analogue 5′-adenylyl-β-γ-imididodiphosphate (AMPPNP; Figure 2.7E). Thus, Dm-Kat60-mediated severing is stimulated by ATP hydrolysis. Severing also probably involves an interaction between Dm-Kat60 and the C-terminal tail of tubulin, because it was almost completely inhibited by the protease subtilisin, which removes the C termini of the tubulin subunits within the microtubule polymer. Subtilisin treatment was previously reported to inhibit katanin-mediated severing of microtubules (McNally and Vale, 1993).

To our surprise, we also observed substantial rDm-Kat60-induced depolymerization of microtubule ends, which generally preceded any obvious severing of the lattice (Figure 2.7 B and C). Similarly to severing, end depolymerization was suppressed by hexokinase and glucose, AMPPNP and subtilisin, indicating that both occur by a similar mechanism (Figure 2.7E). Although both microtubule ends were depolymerized by rDm-Kat60, one end almost always depolymerized faster than the other (Figure 2.7C). When these assays were carried out using polarity-marked microtubules, the plus-end was found to depolymerize approximately three times faster

than the minus-end (Figure 2.7 D and E). To ensure that microtubule end depolymerization did not result from a protein contaminant, identical analyses were carried out using the catalytically inactive Dm-Kat60 (E393Q; Hartman and Vale, 1999) mutant protein. The catalytically inactive Dm-Kat60 was entirely incapable of severing microtubules and, although it did induce some end depolymerization, the rate at which this occurred was approximately five times slower than that induced by the wild-type protein (Figure 2.7E).

In a last set of experiments we examined the morphology of microtubule ends severed or depolymerized by rDm-Kat60 using electron microscopy. Samples of microtubules incubated with rDm-Kat60 and ATP, rDm-Kat60 and AMPPNP, and control microtubules without rDm-Kat60 were applied to electron microscopy grids and fixed by negative staining (Figure 2.7F). We measured an approximate threefold increase in the number of microtubule ends per unit length in the rDm-Kat60/ATP condition relative to the AMPPNP and control samples without rDm-Kat60 (Figure 2.7G) demonstrating that rDm-Kat60 was active in these assays. Interestingly, we observed no substantial difference in the morphology of microtubule ends among any of the above conditions. In all cases, microtubule ends were blunt or had a few straight protofilaments protruding from the end. In contrast, microtubules incubated with the *Drosophila* kinesin-13 KLP59D (Rath et al., 2009) showed numerous curled protofilaments peeling away from the ends (Figure 2.7G), which is typical of kinesin-13-catalyzed microtubule depolymerization (Desai et al., 1999). This indicates that Dm-Kat60 and kinesin-13 proteins remove tubulin from microtubule ends by distinct mechanisms.

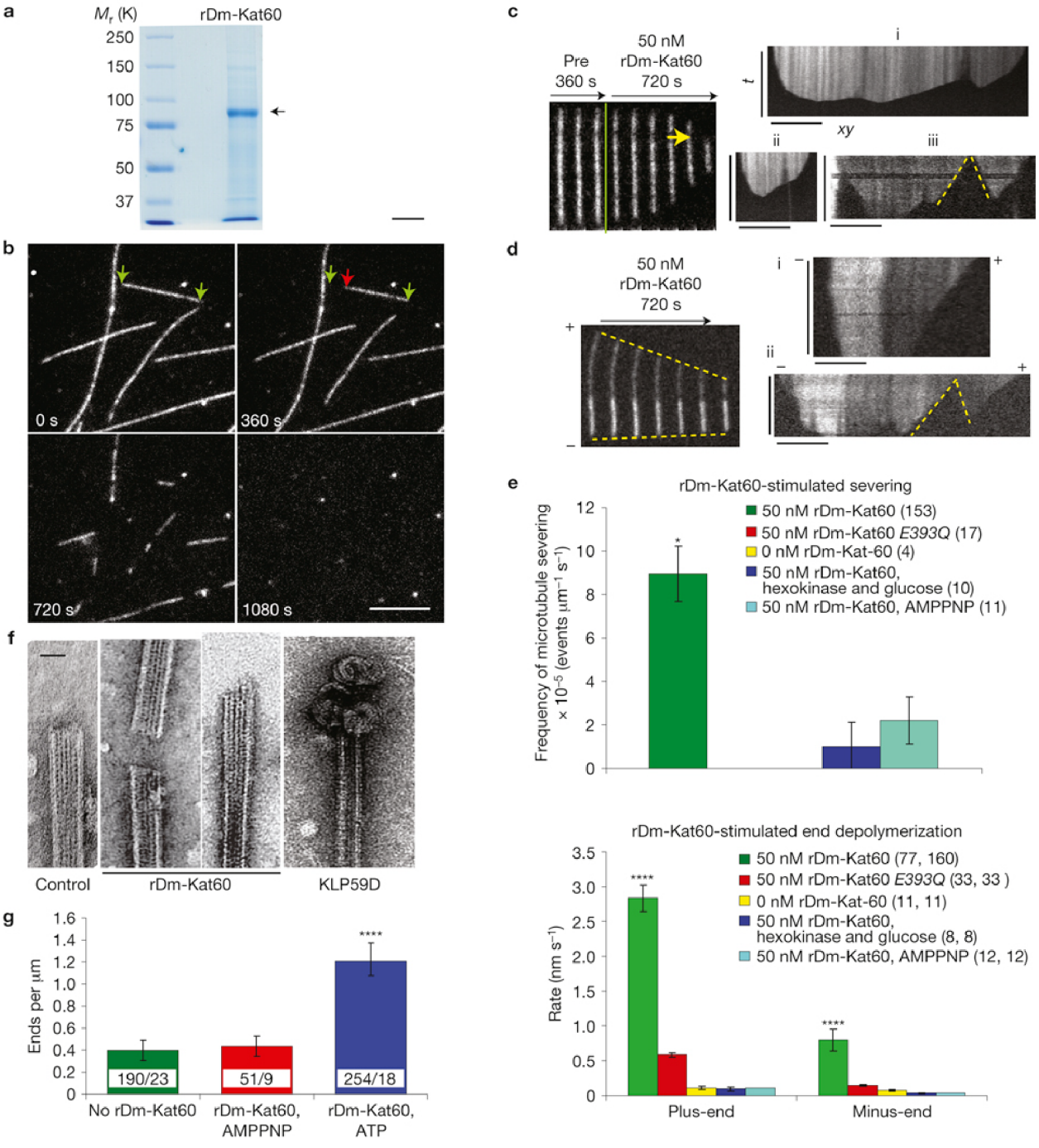

Figure 2.7. Dm-Kat60 severs and depolymerizes microtubules from their ends. (A) Coomassie-blue-stained SDS–polyacrylamide gel electrophoresis of the purified rDm-Kat60 protein used for analysis. The arrow indicates the band corresponding to rDm-Kat60. (B) Time series of TIRF images showing the disassembly of a field of immobilized microtubules by 50 nM rDm-Kat60 and ATP. Green arrows mark the ends of an individual microtubule at the beginning of visualization; a red arrow marks a microtubule end that has shrunk from its initial position. Time (seconds) is indicated. (C) Left, time series of an individual microtubule (marked by arrows in B) before (pre) and

after addition of rDm-Kat60. i–iii, Kymographs showing the depolymerization and severing (indicated by dotted yellow lines) of individual microtubules from other experiments. The time (*t*) axis is vertical and distance (*x*–*y*) axis horizontal in all kymographs shown in this figure. (D) Left, time series of an individual polarity-marked microtubule incubated with rDm-Kat60. The plus-end is dimly labeled and the minus-end is brightly labeled. i,ii, Kymographs showing the depolymerization and severing (dotted yellow lines) of further polarity-marked microtubules. (E) Upper, quantification of the frequency of microtubule severing by rDm-Kat60. All conditions included 2 mM ATP (or 2 mM AMPPNP). P=0.031. Lower, measured rates of microtubule plus- and minus-end depolymerization by rDm-Kat60. P=3.1×10^{-7}. Again, all conditions included 2 mM ATP or AMPPNP. Data in both panels represent mean ± SEM. N= number of microtubules analyzed. (F) Electron micrographs showing the ends of negatively stained microtubules after incubation with: no Dm-Kat60 (control), 50 nM rDm-Kat60 and 2 mM ATP (rDm-Kat60) or full-length KLP59D and ATP (KLP59D). (G) Quantification of microtubule ends per unit microtubule length. Compared with the no Dm-Kat60 and Dm-Kat60 (50 nM)+AMPPNP (2 mM) controls, Dm-Kat60+ATP (50 nM GFP–Dm-Kat60, 2 mM ATP) induces three times more ends (P<0.0001). Numbers in the column indicate numbers of microtubules/electron microscopy fields. Data represent mean ± SEM pooled from two independent experiments. Scale bars, 500 μm (A), 10 μm (B), and 20 nm (F).

Discussion

Our results identify Dm-Kat60 as an important regulator of microtubule dynamics and cell migration. The human katanin KATNA1 behaves similarly. In addition to its cellular roles, *in vitro* analyses indicate that Dm-Kat60 has the capacity to function as both a microtubule-severing enzyme and a microtubule end depolymerase. On the basis of its cortical localization, RNAi phenotypes and catalytic activity, we propose that Dm-Kat60 (and KATNA1) contributes to the generation of a dynamic interface between the microtubule cytoskeleton and the interphase cortex by removing tubulin subunits from any region of the microtubule making contact with Dm-Kat60-rich cortical sites (Figure 2.S7).

Among the more unexpected outcomes of this study is the observation that Dm-Kat60 induces microtubule end depolymerization *in vitro*. However, given present models of the interaction of katanin with the microtubule, such a finding is not entirely surprising. Biophysical and biochemical studies have indicated that severing by katanin is mediated by the transient hexamerization of p60 proteins at the C terminus of a single tubulin within the microtubule (Hartman and Vale, 1999; Roll-Mecak and McNally, 2010). ATP hydrolysis and/or the subsequent disassembly of the hexamer is believed to generate a mechanical force, which, through multiple iterations, induces the removal of the tubulin from the lattice. If katanin works by ‘tugging’ on a single tubulin heterodimer, then the exposed tubulins at the microtubule end are likely to be the easiest to remove because they lack a longitudinal contact. However, we cannot rule out the possibility that Dm-Kat60-mediated end depolymerization is a manifestation of multiple severing events occurring very near the tip.

Within the cell, the severing and depolymerase activities of Dm-Kat60 probably remain under very tight spatial constraints. In this regard, the recruitment of Dm-Kat60 to the cell cortex seems to be central to its interphase functions. Although our data indicate that this process is reliant on the presence of actin, but not microtubules, the specific mechanisms that deliver Dm-Kat60 to the cortex remain a mystery. One appealing hypothesis is that Dm-Kat60 is directly or indirectly linked to the cortical actin array through *Drosophila* p80. The p80 subunit contains repeated WD40 motifs known to mediate protein–protein interactions (Smith et al., 1999). Similar motifs have been identified in some actin-binding proteins (Hudson and Cooley, 2002). The WD40 repeats of p80 are essential for the centrosomal targeting of katanin in other organisms (Hartman et al., 1998; McNally et al., 2000). It has also been suggested that p60 acts independently of p80 in some circumstances (Yu et al., 2005). The identification of the binding partners of Dm-Kat60 represents an important next step in understanding its cellular activities.

At the cortex, Dm-Kat60 suppresses microtubule growth primarily by inducing plus-end catastrophes and transitions from growth to pause. Although other classes of proteins are known to induce microtubule depolymerization, *in vitro* (Desai et al., 1999; Sproul et al., 2005; Gupta et al., 2006; Varga et al., 2006), the presumptive ability of Dm-Kat60 to remove tubulins from any region of the microtubule—end or lattice—may be particularly useful in the more complex cellular environment. For example, such an activity could enable Dm-Kat60 to prevent sustained microtubule growth along the cortex regardless of whether the microtubule contacts the cortex end-on or side-on. The newly created plus-end at the cortical-microtubule interface would then initiate

catastrophe or enter the pause state depending on its association with other microtubule-binding proteins (see below). Moreover, the ends of polymerizing microtubules in cells are often ‘capped’ by plus-end-binding proteins such as EB1 (Mimori-Kiyosue et al., 2000). Dm-Kat60 could remove these by severing the microtubule at the base of the EB1 ‘cap’ and/or directly removing EB1-bound tubulins from the plus-end. The acidic tail of EB1 could mimic the C terminus of tubulin, thereby providing a substrate for Dm-Kat60 (Mishima et al., 2007).

Of course, Dm-Kat60 is not alone in its ability to stimulate the catastrophe of microtubule plus-ends near the cortex of interphase S2 cells, as the *Drosophila* kinesin-13 KLP10A also shows this activity (Mennella et al., 2005). However, aside from the ability of both proteins to promote catastrophes, the activities of Dm-Kat60 and KLP10A are quite distinct. The most notable difference is that KLP10A does not concentrate on the cortex, but instead binds to the ends of polymerizing microtubules to which it is recruited by EB1. Intriguingly, recent work indicates that EB1 can inhibit the depolymerase activity of kinesin-13 proteins by shielding the plus-end (Montenegro Gouveia et al., 2010). If Dm-Kat60 were to generate plus-ends lacking EB1, then it could relieve this inhibition.

We propose that Dm-Kat60 and KLP10A work together as follows. (1) Dm-Kat60 removes tubulins (EB1 bound or otherwise) from regions of the microtubule that come in close proximity to the cortex, thereby creating a free plus-end at the cortical interface. Many of these newly created plus-ends immediately enter a paused state (depletion of EB1 has been shown to strongly promote pause; Rogers et al., 2002). (2) Next, KLP10A, which has already been accumulated near the end by EB1, promotes the

transition of this end from pause to shrinkage—this transition can occur rapidly and may often appear as a catastrophe. Our present study also indicates that KLP10A increases the rate of plus-end depolymerization and thus a small, difficult-to-detect, portion of the protein may remain associated with the microtubule end as it depolymerizes. Why such an effect was not noted in our initial analysis of KLP10A is unknown, but may be due to the more limited region of the cortex analyzed in that study (Mennella et al., 2005).

The finding that Dm-Kat60 targets the leading edge of motile D17 cells and alters their migration provides a broader biological context through which our findings can be viewed and interpreted. Although the depletion of Dm-Kat60 had no obvious influence on the establishment of cell polarity, it did increase both the frequency and displacement of membrane protrusions, at least in S2 cells. The localized suppression of protrusions at the leading edge of motile D17 cells could exert negative control over the rate and persistence of cell movement.

The observation that Dm-Kat60 RNAi results in faster and more persistent migration seems consistent with other studies demonstrating that growing microtubules stimulate the GTPase Rac at the leading edge, which may promote adhesion-complex remodeling, needed to drive and sustain protrusions (Waterman-Storer and Salmon, 1997; Waterman-Storer et al., 1997). In addition, because Dm-Kat60 depletion at the leading edge of migratory cells should decrease catastrophes, microtubules could become unusually persistent and abundant in the extending protrusion, which may intensify other processes that favor protrusion, such as increased kinesin-mediated delivery of vesicles to the protrusion zone (Reed et al., 2006).

A recent study examining hemocyte migration in developing *Drosophila* embryos,

for which we believe D17 cells to be a model, showed that hemocytes migrate less efficiently in response to guidance cues following the disruption of microtubule dynamics (Stramer et al., 2010). Under these conditions, the authors also observed an increase in cell velocities and a decrease in directional persistence, similar to D17 cells depleted of Dm-Kat60 by RNAi. Thus, Dm-Kat60 may modulate microtubule dynamics at the leading edge to 'fine-tune' cell migration by suppressing protrusions.

The findings of this study uncover unexpected roles for the *Drosophila* katanin p60 Dm-Kat60 in the regulation of cortical microtubule dynamics and provide insights into how the microtubule cytoskeleton affects cell migration. The ability of cells to move and change shape is central to organismal development. Defects in these processes have been linked to human diseases such as cancer. Thus, our finding that human KATNA1 has many of the same functions as Dm-Kat60 suggests the former as a potentially useful therapeutic target.

Materials and Methods

S2 cell culture, RNAi, and construction of plasmids

S2 cells expressing GFP–α-tubulin were a gift from R. Vale (University of California, San Francisco). Wild-type S2 cells were obtained from ATCC. Our methods for S2 cell culture, RNAi treatment of S2 cells and production of double-stranded RNA from the 3′ untranslated region of endogenous Dm-Kat60 (including sequences) have been described previously (Zhang et al., 2007).

Immunofluorescence microscopy

S2 cells were plated on concanavalin-A-coated coverslips for 1.5 h, fixed in 100% methanol at −20 °C for 20 min and blocked with 5% normal goat serum in PBS containing 0.1% Triton X-100. Primary antibodies (Dm-Kat60, α-tubulin (DM1a, Sigma-Aldrich) and actin (clone C4, Millipore)) were applied at 1–20 μg ml^{-1} final concentration in blocking buffer. Fluorescent secondary antibodies (Jackson Immuno-Research Laboratories) were used at 7.5 μg ml^{-1}. Imaging was carried out on an Ultraview spinning-disc confocal system (PerkinElmer) mounted on an inverted microscope (Eclipse TE300; Nikon) with a 100x (1.4 NA) or 60x (1.4 NA) objective and captured with an Orca ER digital camera (Hamamatsu). For microtubule disruption, cells were treated with 50 μM colchicine for 18 h before fixation. For microfilament disruption, cells were treated with 5 μM cytochalasin D for 1 h before fixation.

Live-cell imaging and automated tracking

Four-dimensional time-lapse movies of GFP–α-tubulin-expressing S2 cells were acquired using the Ultraview spinning-disc confocal microscope described above.

Microtubule ends were tracked through each series of time-lapse images with an automated tracking program using the following assumptions.

To define the tracking region, for each cell, we tracked microtubules in a hand-selected region of interest consisting of an outer (the cortex; Figure 2.3A) and an inner (to avoid tracking into the crowded interior) boundary. For all calculations, the data from cells of the same treatment (control or Dm-Kat60 RNAi) were pooled.

To define growth and shrinkage, we calculated the angle α between the direction of the displacement of the microtubule tip and the direction of the microtubule itself. A value of $\cos(\alpha)>0.2$ ($\alpha<\sim78^{\circ}$) indicated probable growth, and $\cos(\alpha)<-0.2$ ($\alpha>\sim101^{\circ}$) indicated probable shrinkage. These 'loose' cutoffs were chosen to deal with the curvature of microtubules in the Dm-Kat60 RNAi cells. To qualify as growing or shrinking, we required that the microtubule show the same behavior (either growing or shrinking) for at least two consecutive frames, and that the overall displacement in a run of growth or shrinkage be at least 5 pixels.

The distance to the cortex was defined as the Euclidean distance from a microtubule tip to its closest point on the cortex. The difference in the distance distributions was tested using the Kolmogorov–Smirnov two-distribution test.

To define growth parallel to the cortex, for two consecutive frames t and t+1, the points on the cortex closest to the trajectory segment are given by c(t) and c(t+1), respectively, and the displacement vector along the cortex is $\delta c(t)=c(t+1)-c(t)$. A microtubule was considered to grow parallel to the cortex if the angle between the tip displacement and $\delta c(t)$ was less than 45°. Error bars plotted are the asymptotic standard errors for a binomial distribution: $\sqrt{p(1-p)/N}$, where p is the fraction that

grow along the cortex, and N is the total number of data points. Significance was tested by χ^2 using a 2×2 table of dichotomous outcomes.

To calculate transition rates, catastrophes near the cortex were determined by counting the number of significant shrinkage events away from the cortex. To be counted, a shrinkage event had to begin within 0.63 μm of the cortex (10 pixels), and increase its distance from the cortex by at least 0.32 μm (5 pixels) by the end of the shrinkage run. The catastrophe statistic was calculated as:

$$\frac{1}{N}\sum_{i=1}^{N}\left[\frac{[\text{depolymerization events in cell } i]/[\text{s in cell } i]}{[\text{microtubules near cortex in cell } i]}\right]$$

The standard error was estimated by bootstrap sampling on the terms of the sum with 1,000 resamples. Statistical significance was determined using 1,000 resamples of a one-sided permutation test with the test statistic $\log(S1,i/S2,i)$, where $S1,i$ and $S2,i$ are the catastrophe statistic sums for resample i of control (1) and Dm-Kat60 RNAi (2), respectively. To calculate transition rates (Table 1), each frame of a microtubule trajectory was marked as either grow, shrink or pause. Grow and shrink states were defined as previously described. Pause was defined as neither growing nor shrinking. The lifetimes of states that began and ended in the middle of a trajectory (not on a boundary), as well as the state they transitioned to, were collected. The rate of transition between an initial state k (k=grow, shrink or pause) and a final state l ($l \neq k$) is:

$$\frac{[\text{no. of transitions from } k \text{ to } l]}{[\text{no. of transitions out of } k]} \times \frac{1}{[\text{no. of transitions out of } k]}$$

$$\times \sum_i \left(\frac{1}{[\text{time in state } k \text{ before transition } i]}\right)$$

We used a bootstrap approximation to construct 95% confidence intervals of

each transition, with 1,000 resamples of all lifetimes. Statistical significance was established using a two-sided permutation test with 1,000 resamples of the statistic $r1,i - r2,i$, where $r1,i$ and $r2,i$ correspond to the rates calculated in resample i of control (1) and Kat60-RNAi (2).

Purification of recombinant 6×His–GFP–Dm-Kat60

6xHis–GFP–Dm-Kat60 (rDm-Kat60) was cloned into pFastBac HT-A (Invitrogen) and then transformed into DH10Bac *Escherichia coli* cells. The primers to amplify GFP were: forward, 5′-GAATTCACCATGGTGAGCAAGGGCGAGGAG-3′, and reverse, 5′-AAGGAAAAAAGCGGCCGCCTTGTACAGCTCGTCCATGCCGAG-3′. The primers to amplify Dm-Kat60 were: forward, 5′-AAGGAAAAAAGCGGCCGCCACCATGTCCATAACCTTACTGCGAGGTGG-3′, and reverse, 5′-CCGCTCGAGTCATGACGATCCGAACTCCCTC-3′.

The bacmid was isolated from DH10Bac *E. coli* and then transfected into Sf9 cells. The virus-containing supernatant was used to infect fresh Sf9 cells for 72 h and the procedure was repeated twice to amplify the baculovirus. A 20 µl portion of the third-cycle supernatant was added to Sf9 cells in 250 ml SFM900-II medium (Invitrogen) with 5% fetal bovine serum to express 6xHis–GFP–Dm-Kat60 at a low level (high levels of expression yielded inactive aggregates). Infected cells were lysed with a French press and centrifuged, and the resulting supernatant incubated with 1 ml nickel resin (Qiagen) at 4 °C for 1 h. The resin was then transferred into a 20 ml chromatography column (Biorad) and washed with four column volumes of wash buffer (40 mM imidazole in resuspension buffer without phenylmethylsulphonyl fluoride), and eluted with 500 mM imidazole in resuspension buffer without phenylmethylsulphonyl fluoride. The eluted

rDm-Kat60 was concentrated by centrifugation and exchanged into severing buffer I (20 mM HEPES, at pH 7.0, 300 mM NaCl, 3 mM MgCl2, 10% sucrose, 50 μM ATP, 5 mM dithiothreitol).

***In vitro* assays**

Rhodamine-labelled, taxol-stabilized non-polarity or polarity-marked microtubules were prepared according to an online protocol (http://mitchison.med.harvard.edu.libproxy.lib.unc.edu/protocols.html) and immobilized in the flow chamber with a kinesin rigor mutant (G234A) as reported (McNally and Thomas, 1998). The assay was conducted in severing buffer II (20 mM HEPES, at pH 7.0, 100 mM NaCl, 3 mM MgCl2, 10% sucrose, 2 mM ATP, 10 mM dithiothreitol, 7.5 mg ml^{-1} bovine serum albumin, 0.1% Pluronic F-127) at 24 °C. An oxygen-scavenger system (220 μg ml^{-1} glucose oxidase, 22.5 mM glucose, 36 μg ml^{-1} catalase) was included to minimize photodamage. In some control assays, 5 mM AMPPNP or 4 mM hexokinase was used in place of ATP. Subtilisin pretreatment of microtubules was the same as reported in Roll-Mecak and McNally, 2010. After perfusing microtubules into the flow-chamber cell, the purified rDm-Kat60 construct was introduced into the chamber and fluorescent microtubules were imaged by TIRF. Our TIRF microscope used a home-made laser system assembled around a Nikon Eclipse Ti microscope and a high-numerical-aperture objective (60x,NA=1.49).

Digital images were saved as stacks of Tagged Image File Format files, and time-lapse series were saved as Audio Video Interleave files. Kymographs were generated using the Multiple Kymograph plug-in (ImageJ). From the kymographs of all microtubules recorded for each treatment of the depolymerization assay, we calculated the average angle of the microtubule ends' displacements through time. The

depolymerization rate was determined by calculating the reciprocal of the tangent of the average angle, and then applying the appropriate conversions to derive the distance and time values. The *in vitro* severing frequency was determined by manually counting the number of severing events in every microtubule. The number of severing events in a single movie was divided by the total length of the microtubules at the start of the movie and divided by the total time of the movie.

D17 cell RNAi and migration assays

D17 cells were maintained in a room-temperature incubator in D17 medium: Schneider's medium (Invitrogen) supplemented with 10% fetal bovine serum (Gibco), 1% antibiotic–antimycotic (Gibco) and 1.25 μg ml^{-1} insulin (Invitrogen).

For RNAi, D17 cells were treated on days 0, 2, 4, 6 and 8 with 20 μg of dsRNA in 1 ml serum-containing Schneider cell medium (Life Technologies). On day 9, the RNAi-treated cells were plated on either extracellular-matrix-coated plastic tissue culture dishes for wound-healing experiments or extracellular-matrix-coated glass-bottom tissue culture dishes for single-cell analysis. For wound-healing experiments, cells were allowed to adhere for 4–6 h before manually scraping the cell monolayer with a pipette tip. After replenishing the medium, the scratch-wound regions were imaged 0 and 24 h after wounding using a phase-contrast microscope. For single-cell analysis, cells were imaged every 3 min for 3 h using a phase-contrast microscope equipped with a 10x (0.25 NA) objective.

Electron microscopy

Samples for negative-stain electron microscope experiments were prepared by mixing

1.5 µM of microtubules with 50 nM rDm-Kat60 in severing buffer II (above) for 30 min at 24 °C. A 5 µl portion of this mixture was then loaded onto freshly glow-discharged carbon-supported grids (Electron Microscopy Sciences). The grid was washed and stained with 1% uranyl acetate, followed by observation in a Tecnai F20 microscope (FEI) operating at 120 kV with a nominal magnification of ×50,000.

Statistics

Differences between treatments were analyzed using either a one-way nonparametric analysis of variance (Kruskal–Wallis) for multiple-group comparisons or a nonparametric *t*-test (Mann–Whitney) for two-group comparisons (SigmaStat, Systat Software; or GraphPad Prism, GraphPad Software). Measurement means were taken to be statistically different if $P<0.05$.

REFERENCES

Borghese L, Fletcher G, Mathieu J, Atzberger A, Eades WC, Cagan RL, et al. Systematic analysis of the transcriptional switch inducing migration of border cells. Dev Cell. 2006; 10:497–508.

Burk DH, Zhong RQ, Ye ZH. The katanin microtubule severing protein in plants. J Integr Plant Biol. 2007; 49:1174-82.

Burk DH, Liu B, Zhong RQ, Morrison WH, Ye ZH. A katanin-like protein regulates normal cell wall biosynthesis and cell elongation. Plant Cell. 2001; 13:807–28.

Buster D, McNally K, McNally FJ. Katanin inhibition prevents the redistribution of gamma-tubulin at mitosis. J Cell Sci. 2002; 115:1083–92.

Casanova M, Crobu L, Blaineau C, Bourgeois N, Bastien P, Pagès M. Microtubule-severing proteins are involved in flagellar length control and mitosis in Trypanosomatids. Mol Microbiol. 2009; 71:1353–70.

Desai A, Verma S, Mitchison TJ, Walczak CE. Kin I kinesins are microtubule-destabilizing enzymes. Cell. 1999; 96:69–78.

Gupta ML, Carvalho P, Roof DM, Pellman D. Plus end-specific depolymerase activity of Kip3, a kinesin-8 protein, explains its role in positioning the yeast mitotic spindle. Nat Cell Biol. 2006; 8:913–23.

Hartman JJ, Vale RD. Microtubule disassembly by ATP-dependent oligomerization of the AAA enzyme katanin. Science. 1999; 286:782–5.

Hartman JJ, Mahr J, McNally K, Okawa K, Iwamatsu A, Thomas S, et al. Katanin, a microtubule-severing protein, is a novel AAA ATPase that targets to the centrosome using a WD40-containing subunit. Cell. 1998; 93:277–87.

Hudson AM, Cooley L. Understanding the function of actin-binding proteins through genetic analysis of Drosophila oogenesis. Annu Rev Genet. 2002; 36:455–88.

Jankovics F, Brunner D. Transiently reorganized microtubules are essential for zippering during dorsal closure in Drosophila melanogaster. Dev Cell. 2006; 11:375–85.

Jaworski J, Hoogenraad CC, Akhmanova A. Microtubule plus-end tracking proteins in differentiated mammalian cells. Int J Biochem Cell Biol. 2008; 40:619–37.

Karabay A, Yu W, Solowska JM, Baird DH, Baas PW. Axonal growth is sensitive to the levels of katanin, a protein that severs microtubules. J Neurosci. 2004; 24:5778–88.

Kurtti TJ, Brooks MA. Growth and differentiation of lepidopteran myboblasts in vitro. Exp Cell Res. 1970; 61:407-12.

Lee H, Engel U, Rusch J, Scherrer S, Sheard K, Van Vactor D. The microtubule plus end tracking protein Orbit/MAST/CLASP acts downstream of the tyrosine kinase Abl in mediating axon guidance. Neuron. 2004; 42:913–26.

Martin SG. Microtubule-dependent cell morphogenesis in the fission yeast. Trends Cell Biol. 2009; 19:447–54.

McNally FJ, Thomas S. Katanin is responsible for the M-phase microtubule-severing activity in Xenopus eggs. Mol Biol Cell. 1998; 9:1847–61.

McNally FJ, Vale RD. Identification of katanin, an ATPase that severs and disassembles stable microtubules. Cell. 1993; 75:419–29.

McNally KP, Bazirgan OA, McNally FJ. Two domains of p80 katanin regulate microtubule severing and spindle pole targeting by p60 katanin. J Cell Sci. 2000; 113:1623–33.

McNally K, Audhya A, Oegema K, McNally FJ. Katanin controls mitotic and meiotic spindle length. J Cell Biol. 2006; 175:881–91.

Mennella V, Rogers GC, Rogers SL, Buster DW, Vale RD, Sharp DJ. Functionally distinct kinesin-13 family members cooperate to regulate microtubule dynamics during interphase. Nat Cell Biol. 2005; 7:235–45.

Merchant D, Ertl RL, Rennard SI, Stanley DW, Miller JS. Eicosanoids mediate insect hemocyte migration. J Insect Physiol. 2008; 54:215-21.

Mimori-Kiyosue Y, Shiina N, Tsukita S. The dynamic behavior of the APC-binding protein EB1 on the distal ends of microtubules. Curr Biol. 2000; 10:865–8.

Mishima M, Maesaki R, Kasa M, Watanabe T, Fukata M, Kaibuchi K, et al. Structural basis for tubulin recognition by cytoplasmic linker protein 170 and its autoinhibition. Proc Natl Acad Sci USA. 2007; 104:10346–51.

Montenegro Gouveia S, Leslie K, Kapitein LC, Buey RM, Grigoriev I, Wagenbach M, et al. In vitro reconstitution of the functional interplay between MCAK and EB3 at microtubule plus ends. Curr Biol. 2010; 20:1717–22.

Nakamura M, Ehrhardt DW, Hashimoto T. Microtubule and katanin-dependent dynamics of microtubule nucleation complexes in the acentrosomal Arabidopsis cortical array. Nat Cell Biol. 2010; 12:1064–70.

Ozon S, Guichet A, Gavet O, Roth S, Sobel A. Drosophila stathmin: a microtubule-destabilizing factor involved in nervous system formation. Mol Biol Cell. 2002; 13:698–710.

Quarmby L. Cellular Samurai: katanin and the severing of microtubules. J Cell Sci. 2000; 113:2821–7.

Rasi MQ, Parker JDK, Feldman JL, Marshall WF, Quarmby LM. Katanin knockdown supports a role for microtubule severing in release of basal bodies before mitosis in Chlamydomonas. Mol Biol Cell. 2009; 20:379–88.

Reed NA, Cai D, Blasius TL, Jih GT, Meyhofer E, Gaertig J, et al. Microtubule acetylation promotes kinesin-1 binding and transport. Curr Biol. 2006; 16:2166–72.

Rogers SL, Rogers GC, Sharp DJ, Vale RD. Drosophila EB1 is important for proper assembly, dynamics, and positioning of the mitotic spindle. J Cell Biol. 2002; 158:873–84.

Roll-Mecak A, McNally FJ. Microtubule-severing enzymes. Curr Opin Cell Biol. 2010; 22:96–103.

Roll-Mecak A, Vale RD. The Drosophila homologue of the hereditary spastic paraplegia protein, spastin, severs and disassembles microtubules. Curr Biol. 2005; 15:650–5.

Sharma N, Bryant J, Wloga D, Donaldson R, Davis RC, Jerka-Dziadosz M, et al. Katanin regulates dynamics of microtubules and biogenesis of motile cilia. J Cell Biol. 2007; 178:1065–79.

Siegrist SE, Doe CQ. Microtubule-induced cortical cell polarity. Genes Dev. 2007; 21:483–96.

Siller KH, Doe CQ. Spindle orientation during asymmetric cell division. Nat Cell Biol. 2009; 11:365–74.

Smith TF, Gaitatzes C, Saxena K, Neer EJ. The WD repeat: a common architecture for diverse functions. Trends Biochem Sci. 1999; 24:181–5.

Sonbuchner TM, Rath U, Sharp DJ. KL1 is a novel microtubule severing enzyme that regulates mitotic spindle architecture. Cell Cycle. 2010; 9:2403–11.

Sproul LR, Anderson DJ, Mackey AT, Saunders WS, Gilbert SP. Cik1 targets the minus-end kinesin depolymerase kar3 to microtubule plus ends. Curr Biol. 2005; 15:1420–7.

Srayko M, O'Toole ET, Hyman AA, Müller-Reichert T. Katanin disrupts the microtubule lattice and increases polymer number in C. elegans meiosis. Curr Biol. 2006; 16:1944–9.

Stoppin-Mellet V, Gaillard J, Vantard M. Katanin's severing activity favors bundling of cortical microtubules in plants. Plant J. 2006; 46:1009–17.

Stoppin-Mellet V, Gaillard J, Timmers T, Neumann E, Conway J, Vantard M. Arabidopsis katanin binds microtubules using a multimeric microtubule-binding domain. Plant Physiol and Biochem. 2007; 45:867–77.

Stramer B, Moreira S, Millard T, Evans I, Huang CY, Sabet O, et al. Clasp-mediated microtubule bundling regulates persistent motility and contact repulsion in Drosophila macrophages in vivo. J Cell Biol. 2010; 189:681–9.

Torres JZ, Miller JJ, Jackson PK. High-throughput generation of tagged stable cell lines for proteomic analysis. Proteomics. 2009; 9:2888-91.

Ui K, Ueda R, Miyake T. Cell lines from imaginal discs of Drosophila melanogaster. In Vitro Cell Dev Biol. 1987; 23:707-11.

van der Vaart B, Akhmanova A, Straube A. Regulation of microtubule dynamic instability. Biochem Soc Trans. 2009; 37:1007–13.

Varga V, Helenius J, Tanaka K, Hyman AA, Tanaka TU, Howard J. Yeast kinesin-8 depolymerizes microtubules in a length-dependent manner. Nat Cell Biol. 2006; 8:957–62.

Watanabe T, Noritake J, Kaibuchi K. Regulation of microtubules in cell migration. Trends Cell Biol. 2005; 15:76–83.

Watanabe T, Noritake J, Kaibuchi K. Roles of IQGAP1 in cell polarization and migration. Novartis Found Symp. 2005; 269:92-101.

Waterman-Storer CM, Salmon ED. Actomyosin-based retrograde flow of microtubules in the lamella of migrating epithelial cells influences microtubule dynamic instability and turnover and is associated with microtubule breakage and treadmilling. J Cell Biol. 1997; 139:417–34.

Waterman-Storer CM, Worthylake RA, Liu BP, Burridge K, Salmon ED. Microtubule growth activates Rac1 to promote lamellipodial protrusion in fibroblasts. Nat Cell Biol. 1999; 1:45–50.

Waterman-Storer C, Duey DY, Weber KL, Keech J, Cheney RE, Salmon ED, et al. Microtubules remodel actomyosin networks in Xenopus egg extracts via two mechanisms of F-actin transport. J Cell Biol. 2000; 150:361–76.

Yu W, Qiang L, Solowska JM, Karabay A, Korulu S, Baas PW. The microtubule-severing proteins spastin and katanin participate differently in the formation of axonal branches. Mol Biol Cell. 2008; 19:1485–98.

Yu W, Solowska JM, Qiang L, Karabay A, Baird D, Baas PW. Regulation of microtubule severing by katanin subunits during neuronal development. J Neurosci. 2005; 25:5573–83.

Zhang D, Rogers GC, Buster DW, Sharp DJ. Three microtubule severing enzymes contribute to the “Pacman-flux” machinery that moves chromosomes. J Cell Biol. 2007; 177:231–42.

SUPPORTING INFORMATION

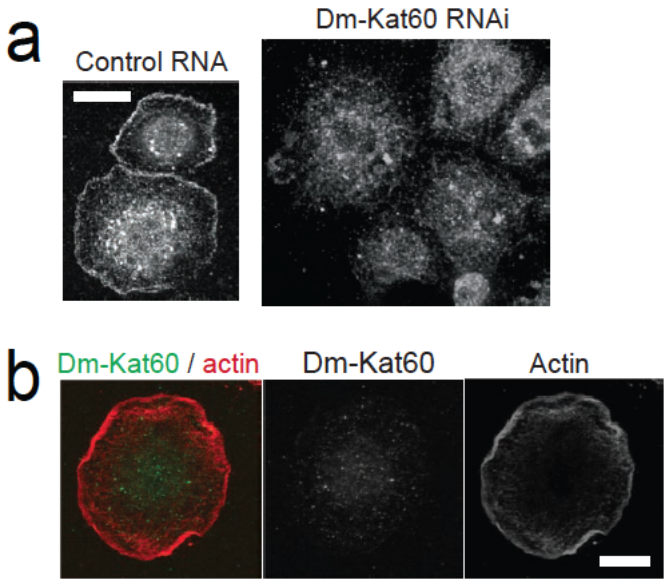

Figure 2.S1. Dm-Kat60's cortical staining is reduced/abolished by Dm-Kat60 RNAi. (A) Comparison of Dm-Kat60 immunofluorescence in a field of control vs. Dm-Kat60 RNAi-treated S2 cells. Dm-Kat60's cortical staining pattern appears to be specific as it was significantly reduced or abolished by the targeted depletion of Dm-Kat60 by RNA-mediated interference. On average, Kat60 RNAi in S2 cells reduced the intensity of cortical Dm-Kat60 immunofluorescence by 71% relative to controls (100 randomly selected cells measured in each condition; $p<0.001$). Moreover, ~30% (31/100) of the RNAi-treated cells displayed no detectable Dm-Kat60 staining at the cortex compared to only 2% (2/100) of controls showing the same. (B) A Dm-Kat60 RNAi treated S2 cell double-labeled for Dm-Kat60 (green) and actin (red) further demonstrating that RNAi reduces the cortical staining of Dm-Kat60 but does not displace cortical actin. Scale bar, 10 μm (A and B).

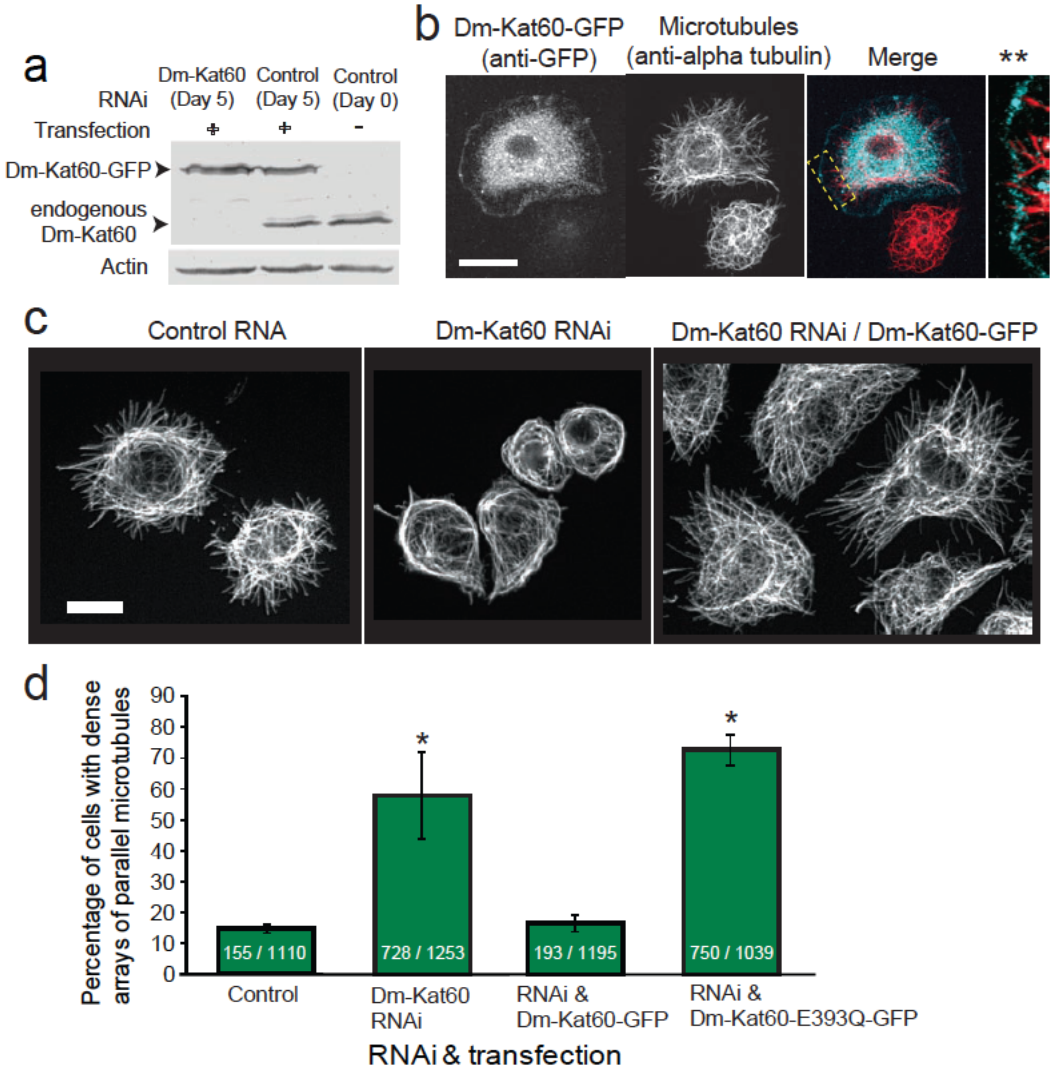

Figure 2.S2. Ectopically expressed GFP-Dm-Kat60 localizes to the cortex of interphase S2 cells and rescues the Dm-Kat60 RNAi phenotype. (A and B) The cortical localization of Dm-Kat60 was confirmed in S2 cells expressing a Dm-Kat60-GFP fusion protein. Because overexpression of this construct is highly toxic to the cell, these experiments were performed in S2 cells depleted of endogenous Dm-Kat60 using dsRNA targeting the 3' untranslated region (UTR) of the Dm-Kat60 mRNA. RNAi-treated cells were then transfected with an inducible plasmid encoding Dm-Kat60 (lacking the endogenous 3'UTR) fused to GFP, which was expressed at a level approximating that of the endogenous protein. Panel A is a Western blot indicating endogenous Dm-Kat60 and Dm-Kat60-GFP expression levels following the indicated treatments. The lower anti-actin blot is included as a loading control. Panel B shows shows the typical localization of Dm-Kat60-GFP (labeled with an anti-GFP antibody) and MTs (labeled with an anti-α-tubulin antibody) in a transfected interphase S2 cell. Far right panel (**) is a high magnification of the boxed region of the cell in the merged panel. Indirect immunofluorescence was used to localize GFP-Dm-Kat60 because the GFP signal alone was too low for the characterization of any specific localization

pattern. Clearly apparent cortical staining was observed in ~67% (311/469) of Dm-Kat60-GFP transfected cells as compared to <5% (11/521) of non-transfected cells stained with the same antibody. (C and D) Replacement of endogenous Dm-Kat60 with the GFP-tagged fusion protein rescued the Dm-Kat60 RNAi phenotype. Panel C shows Immunofluorescence micrographs indicating the typical organization of MT arrays in control, Dm-Kat60 RNAi, and Dm-Kat60 RNAi/Dm-Kat60-GFP transfected interphase S2 cells. (D) Most Dm-Kat60 depleted cells have dense arrays of curled MTs arranged parallel to the cortex, but this phenotype is rescued once Dm-Kat60 RNAi cells are induced to express RNAi resistant Dm-Kat60-GFP. Rescue requires catalytically active Dm-Kat60, as demonstrated by the inability of the inactive mutant, Dm-Kat60 (E393Q; Hartman and Vale, 1999), to restore a normal cortical MT arrangement. $p = 0.0216$. Numbers in the columns indicate the number of cells containing a dense array of curled MTs/total number of cells analyzed. Data represent mean ± SEM from three independent experiments. Scale bars, 10 μm (A and B).

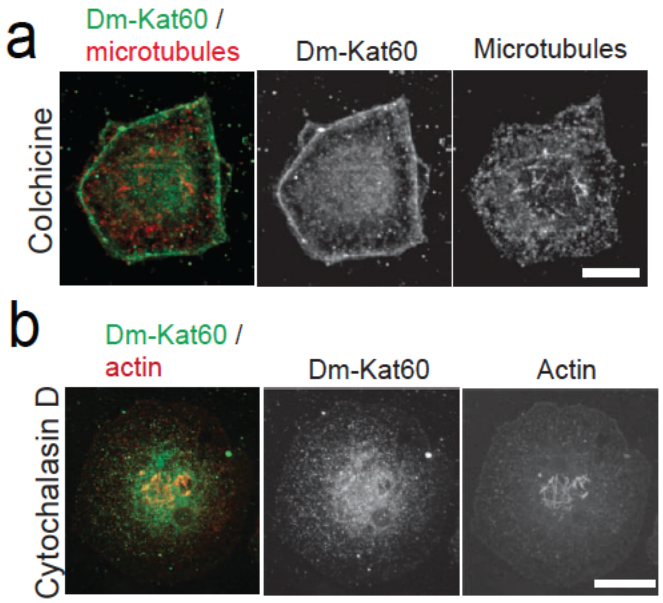

Figure 2.S3. The cortical localization of Dm-Kat60 does not require MTs but is reliant upon actin. (A) Confocal micrographs showing that the localization of Dm-Kat60 at the cortex persists after microtubule disassembly with colchicine. (B) Cortical Dm-Kat-60 staining is lost when actin is disassembled by cytochalasin D. Scale bar, 10 μm (A and B).

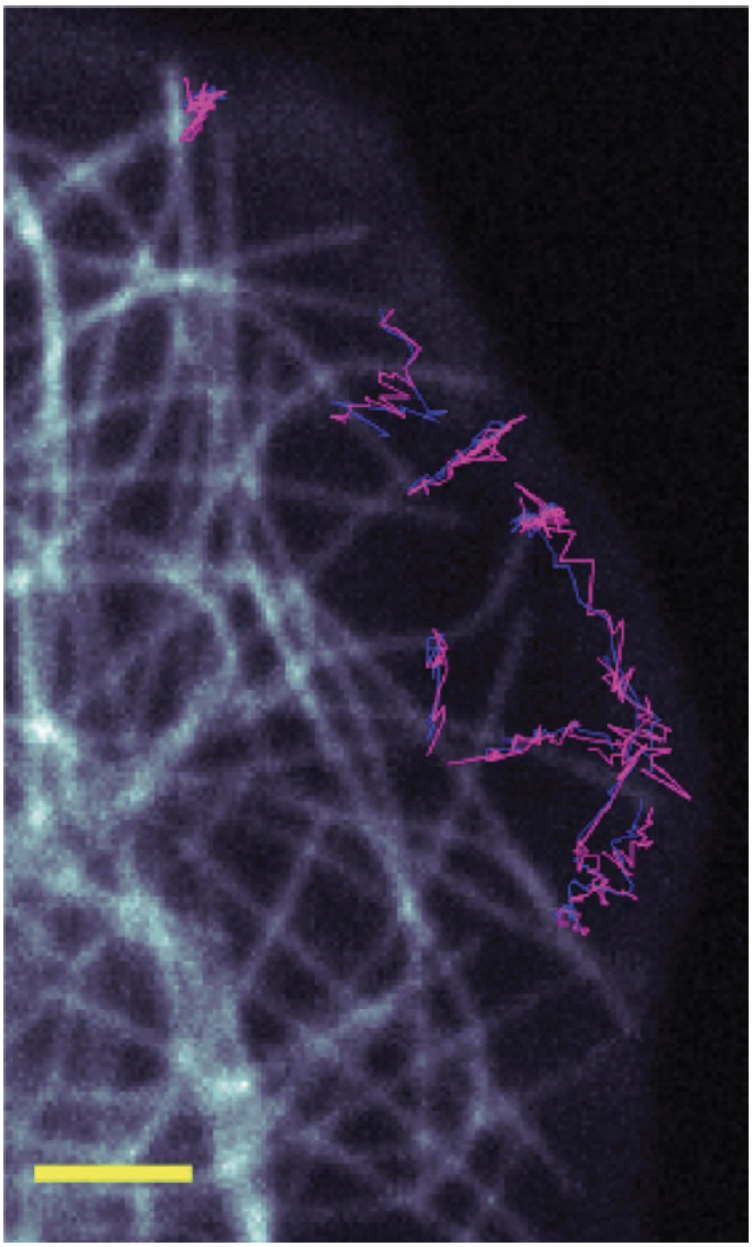

Figure 2.S4. Comparison of MT plus-end trajectories generated using our automated algorithm vs. hand tracking. The image shows an individual time-point from a live cell movie of MT behaviors in a control GFP-α-tubulin expressing interphase S2 cell. The trajectory paths of MT ends generated automatically are shown in magenta while the hand-tracked trajectory paths of these same MT ends are shown in blue. Scale bar, 5 μm. In all, the automated algorithm correctly identified and followed the movement 98.3% of MT plus-ends (n=290).

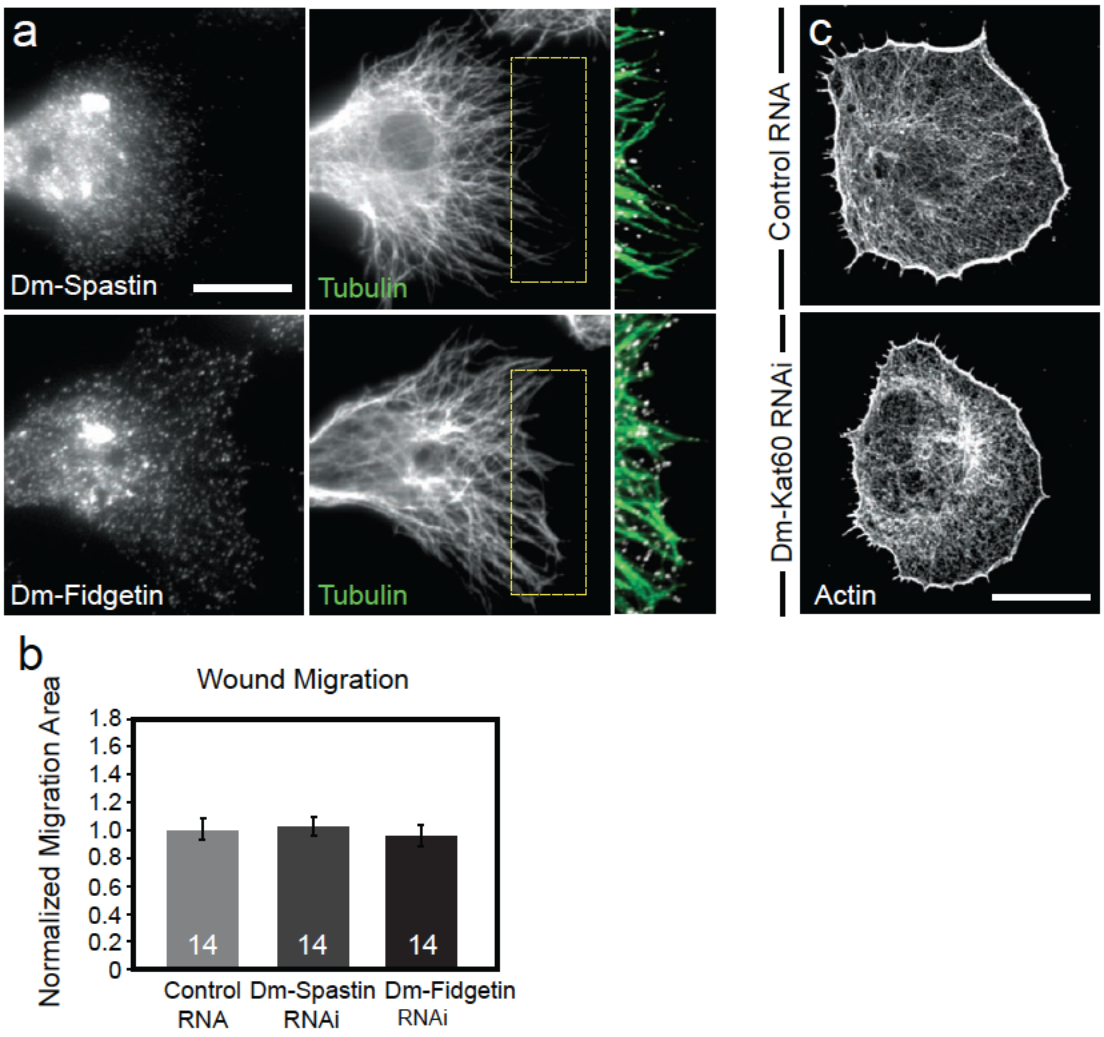

Figure 2.S5. MT severing enzymes in D17 cells. (A) Immunolocalization of Spastin, Fidgetin, and tubulin in *Drosophila* D17 cells. The boxed areas are magnified in the insets. (B) Quantification of migration during wound closure for control, Spastin, and Fidgetin RNA-treated D17 cells. Migration area was calculated by subtracting the total wound area at 24 hr from the total wound area at 0 hr after wounding and normalized to control RNAi. Data represent mean ± SEM. (C) Immunolocalization of actin in control and Dm-Kat60 RNAi-treated D17 cells. Scale bars, 10 μm (A and B).

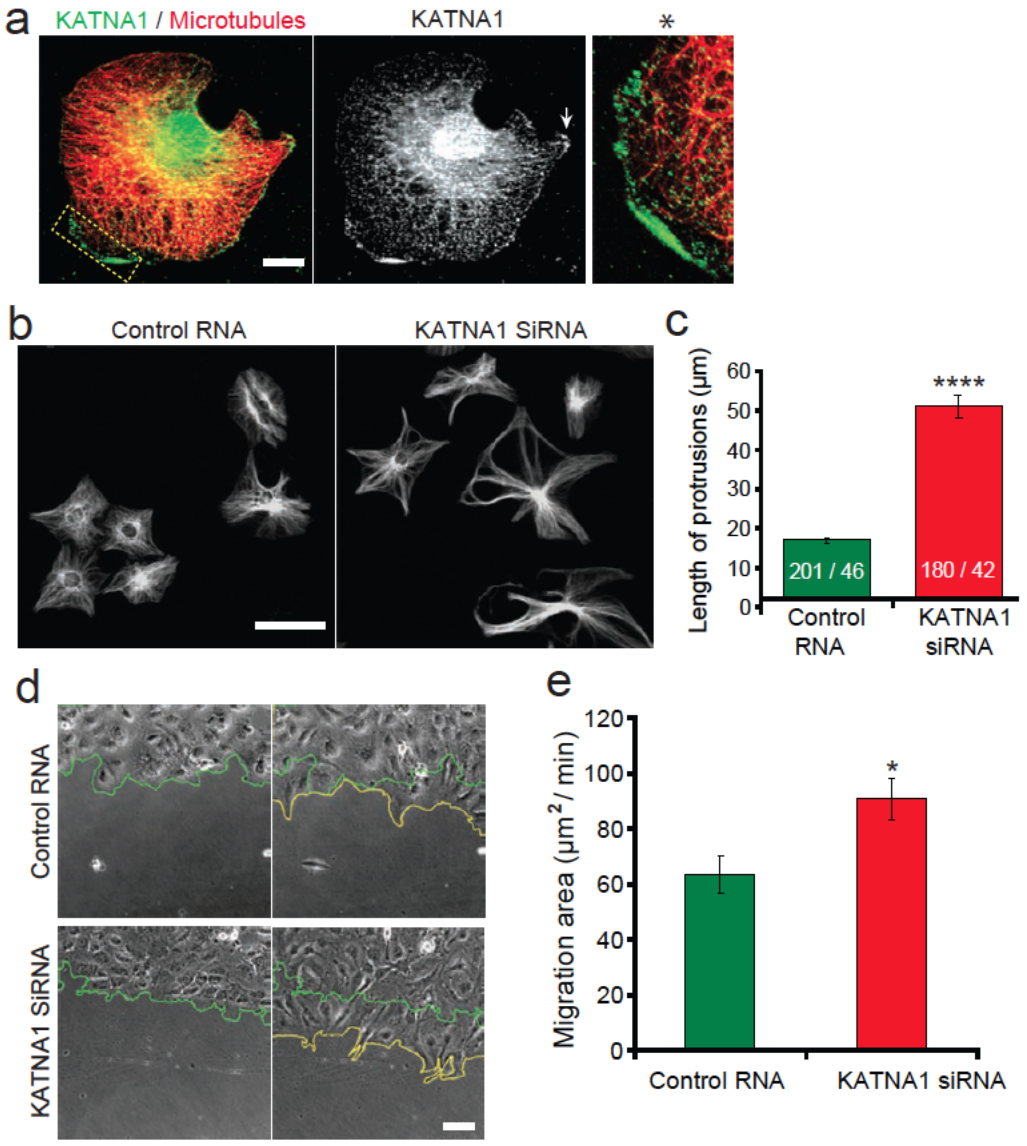

Figure 2.S6. Human KATNA1 localizes to the leading edge of migratory cells and its depletion by RNAi affects microtubule organization and cell migration similarly to Dm-Kat60. (A) Immunofluorescence of human HS578T cells stained with our previously characterized anti-KATNA1 antibody35 revealed that, similarly to Dm-Kat60, KATNA1 adopts a cortical localization that is most prominent at the leading edge of polarized cells as well as the edge of additional cellular protrusions (arrow). The area of the leading edge showing pronounced KATNA1 staining boxed in the merged panel is magnified in the inset. (B) siRNA depletion of KATNA1 induces a dramatic alteration in cell morphology hallmarked by an increase in the length of cellular protrusions which were filled with densely packed arrays of parallel MT. The image in this panel shows representative fields of control and KATNA1 siRNA-treated Hs578T cells immunostained for α-tubulin. (C) siRNA depletion of KATNA1 increases the average length of the cellular protrusions more than 2-fold. $p < 0.0001$. Data represent mean ± SEM. Numbers in the columns indicate the number of protrusions measured / total number of cells analyzed. (D) KATNA1 siRNA treated cells migrated ~1.5 fold faster

than controls in wound healing assays. Monolayers of control and KATNA1 siRNA-treated Hs578T cells were wounded and imaged by phase microscopy immediately and 14 hr later. The relative positions of the wound edge at the beginning and end of the experiment are indicated by green and yellow lines, respectively. (E) Quantification of the rate of wound closure in control vs. KATNA1 siRNA treated cultures. The data represent the mean ± SEM of three independent experiments. $p = 0.0328$. Scale bar, 20 μm (A) or 100 μm (B and D).

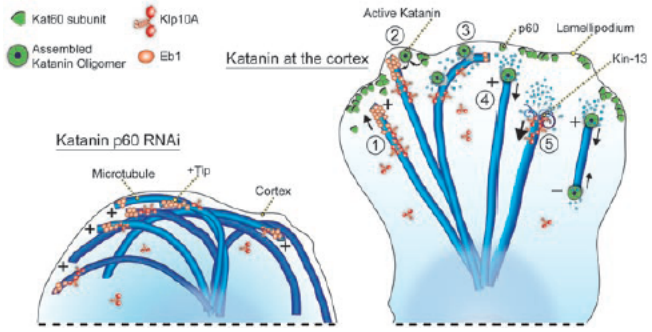

Figure 2.S7. Model of Kat60 activity at the cortex of interphase cells. Dm-Kat60 localizes to the cortex of lamellipodia (right), possibly by interacting with the F-actin enriched in this region. Our results suggest that as plus-ends of growing MTs approach the cortex, Dm-Kat60 attacks both the ends and the walls of MTs and perhaps eliminates stabilizing EB1 “caps” at plus ends. Following Dm-Kat60 induced catastrophe and/or depolymerization at the cortex, kinesin-13 may assume responsibility for plus-end disassembly. If Dm-Kat60 is depleted (left), the loss of this potent catastrophe factor increases the lifetimes of MTs invading the cortex. Consequently, the MTs continue to grow even after reaching the cell boundary, and so the cell periphery fills with dense arrays of MTs running parallel to the cortex. MTs within these arrays could conceivably lose the ability to respond normally to the intra- and extra-cellular cues that optimize their dynamics and organization to stimulate movement, morphogenesis, etc.

CHAPTER 3: THE NON-CATALYTIC DOMAINS OF *DROSOPHILA* KATANIN REGULATE ITS ABUNDANCE AND MICROTUBULE-DISASSEMBLY ACTIVITY[1]

Summary

Microtubule severing is a biochemical reaction that generates an internal break in a microtubule and regulation of microtubule severing is critical for cellular processes such as ciliogenesis, morphogenesis, and meiosis and mitosis. Katanin is a conserved heterodimeric ATPase that severs and disassembles microtubules, but the molecular determinants for regulation of microtubule severing by katanin remain poorly defined. Here we show that the non-catalytic domains of *Drosophila* katanin regulate its abundance and activity in living cells. Our data indicate that the microtubule-interacting and trafficking (MIT) domain and adjacent linker region of the *Drosophila* katanin catalytic subunit Kat60 cooperate to regulate microtubule severing in two distinct ways. First, the MIT domain and linker region of Kat60 decrease its abundance by enhancing its proteasome-dependent degradation. The *Drosophila* katanin regulatory subunit Kat80, which is required to stabilize Kat60 in cells, conversely reduces the proteasome-dependent degradation of Kat60. Second, the MIT domain and linker region of Kat60 augment its microtubule-disassembly activity by enhancing its association with microtubules. On the basis of our data, we propose that the non-catalytic domains of *Drosophila* katanin serve as the principal sites of integration of regulatory inputs, thereby controlling its ability to sever and disassemble microtubules.

[1]Grode KD, Rogers SL. The non-catalytic domains of Drosophila katanin regulate its abundance and microtubule-disassembly activity. PLoS One. 2015; 10:e0123912.

Introduction

Microtubules are cytoskeletal polymers composed of tubulin heterodimers that form complex and highly organized arrays with diverse functions during the cell cycle (Desai and Mitchison, 1997). Microtubules during interphase, for example, form the axonemal structures of cilia and flagella, the bundled arrays of neuronal cells, and the web-like networks of epithelial cells. Microtubule superstructures such as these are required, respectively, for ciliary and flagellar motility, directional molecular transport, and the establishment and maintenance of cytoplasmic polarity (Hirokawa and Takemura, 2005; Satir and Christensen, 2007; Siegrist and Doe, 2007). Microtubules during cell division, by contrast, create a single higher-order structure called a bipolar spindle that is required for the segregation of genetic material within the germline and somatic tissues of multi-cellular organisms (Wittman et al., 2001; Müller-Reichert et al., 2010). Despite their organizational and functional diversity during the cell cycle, microtubule superstructures are built and remodeled by many of the same microtubule-stabilizing and destabilizing activities. One activity that is important for the proper organization and function of microtubule superstructures throughout the cell cycle is the severing of microtubules (Roll-Mecak and McNally, 2010; Sharp and Ross, 2012). Microtubule severing is a biochemical reaction that generates an internal break in a microtubule and catalysis of microtubule severing is mediated by a small family of ATPases called microtubule-severing enzymes. To date, three microtubule-severing enzymes have been identified - katanin, spastin, and fidgetin - and each contains a single catalytic AAA ATPase domain that is highly conserved between these enzymes (Roll-Mecak and McNally, 2010). Recent studies have uncovered diverse cellular roles

for the microtubule-severing enzyme family and these roles are highlighted by the wide range of disorders and diseases that are associated with their mutations such as infertility, microphthalmia, and hereditary spastic paraplegia (Hazan et al., 1999; Cox et al., 2000; O'Donnell et al., 2012; Smith et al., 2012). Central to the cellular roles of the microtubule-severing enzymes is the control of their abundance and activity, however the regulatory mechanisms that coordinate microtubule severing with the normal cellular program remain poorly understood.

Katanin was first purified from sea urchin eggs based on its ATP-dependent microtubule-severing activity and it was the first protein identified that severed and disassembled microtubules (McNally et al., 1993). Katanin is a heterodimer consisting of a catalytic subunit and a regulatory subunit and conserved homologues of both katanin subunits are widely represented in eukaryotes. All canonical katanin catalytic subunits exhibit a bipartite domain structure with an NH_2-terminal microtubule-interacting and trafficking (MIT) domain connected to a COOH-terminal AAA ATPase domain via a poorly conserved linker region (Roll-Mecak and McNally, 2010). The nuclear magnetic resonance structure of the MIT domain from the mouse katanin catalytic subunit KATNA1 revealed that it consists of a three-helix bundle with many potential protein-protein interaction surfaces (Iwaya et al., 2010). Biochemical studies of katanin catalytic subunits from several species have shown that the MIT domain is necessary for binding the katanin regulatory subunit (McNally et al., 2000; McNally and McNally, 2011) and that the MIT domain together with the linker region is sufficient for binding both the katanin regulatory subunit (McNally and McNally, 2011) and microtubules (Hartman and Vale, 1999; Stoppin-Mellet et al., 2007; McNally and

McNally, 2011; Eckert et al., 2012). Based on recent x-ray crystallographic studies of spastin (Roll-Mecak and Vale, 2008; Taylor et al., 2012), the AAA ATPase domain of katanin catalytic subunits likely comprises a canonical α/β nucleotide-binding domain surrounded by structural elements involved in tubulin-binding and oligomerization. Mutagenesis studies of katanin catalytic subunits from several species have established that ATP hydrolysis by the AAA domain is absolutely required for severing microtubules (McNally et al., 2000; Buster et al., 2002; Diaz-Valencia et al., 2011; Zhang et al., 2011). Similar to katanin catalytic subunits, all canonical katanin regulatory subunits exhibit a bipartite domain structure, but with an NH_2-terminal WD40 domain connected to a conserved COOH-terminal domain (CTD) via a proline-rich linker region (Roll-Mecak and McNally, 2010). The WD40 domain of katanin regulatory subunits typically consists of six WD40 repeats that are predicted to fold into a six-bladed β-propeller architecture, whereas the CTD of katanin regulatory subunits is predicted to be mostly α-helical. Biochemical studies of katanin regulatory subunits from several species have demonstrated that the CTD is necessary for binding the katanin catalytic subunit (Hartman et al., 1998) and sufficient for binding both the katanin catalytic subunit (Hartman et al., 1998; McNally et al., 2000; Srayko et al., 2000) and microtubules (McNally et al., 2000). Thus, katanin is thought to form a ring-shaped complex with non-catalytic microtubule-binding sites distributed between its subunits that extend radially from its central ATP-fueled motor. This quaternary structure suggests that the non-catalytic domains of katanin are crucial to its microtubule-severing activity, however this hypothesis has not been rigorously tested by any functional study to date.

Based on their observation that the katanin catalytic subunit forms transient hexamers only in the presence of ATP and microtubules, Hartman and Vale proposed a model - hereafter referred to as the katanin assembly model - for how katanin severs and disassembles microtubules (Hartman and Vale, 1999). In this model, katanin heterodimers are monomeric in the ADP-bound state, but nucleotide exchange for ATP and microtubule-binding increases inter-subunit binding affinity, leading to oligomerization. Once assembled, the katanin complex binds the microtubule polymer with high affinity due to the formation of multiple contacts with tubulin and its ATPase activity is stimulated, resulting in nucleotide-driven conformational changes that sever the microtubule polymer. Thus, the katanin assembly model postulates that the oligomerization of katanin into a catalytically active complex occurs in a concentration- and microtubule-dependent manner via multivalent interaction with the microtubule polymer. The prediction of this model for the roles of the non-catalytic domains of katanin is that they enhance the initial targeting of its subunits to the microtubule polymer and/or influence the subsequent balancing between subunit-microtubule and inter-subunit interactions. Although recent biophysical studies have advanced our understanding of the katanin assembly model (Diaz-Valenica et al., 2011; Loughlin et al., 2011; Eckhert et al., 2012; Whitehead et al., 2012), the relative contribution of the non-catalytic domains of katanin to its microtubule-severing activity in vivo remains unknown. Here we conduct a structure-function analysis of *Drosophila* katanin in cultured *Drosophila* S2 cells to test the hypothesis that the non-catalytic domains of katanin make distinct contributions to microtubule severing in living cells.

Results and Discussion

Cultured *Drosophila* S2 cells overexpressing Kat60 exhibit microtubule-disassembly in a concentration-dependent manner

The *Drosophila* genome contains single genes that encode the canonical katanin catalytic subunit, Kat60, and the canonical katanin regulatory subunit, Kat80 (Figure 3.1A). Previous studies have shown that Kat60 by itself can sever and disassemble microtubules in vitro (Diaz-Valencia et al., 2011; Zhang et al., 2011) and that overexpression of Kat60 is sufficient to promote microtubule disassembly in cultured S2 cells (Zhang et al., 2007) and in larval muscle cells (Mao et al., 2014). To date, there have been no functional studies of Kat80. To begin our structure-function analysis of the microtubule-severing activity of *Drosophila* katanin, we first overexpressed Kat60 in S2 cells and examined the effects on microtubules by immunofluorescence microscopy. Cells overexpressing Kat60 displayed a disorganized array of fragmented microtubules and the overall length of microtubules appeared to decrease with increasing levels of Kat60 (Figure 3.1B). Many of these cells contained individual microtubules with both ends visible and several of these cells had only short microtubule fragments; cells that showed a complete loss of microtubules were never observed. In addition, cells overexpressing Kat60 had reduced levels of alpha-tubulin compared to control cells and the degree of reduction increased with increasing levels of Kat60. The inverse relationship between alpha-tubulin and Kat60 levels indicates that cells overexpressing Kat60 exhibit microtubule disassembly in a concentration-dependent manner and the disorganized array of short microtubules suggests that this disassembly is due to the microtubule-severing activity of Kat60. The effects of overexpression of Kat60 on microtubules and alpha-tubulin levels in S2 cells are similar to those observed in other

animal cell types overexpressing the katanin catalytic subunit (McNally et al., 2000; Yu et al., 2005). To determine if Kat80 possesses microtubule-disassembly activity, we overexpressed Myc-tagged Kat80 (Myc-Kat80) in cells and examined the effects on microtubules by immunofluorescence microscopy. Cells overexpressing Myc-Kat80 did not exhibit microtubule fragmentation or have reduced levels of alpha-tubulin (Figure 3.1C), consistent with a previous report that the sea urchin katanin regulatory subunit KATNB1 cannot sever and disassemble microtubules in vitro (Hartman and Vale, 1998). Taken together, these findings demonstrate that overexpression of Kat60, but not Kat80, is sufficient to promote microtubule disassembly in S2 cells and that the loss of microtubules in these cells occurs as a function of Kat60 levels.

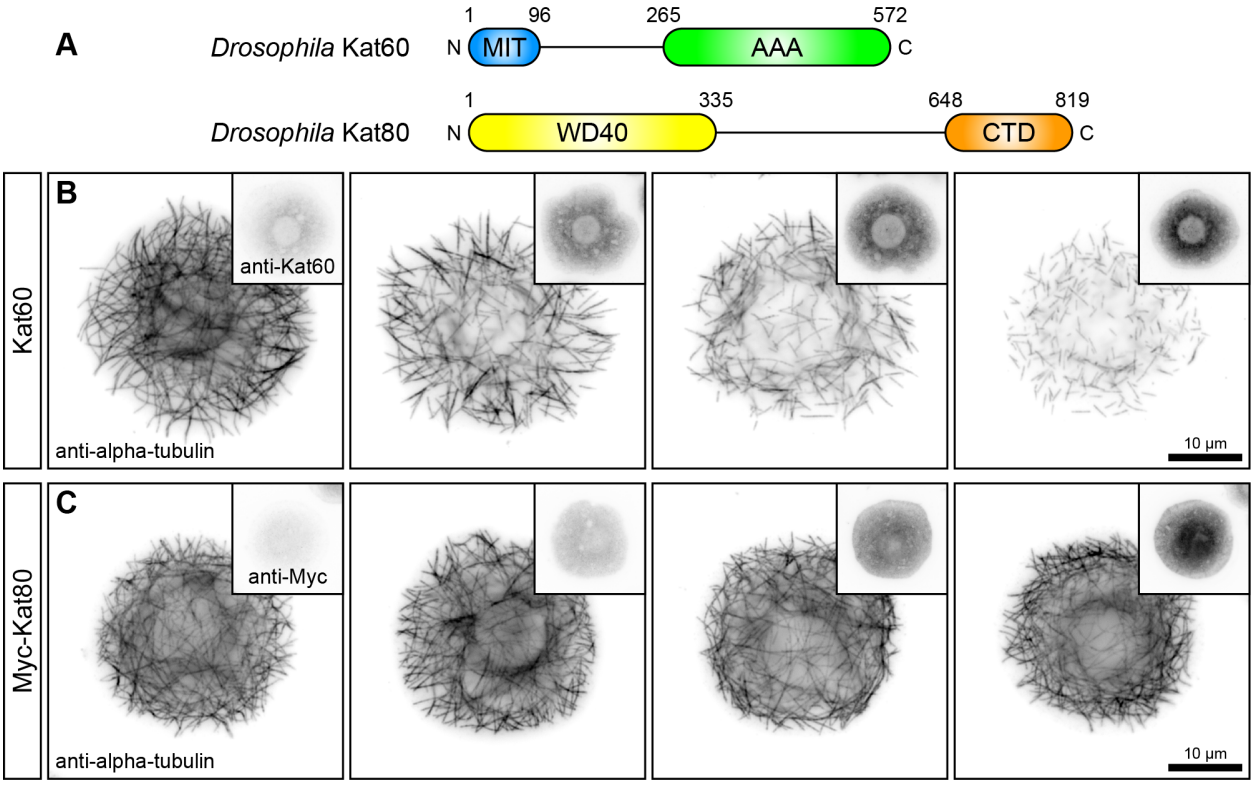

Figure 3.1. Cultured *Drosophila* S2 cells overexpressing Kat60 exhibit microtubule-disassembly in a concentration-dependent manner. (A) Schematic of the domain structure of the *Drosophila* canonical katanin catalytic subunit Kat60 (Top) and the canonical katanin regulatory subunit Kat80 (Bottom). (B and C) Immunofluorescence microscopy images of *Drosophila* S2 cells overexpressing Kat60 (B) or Myc-Kat80 (C) and immunostained for alpha-tubulin and Kat60 (B) or Myc (C). (B) A cell not overexpressing Kat60 (First) and cells overexpressing Kat60 (Second-Fourth). (C) A cell not overexpressing Myc-Kat80 (First) and cells overexpressing Myc-Kat80 (Second-Fourth). Alpha-tubulin, Kat60, and Myc images in each panel are displayed with the same scaling.

Development of a single-cell assay to measure the microtubule-disassembly activity of Kat60 using automated microscopy

To quantitate the effects of overexpression of Kat60 on microtubules in cells, we developed a high-content immunofluorescence microscopy assay to measure the loss of microtubules as a function of Kat60 levels. For this assay, we generated cells that stably express 1) GFP under the control of a constitutive promoter and 2) versions of Kat60 and Kat80, either alone or in combination, under the control of a copper-inducible promoter. In this assay, we first induce cells with $CuSO_4$ and then we acquire images of tens of thousands of cells stained for DNA and immunostained for alpha-tubulin and Kat60 using automated microscopy (Figure 3.S1). Next, we process and analyze the images using the open-source CellProfiler software (Carpenter et al., 2006). The DNA images allow us to first identify nuclei, which then permits the use of the GFP images to identify individual cells and create cell outlines. Finally, we extract the average alpha-tubulin and Kat60 immunofluorescence intensities from each outlined cell based on the alpha-tubulin and Kat60 images, respectively.

To minimize the potential contribution of endogenous Kat60 and Kat80 to the single-cell measurements collected in each experiment, we devised an RNA interference (RNAi) strategy to specifically deplete the endogenous proteins from cells using double-stranded RNAs (dsRNA) that target the untranslated regions (UTR) of Kat60 and Kat80. Before evaluating the efficacy of this strategy, we first sought to determine if dsRNAs targeting the coding sequences (CDS) of Kat60 and Kat80 are effective in eliminating both proteins from cells. As an initial step, we treated cells stably expressing GFP alone with Kat60 or Kat80 CDS dsRNA and analyzed the steady-state levels of Kat60 by immunoblotting. Endogenous Kat60 was undetectable in cells treated

with Kat60 CDS dsRNA and the levels of Kat60 in cells treated with Kat80 CDS dsRNA were dramatically reduced compared to those in cells treated with control dsRNA (Figure 3.2A), suggesting that Kat80 functions to stabilize Kat60. To verify the effectiveness of Kat80 CDS dsRNA treatment, we treated cells stably expressing GFP and copper-inducible FLAG-tagged Kat80 (FLAG-Kat80) with Kat60 or Kat80 CDS dsRNA prior to induction and analyzed the levels of FLAG-Kat80 by immunoblotting. FLAG-Kat80 was undetectable in cells treated with Kat80 CDS dsRNA and the levels of FLAG-Kat80 in cells treated with Kat60 CDS dsRNA were indistinguishable from those in cells treated with control dsRNA (Figure 3.2B). Thus, in addition to demonstrating that Kat60 and Kat80 CDS dsRNA treatments are effective in eliminating both proteins from cells, these findings provide strong evidence that Kat80 is required to stabilize Kat60 in cells. To our knowledge, the loss of Kat60 upon depletion of Kat80 represents the first example of instability of one katanin subunit in the absence of the other subunit.

Having observed that both Kat60 and Kat80 CDS dsRNA treatments reduce steady-state Kat60 levels in cells, we next tested the effectiveness of Kat60 and Kat80 UTR dsRNA treatments in depleting the endogenous proteins from cells. To do this, we treated cells stably expressing GFP alone with Kat60 and Kat80 UTR dsRNA, either alone or in combination, and analyzed the steady-state levels of Kat60 by immunoblotting. The levels of Kat60 in cells treated with Kat60 and Kat80 UTR dsRNA, either alone or in combination, were dramatically reduced compared to those in cells treated with control dsRNA (Figure 3.S2). From these results, we conclude that Kat60 and Kat80 UTR dsRNA treatments effectively deplete the endogenous proteins from

cells and unless otherwise noted, we employed our Kat60 and Kat80 UTR RNAi strategy in all subsequent experiments in this study.

To investigate the effects of depletion of Kat60 and Kat80 on the single-cell measurements collected in each experiment, we used our assay to measure the steady-state levels of alpha-tubulin and Kat60 in cells stably expressing GFP alone that were treated with both Kat60 and Kat80 UTR dsRNA. These cells had only slightly reduced levels of alpha-tubulin compared to cells treated with control dsRNA (Figure 3.S3), indicating that depletion of Kat60 and Kat80 causes minimal perturbation of steady-state alpha-tubulin levels in cells. As expected, these cells had reduced levels of Kat60 compared to cells treated with control dsRNA, demonstrating that a difference in Kat60 levels between control and Kat60 and Kat80 depleted cells can be measured using our assay. Based on such an approximation of endogenous Kat60 levels, we can estimate the fold overexpression levels of Kat60 in cells expressing Kat60 to provide a biological context for the single-cell measurements collected in each experiment.

To establish baseline single-cell measurements for the effects of inducible expression of Kat60 and Kat80 on microtubules, we used our assay to measure the loss of microtubules in cells stably expressing GFP and copper-inducible Kat60 or FLAG-Kat80 that were induced with increasing concentrations of $CuSO_4$. Cells induced to express Kat60 had reduced levels of alpha-tubulin compared to control cells and the degree of reduction increased with increasing concentrations of $CuSO_4$ over a 100-fold $CuSO_4$ concentration range (Figure 3.3A and Table 3.S1). Appropriately, Kat60 accumulated at levels that increased with increasing concentrations of $CuSO_4$ in these cells. As expected, cells induced to express FLAG-Kat80 had almost identical levels of

alpha-tubulin and Kat60 relative to control cells and FLAG-Kat80 accumulated at levels that increased with increasing concentrations of $CuSO_4$ in these cells (Figure 3.3B and Table 3.S1). Collectively, these data demonstrate that inducible expression of Kat60, but not Kat80, results in measurable microtubule disassembly in our single-cell assay.

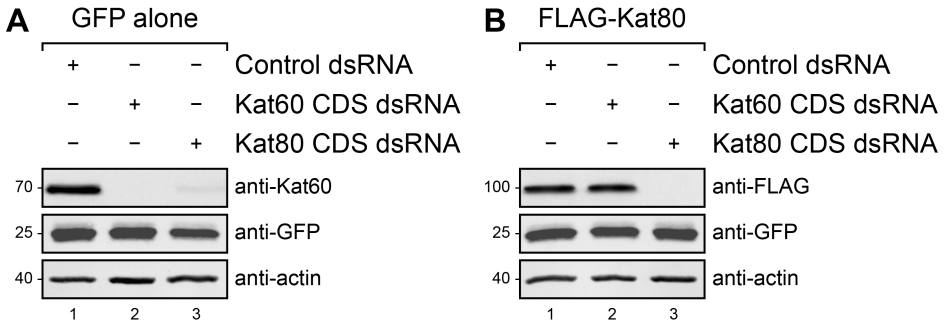

Figure 3.2. Depletion of Kat80 reduces steady-state Kat60 levels in cells. (A and B) Immunoblots of *Drosophila* S2 cell lysates prepared from cells stably expressing GFP alone (A) or GFP and copper-inducible FLAG-Kat80 (B) that were treated with control (lane 1), Kat60 CDS (lane 2), or Kat80 CDS dsRNA (lane 3) for 7 days total. The cells described in B were also treated with 0.1 mM $CuSO_4$ for 20 hours. Molecular weights (in Kd) are shown on the left.

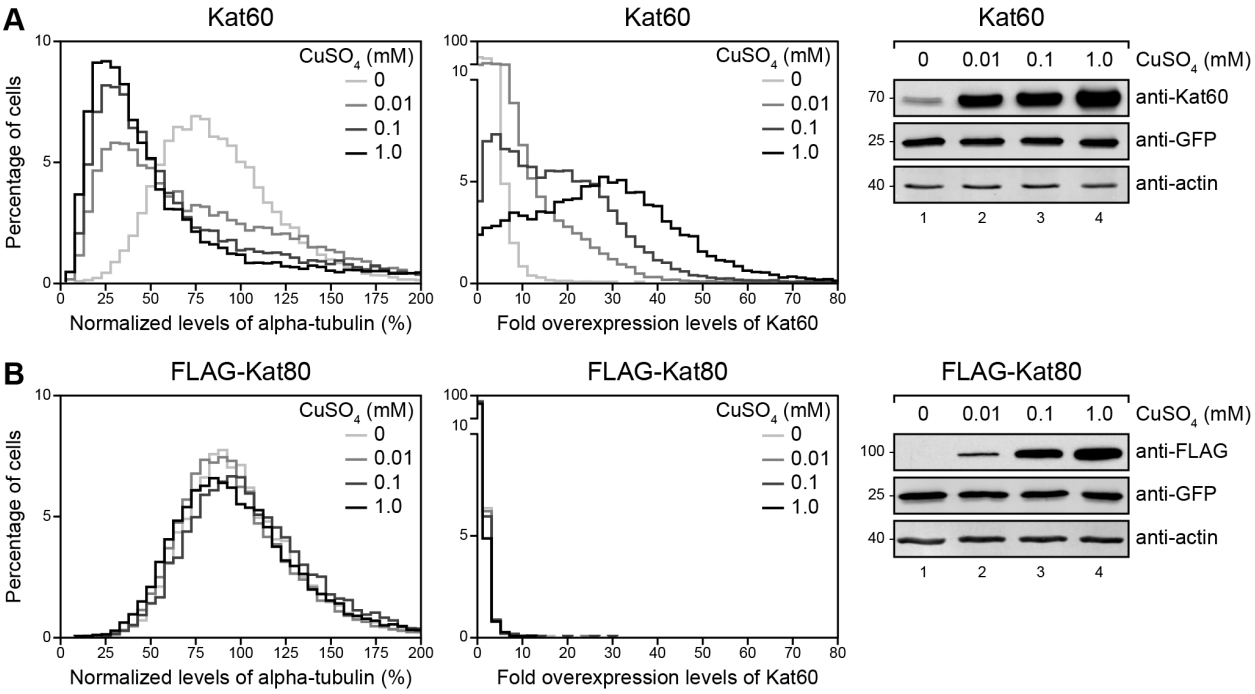

Figure 3.3. Inducible expression of Kat60 results in measurable microtubule disassembly in our single-cell assay. (A and B) Histograms of normalized levels of alpha-tubulin (Left) and fold overexpression levels of Kat60 (Middle) in *Drosophila* S2 cells stably expressing GFP and copper-inducible Kat60 (A) or FLAG-Kat80 (B) that were treated with both Kat60 and Kat80 UTR dsRNA for 7 days total. The cells described in A and B were also treated with 0 (light gray), 0.01 (medium gray), 0.1 (dark gray), or 1.0 mM $CuSO_4$ (black) for 20 hours and immunostained for alpha-tubulin and Kat60. Normalized levels of alpha-tubulin are expressed as a percentage of the mean levels of alpha-tubulin in cells stably expressing GFP alone that were treated with both Kat60 and Kat80 UTR dsRNA for 7 days total. Fold overexpression levels of Kat60 are expressed as a fraction of the difference in the mean levels of Kat60 between cells stably expressing GFP alone that were treated with control and both Kat60 and Kat80 UTR dsRNA for 7 days total. Data are pooled from three independent experiments (see Table 3.S1 for summary statistics of the single-cell measurements collected). (Right) Immunoblots of cell lysates prepared from the cells described in A and B. Molecular weights (in Kd) are shown on the left.

The MIT domain of Kat60 is dispensable for its microtubule-disassembly activity at high levels of accumulation in cells

To assess the contribution of the non-catalytic domains of *Drosophila* katanin to its microtubule-disassembly activity, we used our assay to measure the loss of microtubules in cells induced to express Kat60 alone or together with FLAG-Kat80, Kat60 lacking the MIT domain (Kat60-ΔMIT), or Kat60 lacking the MIT domain and linker region (Kat60-AAA). Compared to cells induced to express Kat60 alone, cells induced to express Kat60 together with FLAG-Kat80 had reduced levels of alpha-tubulin (Figure 3.4 A and B and Table 3.S2), suggesting that Kat80 affects the microtubule-disassembly activity of Kat60. However, uninduced cells also had reduced levels of alpha-tubulin, thereby complicating an assessment of the contribution of Kat80 to the microtubule-disassembly activity of Kat60. In support of the notion that Kat80 increases the abundance of Kat60, Kat60 in the presence of FLAG-Kat80 accumulated at slightly higher levels than Kat60 alone in cells. Surprisingly, cells induced to express Kat60-ΔMIT either did not have reduced levels of alpha-tubulin or they had reduced levels of alpha-tubulin similar to cells induced to express Kat60 (Figure 3.4 A and C and Table 3.S2), indicating that the MIT domain of Kat60 is, at the very least, dispensable for its microtubule-disassembly activity. Coincidentally, Kat60-ΔMIT either did not accumulate at detectable levels or it accumulated at notably higher levels than Kat60 in cells, suggesting that once expressed, the MIT domain of Kat60 functions to decrease its abundance. Thus, in addition to providing strong evidence that the MIT domain of Kat60 is dispensable for its microtubule-disassembly activity at high levels of accumulation, these results point to the need for alternative strategies to accurately assess the importance of the MIT domain of Kat60 to its activity. Consistent with the hypothesis

that the non-catalytic domains of katanin are crucial to its microtubule-disassembly activity, cells induced to express Kat60-AAA did not have reduced levels of alpha-tubulin relative to cells induced to express Kat60 (Figure 3.4 A and D and Table 3.S2). Remarkably, Kat60-AAA accumulated at higher levels than Kat60-ΔMIT in cells, strongly suggesting that the MIT domain and linker region of Kat60 cooperate to decrease its abundance.

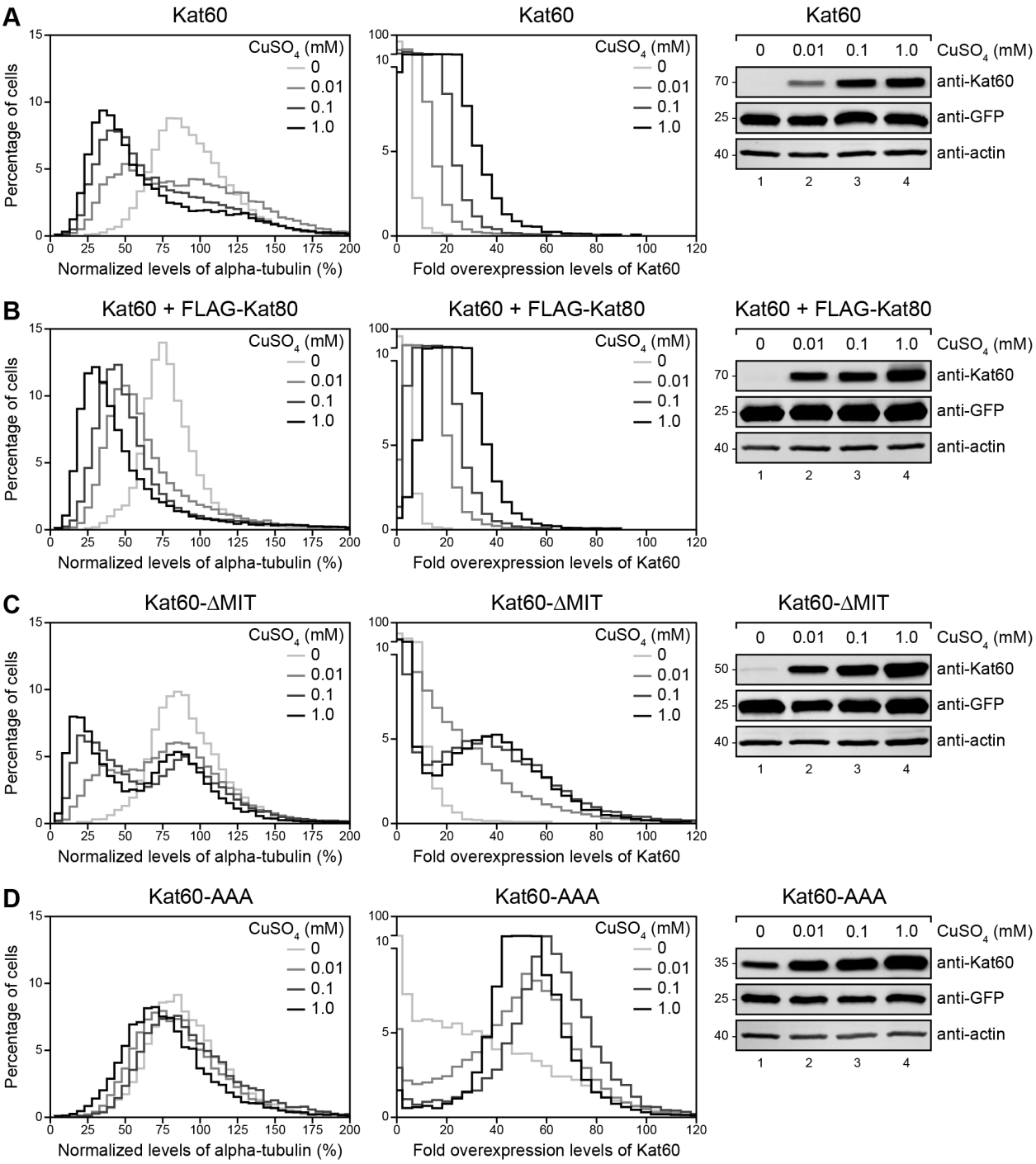

Figure 3.4. Kat60 lacking the MIT domain disassembles microtubules at high levels of accumulation in cells. (A-D) Histograms of normalized levels of alpha-tubulin (Left) and fold overexpression levels of Kat60 (Middle) in *Drosophila* S2 cells stably expressing GFP and copper-inducible Kat60 (A), Kat60 and FLAG-Kat80 (B), Kat60-ΔMIT (C), or Kat60-AAA (D) that were treated with both Kat60 and Kat80 UTR dsRNA for 7 days total. The cells described in A-D were also treated with 0 (light gray), 0.01 (medium gray), 0.1 (dark gray), or 1.0 mM $CuSO_4$ (black) for 20 hours and

immunostained for alpha-tubulin and Kat60. Normalized levels of alpha-tubulin are expressed as a percentage of the mean levels of alpha-tubulin in cells stably expressing GFP alone that were treated with both Kat60 and Kat80 UTR dsRNA for 7 days total. Fold overexpression levels of Kat60 are expressed as a fraction of the difference in the mean levels of Kat60 between cells stably expressing GFP alone that were treated with control and both Kat60 and Kat80 UTR dsRNA for 7 days total. Data are pooled from three independent experiments (see Table 3.S2 for summary statistics of the single-cell measurements collected). (Right) Immunoblots of cell lysates prepared from the cells described in A-D. Molecular weights (in Kd) are shown on the left.

The MIT domain and linker region of Kat60 are required for its proteasome-dependent degradation in cells

Given our unexpected findings that both Kat60-ΔMIT and Kat60-AAA accumulate at higher levels than Kat60 in cells, we next explored how the non-catalytic domains of *Drosophila* katanin regulate its abundance. Because katanin catalytic subunits from several species have been shown to be ubiquitinated by ubiquitin ligase complexes (Furukawa et al., 2003; Cummings et al., 2009; Maddika and Chen, 2009; Yang et al., 2013) and degraded by the proteasome (Wilson et al., 2012; Yang et al., 2013), we speculated that the non-catalytic domains of *Drosophila* katanin regulate its abundance by affecting its degradation via the ubiquitin-proteasome system. To test this hypothesis, we first pulsed the expression of Kat60 alone or together with Myc-Kat80, Kat60-ΔMIT, or Kat60-AAA in cells and then we used immunoblotting to analyze the degradation of these proteins in cells treated with DMSO or the 26S proteasome inhibitor MG132. Whereas Kat60 was markedly degraded in control cells, it was not detectably degraded in cells treated with MG132 (Figure 3.5A), demonstrating that the degradation of Kat60 is proteasome-dependent. In contrast to Kat60 alone, Kat60 in the presence of Myc-Kat80 was only slightly degraded in control cells (Figure 3.5B), indicating that Kat80 reduces the proteasome-dependent degradation of Kat60. Strikingly, both Kat60-ΔMIT and Kat60-AAA were not detectably degraded in control cells (Figure 3.5 C and D), providing strong evidence that the MIT domain and linker region of Kat60 are required for its proteasome-dependent degradation. From these results, we conclude that the MIT domain and linker region of Kat60 decrease its abundance by enhancing its proteasome-dependent degradation and that Kat80

conversely increases the abundance of Kat60 by reducing its proteasome-dependent degradation.

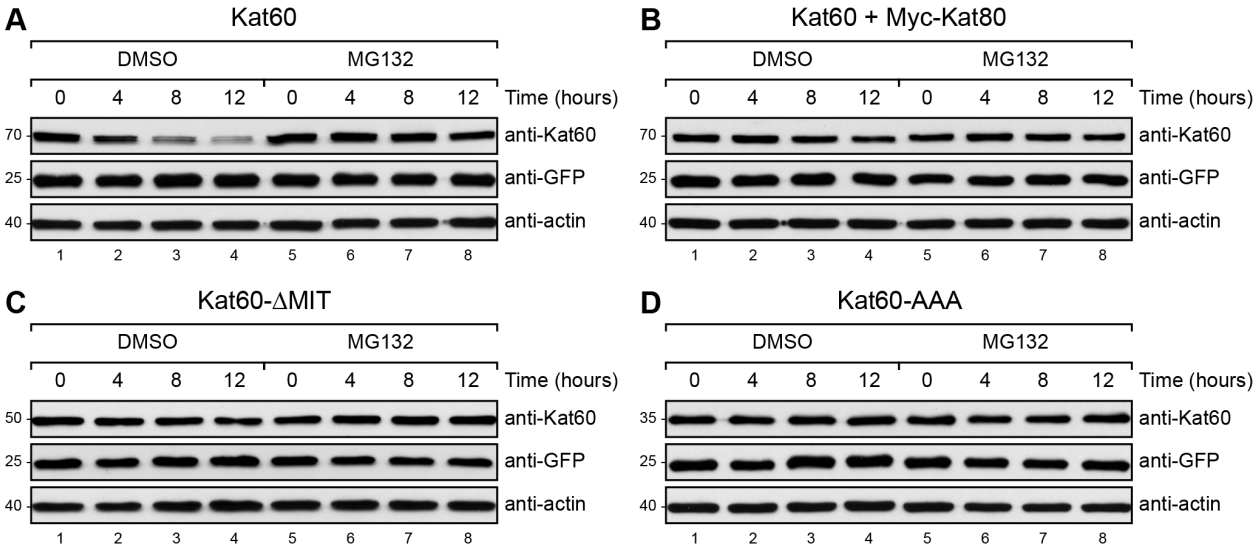

Figure 3.5. Kat60 lacking the MIT domain or the MIT domain and linker region is not detectably degraded in cells. (A-D) Immunoblots of *Drosophila* S2 cell lysates prepared from cells stably expressing GFP and copper-inducible Kat60 (A), Kat60 and Myc-Kat80 (B), Kat60-ΔMIT (C), or Kat60-AAA (D) that were treated with both Kat60 and Kat80 UTR dsRNA for 7 days total. The cells described in A-D were also treated with 1.0 (A), 1.0 (B), 0.1 (C), or 0.01 mM $CuSO_4$ (D) for 16 hours, washed with S2M, and treated with DMSO (lanes 1-4) or 50 μM MG132 (lanes 5-8) for 0 (lanes 1 and 5), 4 (lanes 2 and 6), 8 (lanes 3 and 7), or 12 hours (lanes 4-8). Molecular weights (in Kd) are shown on the left.

The MIT domain of Kat60 is important for its ability to disassemble microtubules at low levels of accumulation in cells

To circumvent the limitations highlighted above and reassess the contribution of the non-catalytic domains of *Drosophila* katanin to its microtubule-disassembly activity, we first expressed Kat60 alone or together with FLAG-Kat80, Kat60-ΔMIT, or Kat60-AAA over a broad range of levels in cells. We then used immunofluorescence microscopy and our single-cell assay to carefully examine the effects on microtubules as a function of the levels of these proteins. Cells expressing Kat60 together with FLAG-Kat80 exhibited microtubule disassembly in a concentration-dependent manner analogous to cells expressing Kat60 alone (Figure 3.6 A and B). Likewise, these cells had reduced levels of alpha-tubulin similar to cells expressing full-length Kat60 alone (Figure 3.6E and Table 3.S3), suggesting that Kat80 does not affect the ability of Kat60 to disassemble microtubules. By contrast, cells expressing Kat60-ΔMIT at low levels did not display noticeably disassembled microtubules, although cells expressing Kat60-ΔMIT at high levels showed partially disassembled microtubules similar to cells expressing Kat60 at low levels (Figure 3.6 A and C). Accordingly, the former cells did not have notably reduced levels of alpha-tubulin, whereas the latter cells had equivalent levels of alpha-tubulin compared to cells expressing Kat60 at low levels (Figure 3.6E and Table 3.S3). Thus, in addition to providing strong evidence that the MIT domain of Kat60 is important for its ability to disassemble microtubules at low levels of accumulation, these data further underscore the unique concentration-dependent contribution of the MIT domain of Kat60 to its activity. As predicted from our previous observations, cells expressing Kat60-AAA did not exhibit microtubule disassembly or have reduced levels of alpha-tubulin like cells expressing full-length Kat60 (Figure 3.6

A, D, and E and Table 3.S3), strongly suggesting that the MIT domain and linker region of Kat60 cooperate to augment its microtubule-disassembly activity.

To verify that Kat60 alone or in the presence of FLAG-Kat80, Kat60-ΔMIT, and Kat60-AAA all required ATP to disassemble microtubules, we first expressed each of these proteins harboring a well-characterized mutation in a critical Walker A residue (K339A) designed to prevent ATP binding in cells. We then used our assay to measure the loss of microtubules in cells expressing each of these ATP-binding deficient mutants of Kat60 over an identical range of levels. As expected, cells expressing Kat60-K339A alone or together with FLAG-Kat80, Kat60-ΔMIT-K339A, or Kat60-AAA-K339A did not have reduced levels of alpha-tubulin compared to control cells (Figure 3.S4), demonstrating that ATP-binding deficient mutants of Kat60 do not disassemble microtubules.

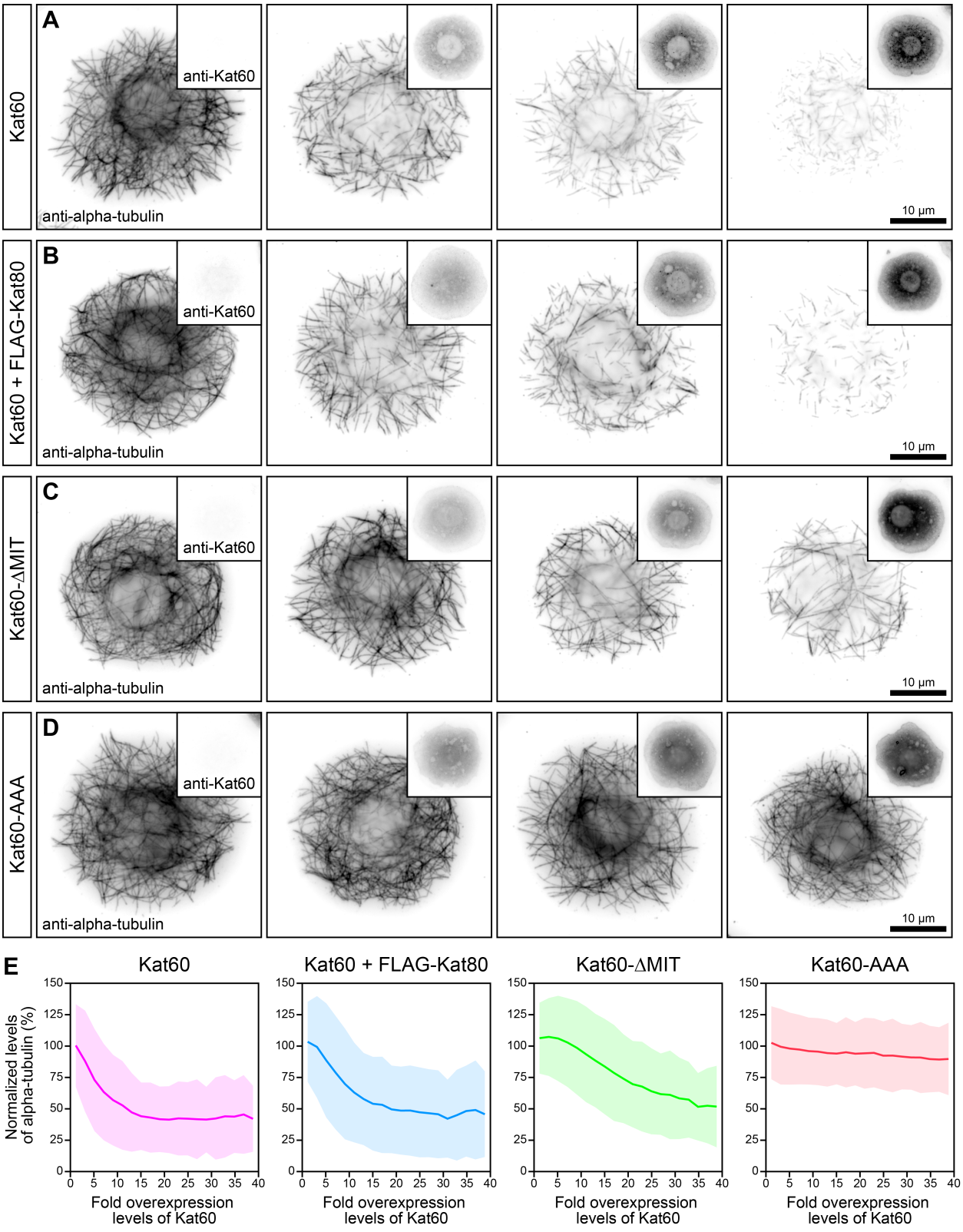

Figure 3.6. Kat60 lacking the MIT domain does not disassemble microtubules at low levels of accumulation in cells. (A-D) Immunofluorescence microscopy images of

Drosophila S2 cells stably expressing GFP and copper-inducible Kat60 (A), Kat60 and FLAG-Kat80 (B), Kat60-ΔMIT (C), or Kat60-AAA (D) that were treated with both Kat60 and Kat80 UTR dsRNA for 7 days total. The cells described in A-D were also treated with 0-1.0 (A), 0-1.0 (B), 0-0.01 (C), or 0-0.01 mM $CuSO_4$ (D) for 20 hours and immunostained for alpha-tubulin and Kat60. Alpha-tubulin and Kat60 images in each panel are displayed with the same scaling. (E) Line graphs of normalized levels of alpha-tubulin as a function of fold overexpression levels of Kat60 for the cells described in A-D. Normalized levels of alpha-tubulin are expressed as a percentage of the mean levels of alpha-tubulin in cells with fold overexpression levels of Kat60 below 0. Fold overexpression levels of Kat60 are expressed as a fraction of the difference in the mean levels of Kat60 between cells stably expressing GFP alone that were treated with control and both Kat60 and Kat80 UTR dsRNA for 7 days total. Data represent mean values ± standard deviation from cells with fold overexpression levels of Kat60 between 0 and 40, pooled from six independent experiments (see Table 3.S3 for summary statistics of the single-cell measurements collected).

The MIT domain and linker region of Kat60 are required for its association with microtubules in cells

Given our findings that both Kat60-ΔMIT and Kat60-AAA do not disassemble microtubules like Kat60 in cells, we next investigated how the non-catalytic domains of *Drosophila* katanin regulate its microtubule-disassembly activity. Because the non-AAA region of katanin catalytic subunits from several species has been to shown to bind microtubules in vitro (Hartman and Vale, 1999; Stoppin-Mellet et al., 2007; McNally and McNally, 2011; Eckert et al., 2012) and because a putative human katanin regulatory subunit has also been shown to bind microtubules in vitro (McNally and McNally, 2011), we reasoned that the non-catalytic domains of *Drosophila* katanin regulate its microtubule-disassembly activity by affecting its association with microtubules. In order to test this hypothesis, we developed a fluorescence microscopy assay to visualize the colocalization of Kat60 with microtubules in living cells. For this assay, we generated cells that stably express 1) RFP-tagged alpha-tubulin (RFP-alpha-tubulin) under the control of its own endogenous promoter and 2) GFP-tagged versions of Kat60 harboring the K339A mutation, either alone or together with Myc-Kat80, under the control of a copper-inducible promoter. We chose to examine the colocalization of ATP-binding deficient mutants of Kat60 with microtubules in this assay because they do not possess microtubule-disassembly activity and because an equivalent mutant of the human katanin catalytic subunit KATNA1 has been shown to possess microtubule-binding activity (McNally et al., 2000). In this assay, we first induce cells with $CuSO_4$ and then we acquire snapshot images of cells using total internal reflection fluorescence (TIRF) microscopy.

To test the hypothesis that the non-catalytic domains of *Drosophila* katanin affect its association with microtubules, we first expressed GFP-Kat60-K339A alone or together with Myc-Kat80, GFP-Kat60-ΔMIT-K339A, or GFP-Kat60-AAA-K339A in cells. We then used our live-cell assay to examine the colocalization of each of these proteins with microtubules. GFP-Kat60-K339A colocalized with the majority of microtubules in cells and it exhibited a discontinuous and punctate localization pattern on these microtubules (Figure 3.7A). Interestingly, GFP-Kat60-K339A in the presence of Myc-Kat80 also colocalized with the majority of microtubules in cells, however it exhibited a continuous localization pattern on these microtubules (Figure 3.7B), suggesting that Kat80 alters the association of Kat60 with microtubules. In contrast, GFP-Kat60-ΔMIT-K339A and GFP-Kat60-AAA-K339A detectably colocalized with only a few, if any, microtubules in cells (Figure 3.7 C and D), providing strong evidence that the MIT domain and linker region of Kat60 are required for its association with microtubules. From these results, we conclude that the MIT domain and linker region of Kat60 augment its microtubule-disassembly activity by enhancing its association with microtubules.

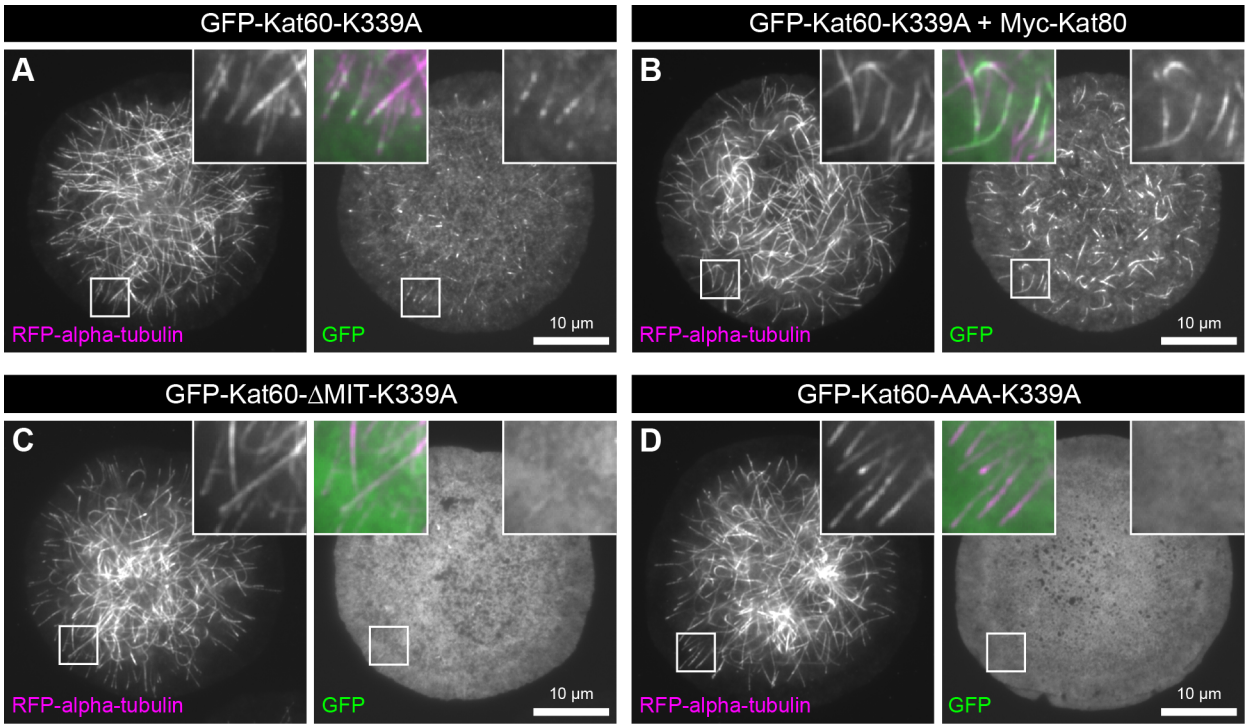

Figure 3.7. Kat60 lacking the MIT domain or the MIT domain and linker region detectably colocalizes with only a few, if any, microtubules in cells. (A-D) TIRF microscopy images of living *Drosophila* S2 cells stably expressing RFP-alpha-tubulin and copper-inducible GFP-Kat60-K339A (A), GFP-Kat60-K339A and Myc-Kat80 (B), GFP-Kat60-ΔMIT-K339A (C), or GFP-Kat60-AAA-K339A (D) that were treated with both Kat60 and Kat80 UTR dsRNA for 7 days total. The cells described in A-D were also treated with 0.1 (A), 0.1 (B), 0.1 (C), or 0.01 mM $CuSO_4$ (D) for 20 hours. GFP images are displayed with the same scaling.

Model for regulation of *Drosophila* katanin by its non-catalytic domains

Collectively, our data suggest a model for how the non-catalytic domains of *Drosophila* katanin regulate microtubule severing (Figure 3.8). First, we speculate that the MIT domain of Kat60 physically interacts with Kat80 – a well-established mode of interaction between katanin catalytic and regulatory subunits from several species (McNally et al., 2000; McNally and McNally, 2011) – and that the primary function of this interaction is to regulate the abundance of Kat60 itself. Our data and those of others (Pintard et al., 2003; Stitzel et al., 2006; Maddika and Chen, 2009) are consistent with a mechanism in which the MIT domain and linker region of Kat60 enhance its proteasome-dependent degradation by promoting interactions with ubiquitin ligase complexes, whereas Kat80 reduces the proteasome-dependent degradation of Kat60 by antagonizing such interactions. This mechanism could serve to maintain stoichiometric levels of Kat60 and Kat80 to ensure proper heterodimeric complex formation. In addition to regulating the abundance of Kat60, our data also demonstrate that the MIT domain and linker region of Kat60 regulate its microtubule-disassembly activity. In support of the katanin assembly model proposed by Hartman and Vale (Hartman and Vale, 1999), our data suggest that the MIT domain and linker region of Kat60 enhance its initial targeting to microtubules. We speculate that the MIT domain and linker region of Kat60 also influence the subsequent balancing between Kat60-microtubule and Kat60-Kat60 interactions, however our data indicate that the MIT domain cannot be required for these interactions. On the other hand, our data suggest that Kat80 does not affect the microtubule-disassembly activity of Kat60 despite altering the association of Kat60 with microtubules. Previous studies of katanin from several

species have shown that the katanin regulatory subunit potently stimulates the microtubule-severing activity of the katanin catalytic subunit in vitro (Hartman et al., 1998) and that the heterodimeric complex exhibits distinct microtubule-binding properties in vitro (McNally et al., 2014). Thus, we speculate Kat80 might function to target Kat60 to unique structural features or post-translational modifications of microtubules where it requires activation via some regulatory input to stimulate microtubule severing. Future work will focus on determining the functional importance of the microtubule-binding activity of Kat80 in living cells.

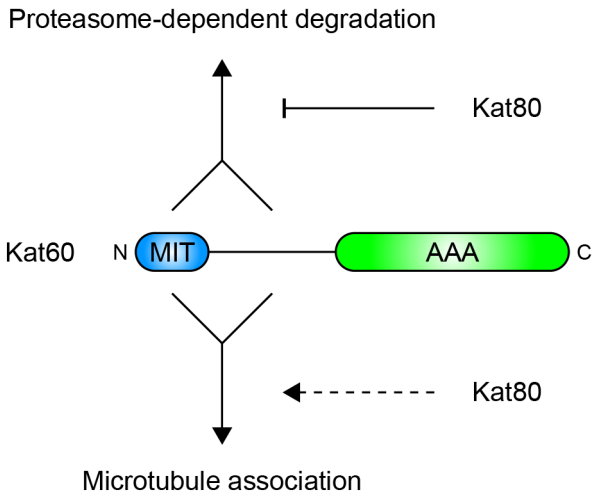

Figure 3.8 Model for regulation of *Drosophila* katanin by its non-catalytic domains. Schematic representation of the proposed contributions of the non-catalytic domains of *Drosophila* katanin to its proteasome-dependent degradation and microtubule association. Converging solid lines indicate cooperation between the MIT domain and linker region of Kat60 and solid lines with arrowheads indicate enhancement of the proteasome-dependent degradation and microtubule association of Kat60 by its MIT domain and linker region. The solid line with a blunt arrowhead indicates reduction of the proteasome-dependent degradation of Kat60 by Kat80 and the dashed line with an arrowhead indicates alteration of the microtubule association of Kat60 by Kat80. See text for details.

Materials and Methods

Plasmid construction

Multi-expression plasmids were constructed in the pMT/V5-His A expression plasmid backbone (Invitrogen) and additional expression cassettes were cloned into unique restriction enzyme sites engineered into regions outside of the copper-inducible expression cassette. Constitutive expression cassettes were obtained by PCR amplification of the pIZ/V5-His expression plasmid (Invitrogen) containing the CDS of GFP, the pCoBlast expression plasmid containing the CDS of the blasticidin-resistance protein (Invitrogen), or the pCoHygro expression plasmid containing the CDS of the hygromycin-resistance protein (Invitrogen). The *Drosophila* alpha-tubulin expression cassette was created by PCR amplification of *Drosophila* S2 cell genomic DNA containing the 5' and 3' UTR of alpha-tubulin and expression plasmids containing the CDS of RFP (Currie et al., 2011) and alpha-tubulin (Rogers et al., 2002) and fusion of the resulting PCR products using the In-Fusion HD cloning kit (Clontech Laboratories, Inc.). All copper-inducible transgenes were created by cloning PCR-amplified CDS into the multiple cloning site of the copper-inducible expression cassette. Transgenes encoding untagged full-length and deletion mutants of *Drosophila* Kat60 were created by PCR amplification of the CDS of full-length Kat60 (amino acids 1-572), Kat60-ΔMIT (amino acids 97-572), or Kat60-AAA (amino acids 265-572) from the Berkeley *Drosophila* Genome Project (BDGP) cDNA clone RE17942 (*Drosophila* Genomics Resource Center). The transgene encoding internally GFP-tagged full-length Kat60 was created by PCR amplification of the CDS of Kat60-MIT (amino acids 1-96), GFP, and Kat60-ΔMIT and fusion of the resulting PCR products using the In-Fusion HD cloning kit

(Clontech Laboratories, Inc.). Transgenes encoding NH_2-terminally GFP-tagged deletion mutants of Kat60 were created by PCR amplification of the CDS of GFP and Kat60-ΔMIT or Kat60-AAA and fusion of the resulting PCR products using the In-Fusion HD cloning kit (Clontech Laboratories, Inc.). Transgenes encoding NH_2-terminally epitope-tagged full-length *Drosophila* Kat80 were created by PCR amplification of the CDS of full-length Kat80 (amino acids 1-819) from the BDGP cDNA clone LD44201 (*Drosophila* Genomics Resource Center) with the CDS of Myc or FLAG engineered onto the 5' end of the PCR product. All point mutations were introduced by a PCR-based site-directed mutagenesis method and all plasmids were fully sequenced. The multi-expression plasmids constructed in this study are shown in Table 3.S4.

Cell culture and generation of stable cell lines

Drosophila S2 cells were maintained in a room temperature (RT) incubator in S2 cell medium (S2M: Schneider's *Drosophila* medium (Invitrogen) supplemented with 10% heat-inactivated FBS (Invitrogen) and 1x antibiotic-antimycotic solution (Invitrogen)). For generation of stable cell lines, cells were transiently transfected with the multi-expression plasmids described in Table 3.S4 using the FuGENE HD transfection reagent (Promega) according to the manufacturer's instructions. After transfection, cells were treated with 50 μg/mL blasticidin (Invitrogen), either alone or in combination, with 500 μg/mL hygromycin (Invitrogen) every 3 days for 4 weeks total. The stable cell lines generated in this study are shown in Table 3.S5.

RNAi and inducible protein expression

DNA templates for dsRNA synthesis were obtained by PCR amplification of the pFastBacHT-CAT expression plasmid (Invitrogen), BDGP cDNA clones, or S2 cell genomic DNA using the gene-specific primer sequences shown in Table 3.S6 dsRNA was synthesized using the T7 RiboMAX large scale RNA production system (Promega) according to the manufacturer's instructions. For RNAi, cells were treated with 20 μg/mL dsRNA every 2 days for 7 days total. For inducible protein expression, cells were treated with 0.01-1.0 mM $CuSO_4$ for 16-20 hours.

Pulsed-induction of protein expression and drug treatment

Cells were treated with 0.01-1.0 mM $CuSO_4$ for 16 hours, washed thrice with S2M, and treated with DMSO (Sigma-Aldrich) or 50 μM MG132 (Sigma-Aldrich) for 0-12 hours.

Antibody production

6xHis- and GST-tagged Kat60-AAA proteins were bacterially expressed and purified using Ni-NTA agarose (Qiagen) or glutathione sepharose (GE Healthcare). Polyclonal antibodies were generated against the 6xHis-tagged purified protein (Pocono Rabbit Farm and Laboratory) and affinity purified from sera using the GST-tagged purified protein coupled to CNBr-activated sepharose (GE Healthcare).

Immunoblotting

Protein samples were resolved by SDS-PAGE and transferred to nitrocellulose membranes (Whatman). Membranes were blocked with membrane blocking buffer (MBB: 5% non-fat milk (LabScientific) in PBS containing 0.1% Tween-20) for 1 hour at RT. For chemiluminescent immunodetection of proteins, membranes were first incubated with rabbit anti-Kat60 (0.1-1 μg/mL) or mouse anti-FLAG (2 μg/mL; clone M2;

Sigma-Aldrich) antibodies in MBB for 24 hours at 4°C and then incubated with HRP-conjugated goat anti-rabbit IgG (0.1-1 µg/mL; Sigma-Aldrich) or HRP-conjugated goat anti-mouse IgG (2 µg/mL; Sigma-Aldrich) antibodies in MBB for 1 hour at RT. Protein bands were visualized by incubating the membranes with enhanced chemiluminescent substrate (Pierce) and exposing the membranes to autoradiography film (GeneMate). For fluorescent immunodetection of proteins, membranes were first incubated with mouse anti-actin (1:10,000; clone C4; Millipore) or mouse anti-GFP (0.1 µg/mL; clone JL-8; Clontech Laboratories, Inc.) antibodies in MBB for 24 hours at 4°C and then incubated with Cy3-conjugated goat anti-mouse IgG (0.02 µg/mL; Jackson ImmunoResearch Laboratories, Inc.) antibodies in MBB for 1 hour at RT. Protein bands were visualized by fluorescence scanning of the membranes using a variable mode imager (Typhoon Trio; GE Healthcare).

Cell plating

Cells were plated at a density of 6 x 10^4 cells per well into 96-well glass-bottom microplates (0.17 mm glass; Matrical Bioscience) pre-washed with alcoholic potassium hydroxide and pre-coated with 0.5 mg/mL concanavalin A (MP Biomedicals). After plating, cells were washed with S2M prior to immunostaining or imaging in fresh S2M.

Immunostaining

Cells were washed with cell fixation buffer (CFB: 100 mM PIPES, pH 6.8, 1 mM EGTA, and 1 mM $MgCL_2$) and fixed with 10% paraformaldehyde (Electron Microscopy Sciences) in CFB for 10 minutes. Cells were permeabilized by washing with PBS containing 0.1% Triton X-100 (PBST) and blocked by incubating with cell blocking buffer

(CBB: 5% normal goat serum (Sigma-Aldrich) in PBST) for 10 minutes at RT. For immunostaining, cells were first incubated with rabbit anti-Kat60 (1 µg/mL), rabbit anti-Myc (1 µg/mL; Sigma-Aldrich), or mouse anti-alpha-tubulin (10 µg/mL; clone DM1A; Sigma-Aldrich) antibodies in CBB for 24 hours at 4°C and then incubated with Cy5-conjugated goat anti-rabbit IgG (1 µg/mL; Jackson ImmunoResearch, Inc.) or Cy3-conjugated goat anti-mouse IgG (2 µg/mL; Jackson ImmunoResearch, Inc.) antibodies in CBB for 2 hours at RT. After immunostaining, cells were incubated with 10 µg/mL Hoechst 33342 (Invitrogen) in PBST for 10 minutes at RT and cells were mounted in fluorescence mounting medium (Dako).

Imaging

Images were acquired using an inverted microscope (Eclipse Ti-E; Nikon) equipped with a 20x 0.75 NA Plan Apochromat (Nikon) or 100x 1.49 NA TIRF Plan Apochromat objective (Nikon), a cooled charge-coupled device camera (Clara; Andor), a mercury lamp illumination system for epi-fluorescence (Intensilight; Nikon), a motorized shutter for epi-fluorescence (Ludl Electronic Products Ltd.), a laser unit (Nikon) housing 488 nm and 561 nm solid-state lasers (Sapphire LP; Coherent, Inc.), a TI-LUSU shutter unit for controlling motorized shutters in the laser unit (Nikon), a motorized laser TIRF illumination unit (Nikon), a motorized fluorescence filter cube rotating turret (Nikon), single-band fluorescence filter sets for Hoechst 33342 (exciter (EX): 360/20x, beam splitter (BS): 400, emitter (EM): 460/15m; Nikon), GFP (EX: ZET488/10x, BS: ZT488rdc, EM: ET525/50m + HHQ500lp; Chroma Technology Corporation), RFP/Cy3 (EX: ZET561/10x, BS: ZT561rdc, EM: ET600/50m + HHQ575lp; Chroma Technology Corporation), and Cy5 (EX: ZET635/20x, BS: ZT640rdc, EM: ET655lp + HHQ660lp;

Chroma Technology Corporation), a motorized XY stage (Nikon), and a motorized nosepiece combined with the Perfect Focus System for Z-axis control (Nikon). NIS-Elements AR software (Nikon) was used to control the imaging system and images were acquired using identical system settings (e.g. exposure times, camera bit depth, binning, and gain) for each well of the same 96-well glass-bottom microplate.

Image processing and analysis

High-content immunofluorescence microscopy image processing and analysis was performed using the open-source CellProfiler software (Carpenter et al., 2006). In brief, images were illumination corrected and background subtracted prior to identification of objects and measurement of immunofluorescence intensities. For identification of nuclei, the DNA images were segmented using the Otsu Global two-class thresholding method and the identified nuclei were used to seed the identification of individual cells. For identification of individual cells, the GFP images were segmented using the Watershed - Image method and the Otsu Global three-class thresholding method and the identified cells were used to create cell outlines. For single-cell measurement of alpha-tubulin and Kat60 immunofluorescence intensities, the average pixel intensities were extracted from each outlined cell based on the alpha-tubulin and Kat60 images, respectively.

REFERENCES

Buster D, McNally K, McNally FJ. Katanin inhibition prevents the redistribution of gamma-tubulin at mitosis. J Cell Sci. 2002; 115:1083–92.

Carpenter AE, Jones TR, Lamprecht MR, Clarke C, Kang IH, Friman O, et al. CellProfiler: image analysis software for identifying and quantifying cell phenotypes. Genome Biol. 2006; 7:R100.

Cox GA, Mahaffey CL, Nystuen A, Letts VA, Frankel WN. The mouse fidgetin gene defines a new role for AAA family proteins in mammalian development. Nat Genet. 2000; 26:198–202.

Cummings CM, Bentley CA, Perdue SA, Baas PW, Singer JD. The Cul3/Klhdc5 E3 ligase regulates p60/katanin and is required for normal mitosis in mammalian cells. J Biol Chem. 2009; 284:11663–75.

Currie JD, Stewman S, Schimizzi G, Slep KC, Ma A, Rogers SL. The microtubule lattice and plus-end association of Drosophila Mini spindles is spatially regulated to fine-tune microtubule dynamics. Mol Biol Cell. 2011; 22:4343–61.

Desai A, Mitchison TJ. Microtubule polymerization dynamics. Annu Rev Cell Dev Biol. 1997; 13:83–117.

Diaz-Valencia JD, Morelli MM, Bailey M, Zhang D, Sharp DJ, Ross JL. Drosophila Katanin-60 Depolymerizes and Severs at Microtubule Defects. Biophys J. 2011; 100:2440–9.

Eckert T, Le DT-V, Link S, Friedmann L, Woehlke G. Spastin's microtubule-binding properties and comparison to katanin. PLoS ONE. 2012; 7:e50161.

Furukawa M, He YJ, Borchers C, Xiong Y. Targeting of protein ubiquitination by BTB-Cullin 3-Roc1 ubiquitin ligases. Nat Cell Biol. 2003; 5:1001–7.

Hartman JJ, Vale RD. Microtubule disassembly by ATP-dependent oligomerization of the AAA enzyme katanin. Science. 1999; 286:782–5.

Hartman JJ, Mahr J, McNally K, Okawa K, Iwamatsu A, Thomas S, et al. Katanin, a microtubule-severing protein, is a novel AAA ATPase that targets to the centrosome using a WD40-containing subunit. Cell. 1998; 93:277–87.

Hazan J, Fonknechten N, Mavel D, Paternotte C, Samson D, Artiguenave F, et al. Spastin, a new AAA protein, is altered in the most frequent form of autosomal dominant spastic paraplegia. Nat Genet. 1999; 23:296–303.

Hirokawa N, Takemura R. Molecular motors and mechanisms of directional transport in neurons. Nat Rev Neurosci. 2005; 6:201–14.

Iwaya N, Kuwahara Y, Fujiwara Y, Goda N, Tenno T, Akiyama K, et al. A Common Substrate Recognition Mode Conserved between Katanin p60 and VPS4 Governs Microtubule Severing and Membrane Skeleton Reorganization. J Biol Chem. 2010; 285:16822–9.

Loughlin R, Wilbur JD, McNally FJ, Nédélec FJ, Heald R. Katanin contributes to interspecies spindle length scaling in Xenopus. Cell. 2011; 147:1397–407.

Maddika S, Chen J. Protein kinase DYRK2 is a scaffold that facilitates assembly of an E3 ligase. Nat Cell Biol. 2009; 11:409–19.

Mao C-X, Xiong Y, Xiong Z, Wang Q, Zhang YQ, Jin S. Microtubule-severing protein Katanin regulates neuromuscular junction development and dendritic elaboration in Drosophila. Development. 2014; 141:1064–74.

McNally FJ, Vale RD. Identification of katanin, an ATPase that severs and disassembles stable microtubules. Cell. 1993; 75:419–29.

McNally KP, McNally FJ. The spindle assembly function of C. elegans katanin does not require microtubule-severing activity. Mol Biol Cell. 2011; 22:1550-60.

McNally KP, Bazirgan OA, McNally FJ. Two domains of p80 katanin regulate microtubule severing and spindle pole targeting by p60 katanin. J Cell Sci. 2000; 113:1623–33.

McNally K, Berg E, Cortes DB, Hernandez V, Mains PE, McNally FJ. Katanin maintains meiotic metaphase chromosome alignment and spindle structure in vivo and has multiple effects on microtubules in vitro. Mol Biol Cell. 2014; 25:1037–49.

Müller-Reichert T, Greenan G, O'Toole E, Srayko M. The elegans of spindle assembly. Cell Mol Life Sci. 2010; 67:2195–213.

O'Donnell L, Rhodes D, Smith SJ, Merriner DJ, Clark BJ, Borg C, et al. An essential role for katanin p80 and microtubule severing in male gamete production. PLoS Genet. 2012; 8:e1002698.

Pintard L, Willis JH, Willems A, Johnson J-LF, Srayko M, Kurz T, et al. The BTB protein MEL-26 is a substrate-specific adaptor of the CUL-3 ubiquitin-ligase. Nature. 2003; 425:311–6.

Rogers SL, Rogers GC, Sharp DJ, Vale RD. Drosophila EB1 is important for proper assembly, dynamics, and positioning of the mitotic spindle. J Cell Biol. 2002; 158:873–84.

Roll-Mecak A, McNally FJ. Microtubule-severing enzymes. Curr Opin Cell Biol. 2010; 22:96–103.

Roll-Mecak A, Vale RD. Structural basis of microtubule severing by the hereditary spastic paraplegia protein spastin. Nature. 2008; 451:363–7.

Satir P, Christensen ST. Overview of Structure and Function of Mammalian Cilia. Annu Rev Physiol. 2007; 69:377–400.

Sharp DJ, Ross JL. Microtubule-severing enzymes at the cutting edge. J Cell Sci. 2012; 125:2561–9.

Siegrist SE, Doe CQ. Microtubule-induced cortical cell polarity. Genes Dev. 2007; 21:483–96.

Smith LB, Milne L, Nelson N, Eddie S, Brown P, Atanassova N, et al. KATNAL1 regulation of sertoli cell microtubule dynamics is essential for spermiogenesis and male fertility. PLoS Genet. 2012; 8:e1002697.

Srayko M, Buster DW, Bazirgan OA, McNally FJ, Mains PE. MEI-1/MEI-2 katanin-like microtubule severing activity is required for Caenorhabditis elegans meiosis. Genes Dev. 2000; 14:1072–84.

Stitzel ML, Pellettieri J, Seydoux G. The C. elegans DYRK Kinase MBK-2 Marks Oocyte Proteins for Degradation in Response to Meiotic Maturation. Curr Biol. 2006; 16:56–62.

Stoppin-Mellet V, Gaillard J, Timmers T, Neumann E, Conway J, Vantard M. Arabidopsis katanin binds microtubules using a multimeric microtubule-binding domain. Plant Physiol and Biochem. 2007; 45:867–77.

Taylor JL, White SR, Lauring B, Kull FJ. Crystal structure of the human spastin AAA domain. J Struct Biol. 2012; 179:133–7.

Whitehead E, Heald R, Wilbur JD. N-Terminal Phosphorylation of p60 Katanin Directly Regulates Microtubule Severing. J Mol Biol. 2012; 425:214-21.

Wilson KJ, Qadota H, Mains PE, Benian GM. UNC-89 (obscurin) binds to MEL-26, a BTB-domain protein, and affects the function of MEI-1 (katanin) in striated muscle of Caenorhabditis elegans. Mol Biol Cell. 2012; 23:2623–34.

Wittmann T, Hyman A, Desai A. The spindle: a dynamic assembly of microtubules and motors. Nat Cell Biol. 2001; 3:E28-34.

Yang SW, Oh KH, Park E, Chang HM, Park JM, Seong MW, et al. USP47 and C terminus of Hsp70-interacting protein (CHIP) antagonistically regulate katanin-p60-mediated axonal growth. J Neurosci. 2013; 33:12728–38.

Yu W, Solowska JM, Qiang L, Karabay A, Baird D, Baas PW. Regulation of microtubule severing by katanin subunits during neuronal development. J Neurosci. 2005; 25:5573–83.

Zhang D, Grode KD, Stewman SF, Diaz-Valencia JD, Liebling E, Rath U, et al. Drosophila katanin is a microtubule depolymerase that regulates cortical-microtubule plus-end interactions and cell migration. Nat Cell Biol. 2011; 13:361–9.

Zhang D, Rogers GC, Buster DW, Sharp DJ. Three microtubule severing enzymes contribute to the “Pacman-flux” machinery that moves chromosomes. J Cell Biol. 2007; 177:231–42.

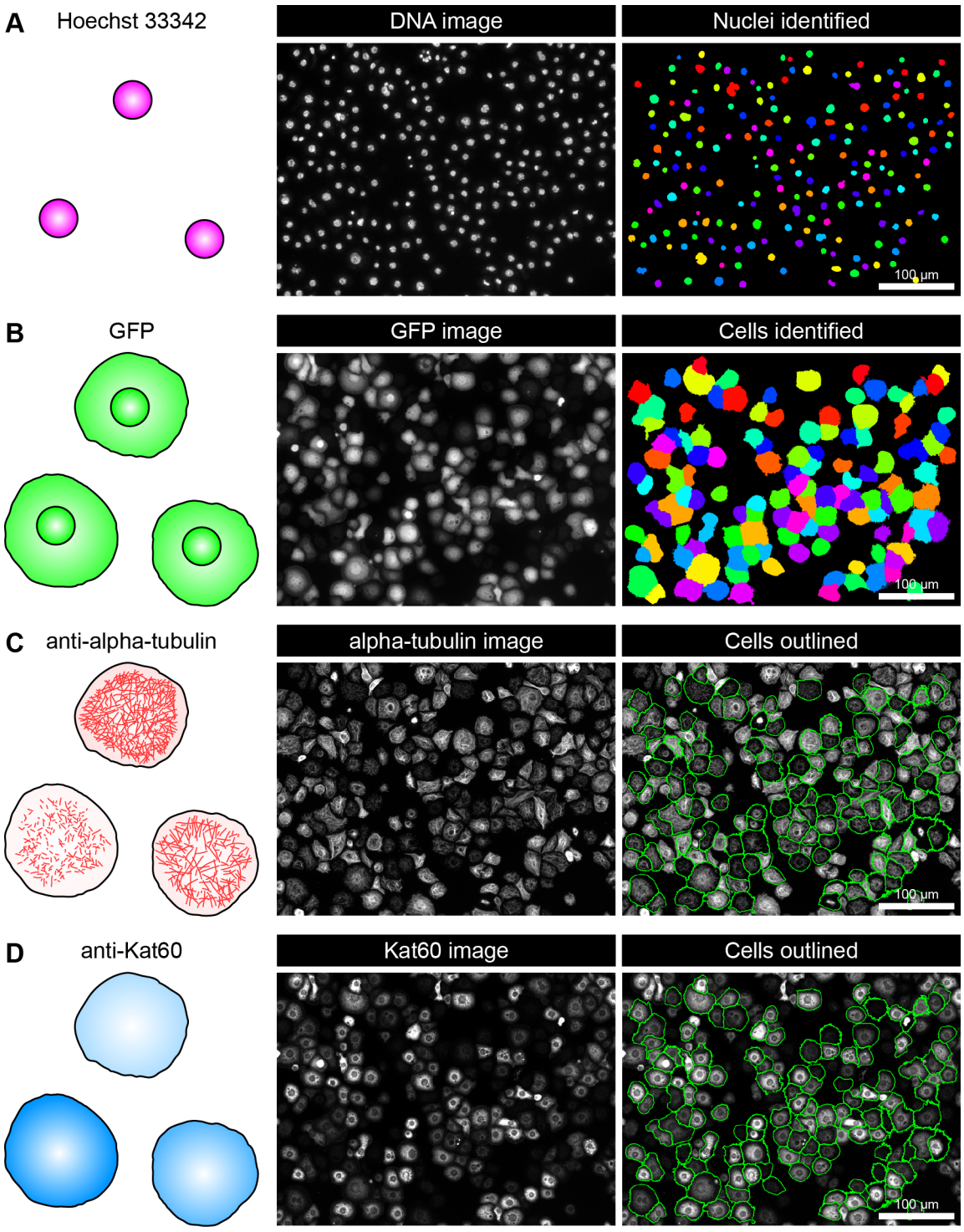

Figure 3.S1. Development of a single-cell assay to measure the microtubule-disassembly activity of Kat60 using automated microscopy. (A-D) Schematic representation (Left) and example high-content immunofluorescence microscopy images (Middle and Right) of *Drosophila* S2 cells stably expressing GFP and copper-

inducible Kat60 that were treated with both Kat60 and Kat80 UTR dsRNA for 7 days total. The cells were also treated with 1.0 mM $CuSO_4$ for 20 hours and stained for DNA and immunostained for alpha-tubulin and Kat60. (A) Original DNA image (Middle) and image of nuclei identified from the DNA image created by CellProfiler software (Right). (B) Original GFP image (Middle) and image of individual cells identified from the GFP image created by CellProfiler software (Right). (C) Original alpha-tubulin image (Middle) and alpha-tubulin image with cell outlines created by CellProfiler software (Right). (D) Original Kat60 image (Middle) and Kat60 image with cell outlines created by CellProfiler software (Right).

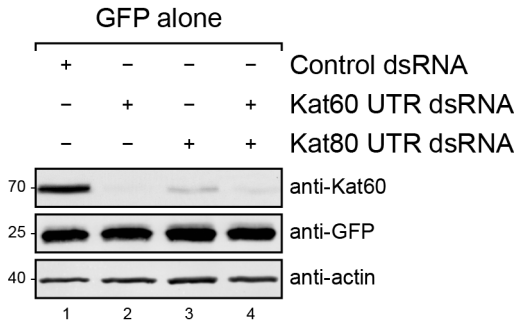

Figure 3.S2. Both Kat60 and Kat80 UTR dsRNA treatments reduce steady-state Kat60 levels in cells. Immunoblots of *Drosophila* S2 cell lysates prepared from cells stably expressing GFP alone that were treated with control (lane 1), Kat60 UTR (lane 2), Kat80 UTR (lane 3), or both Kat60 and Kat80 UTR dsRNA (lane 4) for 7 days total. Molecular weights (in Kd) are shown on the left.

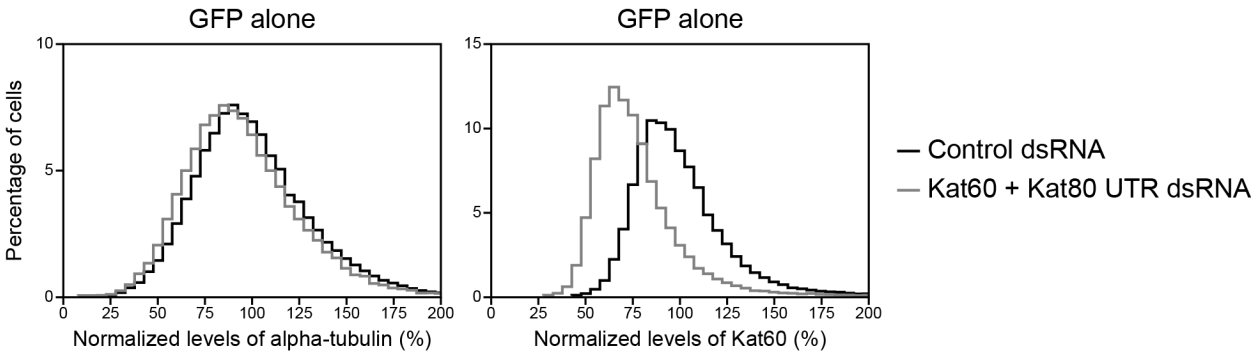

Figure 3.S3. Depletion of Kat60 and Kat80 causes minimal perturbation of steady-state alpha-tubulin levels in cells. Histograms of normalized levels of alpha-tubulin (Left) and normalized levels of Kat60 (Right) in *Drosophila* S2 cells stably expressing GFP alone that were treated with control (black, 32,389 total cells) or both Kat60 and Kat80 UTR dsRNA (gray, 32,142 total cells) for 7 days total. Normalized levels of alpha-tubulin and Kat60 are expressed as a percentage of the mean levels of alpha-tubulin and Kat60, respectively, in cells stably expressing GFP alone that were treated with control dsRNA for 7 days total. Data are pooled from three independent experiments.

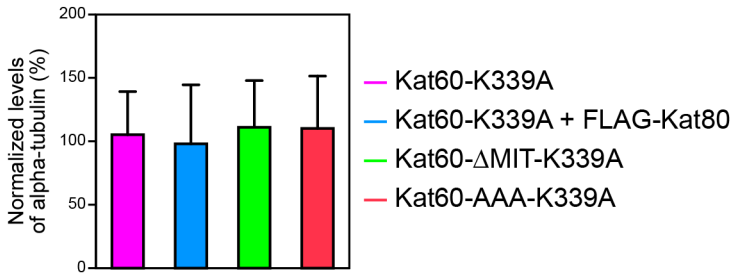

Figure 3.S4. ATP-binding deficient mutants of Kat60 do not disassemble microtubules in cells. Bar graph of normalized levels of alpha-tubulin in *Drosophila* S2 cells stably expressing GFP and copper-inducible Kat60-K339A (magenta, 11,938 total cells), Kat60-K339A and FLAG-Kat80 (blue, 7,956 total cells), Kat60-ΔMIT-K339A (green, 9,494 total cells), or Kat60-AAA-K339A (red, 4,240 total cells) that were treated with both Kat60 and Kat80 UTR dsRNA for 7 days total. The cells were also treated with 0-1.0 (magenta), 0-1.0 (blue), 0-0.01 (green), or 0-0.01 mM $CuSO_4$ (red) for 20 hours. Normalized levels of alpha-tubulin are expressed as a percentage of the mean levels of alpha-tubulin in cells stably expressing GFP alone that were treated with both Kat60 and Kat80 UTR dsRNA for 7 days total. Fold overexpression levels of Kat60 are expressed as a fraction of the difference in the mean levels of Kat60 between cells stably expressing GFP alone that were treated with control and both Kat60 and Kat80 UTR dsRNA for 7 days total. Data represent mean values ± standard deviation from cells with fold overexpression levels of Kat60 between 0 and 40, pooled from three independent experiments.

Table 3.S1. Summary statistics of the single-cell measurements shown in Figure 3.3.

Stable cell line treated with $CuSO_4$ (mM)	Total	Normalized levels of alpha-tubulin (%)		Fold overexpression levels of Kat60	
		Mean ± SD	Median (IQR)	Mean ± SD	Median (IQR)
Kat60 (0)	16,652	87.4 ± 31.5	83.3 (64.5-105.9)	1.9 ± 2.5	1.3 (0.4-2.7)
Kat60 (0.01)	14,190	76.6 ± 49.4	64.0 (36.5-108.1)	9.2 ± 9.1	6.2 (2.6-13.1)
Kat60 (0.1)	13,729	63.0 ± 48.4	46.3 (28.9-82.1)	17.3 ± 12.5	15.9 (7.1-25.3)
Kat60 (1.0)	11,369	57.5 ± 50.9	39.8 (25.1-68.6)	27.8 ± 16.5	27.3 (15.6-38.1)
FLAG-Kat80 (0)	12,755	100.2 ± 30.9	95.8 (79.0-117.1)	-0.2 ± 1.0	-0.4 (-0.8-0.1)
FLAG-Kat80 (0.01)	13,106	97.5 ± 31.0	93.0 (75.8-114.1)	-0.2 ± 0.9	-0.4 (-0.8-0.1)
FLAG-Kat80 (0.1)	9,824	106.0 ± 35.1	100.8 (81.4-125.4)	-0.2 ± 1.0	-0.4 (-0.8-0.1)
FLAG-Kat80 (1.0)	9,849	98.9 ± 34.7	93.9 (74.3-117.6)	-0.4 ± 1.0	-0.6 (-1.0-(-0.1))

Table 3.S1. Summary statistics of the single-cell measurements shown in Figure 3.3. Normalized levels of alpha-tubulin and fold overexpression levels of Kat60 in *Drosophila* S2 cells stably expressing GFP and copper-inducible Kat60 (rows 1-4) or FLAG-Kat80 (rows 5-8) that were treated with both Kat60 and Kat80 UTR dsRNA for 7 days total. The cells were also treated with 0 (rows 1 and 5), 0.01 (rows 2 and 6), 0.1 (rows 3 and 7), or 1.0 mM $CuSO_4$ (rows 4 and 8) for 20 hours and immunostained for alpha-tubulin and Kat60. Normalized levels of alpha-tubulin are expressed as a percentage of the mean levels of alpha-tubulin in cells stably expressing GFP alone that were treated with both Kat60 and Kat80 UTR dsRNA for 7 days total. Fold overexpression levels of Kat60 are expressed as a fraction of the difference in the mean levels of Kat60 between cells stably expressing GFP alone that were treated with control and both Kat60 and Kat80 UTR dsRNA for 7 days total. Data are pooled from three independent experiments. The following abbreviations are used: total, total cell number; SD, standard deviation; and IQR, interquartile range.

Table 3.S2. Summary statistics of the single-cell measurements shown in Figure 3.4.

Stable cell line treated with $CuSO_4$ (mM)	Total	Normalized levels of alpha-tubulin (%)		Fold overexpression levels of Kat60	
		Mean ± SD	Median (IQR)	Mean ± SD	Median (IQR)
Kat60 (0)	15,953	94.5 ± 26.2	91.0 (76.5-109.2)	1.5 ± 1.9	1.0 (0.3-2.1)
Kat60 (0.01)	13,137	89.8 ± 41.0	85.8 (55.5-118.4)	5.2 ± 5.4	3.5 (1.4-7.1)
Kat60 (0.1)	15,753	70.3 ± 36.8	59.8 (41.9-93.5)	10.1 ± 8.3	8.3 (3.5-15.1)
Kat60 (1.0)	15,333	64.0 ± 38.8	50.9 (35.7-83.6)	17.5 ± 12.5	16.6 (7.4-24.9)
Kat60 + FLAG-Kat80 (0)	21,682	80.0 ± 19.4	77.5 (68.3-89.2)	1.7 ± 1.6	1.4 (0.7-2.3)
Kat60 + FLAG-Kat80 (0.01)	19,094	65.0 ± 30.5	56.7 (45.0-75.8)	10.1 ± 6.3	9.1 (5.3-13.7)
Kat60 + FLAG-Kat80 (0.1)	19,639	55.7 ± 31.7	47.4 (37.2-62.5)	15.2 ± 7.5	14.6 (10.2-19.1)
Kat60 + FLAG-Kat80 (1.0)	16,821	47.9 ± 34.0	37.8 (27.1-56.0)	22.6 ± 10.0	21.6 (16.0-28.1)
Kat60-ΔMIT (0)	16,961	91.3 ± 23.8	88.6 (75.5-104.6)	3.6 ± 5.6	1.8 (0.3-4.8)
Kat60-ΔMIT (0.01)	16,035	78.2 ± 34.9	78.8 (51.3-100.3)	18.7 ± 20.9	12.0 (2.0-28.7)
Kat60-ΔMIT (0.1)	15,805	67.7 ± 39.9	64.5 (32.3-96.2)	27.4 ± 26.0	23.5 (2.2-44.8)
Kat60-ΔMIT (1.0)	17,305	60.0 ± 37.6	58.6 (24.7-88.9)	25.4 ± 24.1	22.2 (2.3-43.2)
Kat60-AAA (0)	9,126	91.6 ± 26.0	88.3 (74.2-106.1)	32.0 ± 26.5	27.3 (9.2-50.0)
Kat60-AAA (0.01)	8,832	85.8 ± 28.6	82.0 (65.6-101.6)	47.4 ± 23.4	50.4 (33.1-63.0)
Kat60-AAA (0.1)	7,021	94.0 ± 31.9	88.4 (71.5-110.7)	58.8 ± 21.9	60.6 (49.2-71.5)
Kat60-AAA (1.0)	8,681	78.6 ± 29.6	74.4 (58.4-93.7)	51.6 ± 16.5	51.4 (43.4-60.7)

Table 3.S2. Summary statistics of the single-cell measurements shown in Figure 3.4. Normalized levels of alpha-tubulin and fold overexpression levels of Kat60 in *Drosophila* S2 cells stably expressing GFP and copper-inducible Kat60 (rows 1-4), Kat60 and FLAG-Kat80 (rows 5-8), Kat60-ΔMIT (rows 9-12), or Kat60-AAA (rows 13-16) that were treated with both Kat60 and Kat80 UTR dsRNA for 7 days total. The cells described were also treated with 0 (rows 1, 5, 9, and 13), 0.01 (rows 2, 6, 10, and 14), 0.1 (rows 3, 7, 11, and 15), or 1.0 mM $CuSO_4$ (rows 4, 8, 12, and 16) for 20 hours and immunostained for alpha-tubulin and Kat60. Normalized levels of alpha-tubulin are expressed as a percentage of the mean levels of alpha-tubulin in cells stably expressing GFP alone that were treated with both Kat60 and Kat80 UTR dsRNA for 7 days total. Fold overexpression levels of Kat60 are expressed as a fraction of the difference in the mean levels of Kat60 between cells stably expressing GFP alone that were treated with control and both Kat60 and Kat80 UTR dsRNA for 7 days total. Data are pooled from three independent experiments. The following abbreviations are used: total, total cell number; SD, standard deviation; and IQR, interquartile range.

Table 3.S3. Summary statistics of the single-cell measurements shown in Figure 3.6

Fold overexpression levels of Kat60	Kat60		Kat60 + FLAG-Kat80		Kat60-ΔMIT		Kat60-AAA	
	Total	Mean ± SD	Total	Mean ± SD	Total	Mean ± SD	Total	Mean ± SD
0-2	9,548	100.5 ± 33.2	11,967	103.5 ± 32.1	14,120	106.4 ± 28.5	3,345	102.7 ± 29.3
2-4	6,921	87.9 ± 40.6	9,722	99.3 ± 40.9	8,947	107.4 ± 31.3	2,217	99.52 ± 30.4
4-6	5,059	72.2 ± 41.0	7,638	88.5 ± 45.9	6,159	106.2 ± 34.3	1,820	98.0 ± 28.9
6-8	3,880	63.0 ± 38.7	6,345	78.6 ± 45.6	4,659	102.9 ± 35.6	1,848	97.3 ± 27.9
8-10	3,146	56.5 ± 36.4	5,641	69.6 ± 44.5	3,934	98.7 ± 37.6	1,711	96.1 ± 26.9
10-12	2,682	52.4 ± 35.7	4,965	62.6 ± 40.0	3,346	93.4 ± 38.4	1,597	95.6 ± 26.9
12-14	2,412	46.7 ± 31.6	4,371	57.5 ± 37.01	2,918	88.4 ± 37.6	1,589	94.4 ± 26.9
14-16	2,028	43.7 ± 27.1	3,805	53.7 ± 37.7	2,542	83.6 ± 38.3	1,532	94.0 ± 24.6
16-18	1,680	42.6 ± 28.2	3,283	52.8 ± 38.7	2,276	78.4 ± 38.6	1,548	95.1 ± 28.2
18-20	1,340	41.2 ± 26.3	2,795	49.1 ± 35.2	2,073	73.8 ± 35.7	1,419	93.9 ± 25.4
20-22	1,044	40.9 ± 26.9	2,371	48.2 ± 36.2	1,768	69.4 ± 34.7	1,350	94.3 ± 28.4
22-24	844	41.9 ± 29.7	2,145	48.2 ± 36.2	1,612	67.5 ± 36.1	1,283	94.6 ± 27.7
24-26	670	41.6 ± 29.4	1,752	46.8 ± 36.2	1,510	63.7 ± 34.6	1,281	92.3 ± 27.5
26-28	553	41.2 ± 32.0	1,542	46.1 ± 35.3	1,362	61.4 ± 32.7	1,354	92.5 ± 29.5
28-30	409	40.9 ± 26.3	1,302	45.2 ± 35.3	1,234	60.8 ± 35.6	1,174	91.6 ± 26.3
30-32	341	41.9 ± 33.0	1,111	41.7 ± 31.3	1,063	58.0 ± 32.7	1,170	90.9 ± 25.9
32-34	259	43.6 ± 33.1	897	44.5 ± 36.5	871	57.0 ± 30.5	1,125	90.8 ± 28.5
34-36	188	43.4 ± 29.1	713	47.8 ± 36.6	869	51.2 ± 27.1	1,099	89.6 ± 26.7
36-38	150	45.0 ± 31.6	655	48.7 ± 39.7	748	52.1 ± 30.1	1,094	89.3 ± 25.9
38-40	111	41.6 ± 26.5	495	45.2 ± 34.4	632	51.4 ± 32.8	1,044	89.7 ± 29.1

Table 3.S3. Summary statistics of the single-cell measurements shown in Figure 3.6. Normalized levels of alpha-tubulin in *Drosophila* S2 cells stably expressing GFP and copper-inducible Kat60 (column 1), Kat60 and FLAG-Kat80 (column 2), Kat60-ΔMIT (column 3), or Kat60-AAA (column 4) that were treated with both Kat60 and Kat80 UTR dsRNA for 7 days total. The cells were also treated with 0-1.0 (column 1), 0-1.0 (column 2), 0-0.01 (column 3), or 0-0.01 mM $CuSO_4$ (column 4) for 20 hours and immunostained for alpha-tubulin and Kat60. Normalized levels of alpha-tubulin are expressed as a percentage of the mean levels of alpha-tubulin in cells with fold overexpression levels of Kat60 below 0. Fold overexpression levels of Kat60 are expressed as a fraction of the difference in the mean levels of Kat60 between cells stably expressing GFP alone that were treated with control and both Kat60 and Kat80 UTR dsRNA for 7 days total. Data are pooled from six independent experiments. The following abbreviations are used: total, total cell number; and SD, standard deviation.

Table 3.S4. List of the multi-expression plasmids constructed in this study.

Name	Description
pKG01	MT::Empty / OP::GFP / CO::Blast
pKG02	MT::Kat60 / OP::GFP / CO::Blast
pKG03	MT::Kat60-K339A / OP::GFP / CO::Blast
pKG04	MT::Kat60-ΔMIT / OP::GFP / CO::Blast
pKG05	MT::Kat60-ΔMIT-K339A / OP::GFP / CO::Blast
pKG06	MT::Kat60-AAA / OP::GFP / CO::Blast
pKG07	MT::Kat60-AAA-K339A / OP::GFP / CO::Blast
pKG08	MT::Myc-Kat80 / CO::Hygro
pKG09	MT::FLAG-Kat80 / OP::GFP / CO::Blast
pKG10	MT::FLAG-Kat80 / CO::Hygro
pKG11	MT::Empty / AT::RFP-alpha-tubulin / CO::Blast
pKG12	MT::GFP-Kat60-K339A / AT::RFP-alpha-tubulin / CO::Blast
pKG13	MT::GFP-Kat60-ΔMIT-K339A / AT::RFP-alpha-tubulin / CO::Blast
pKG14	MT::GFP-Kat60-AAA-K339A / AT::RFP-alpha-tubulin / CO::Blast

Table 3.S4. List of the multi-expression plasmids constructed in this study. Multi-expression plasmids are shown with individual expression cassettes separated by forward slashes and with CDS separated from promoters by double colons. The following abbreviations are used: MT, copper-inducible metallothionein promoter; OP, constitutive OpIE2 promoter. CO, constitutive copia promoter; AT, endogenous alpha-tubulin promoter; Blast, blasticidin-resistance protein; and Hygro, hygromycin-resistance protein.

Table 3.S5. List of the stable *Drosophila* S2 cell lines generated in this study.

Name	Description
cKG01	GFP
cKG02	GFP and copper-inducible Kat60[a]
cKG03	GFP and copper-inducible Kat60-K339A
cKG04	GFP and copper-inducible Kat60-ΔMIT
cKG05	GFP and copper-inducible Kat60-ΔMIT-K339A
cKG06	GFP and copper-inducible Kat60-AAA
cKG07	GFP and copper-inducible Kat60-AAA-K339A
cKG08	GFP and copper-inducible Kat60 + FLAG-Kat80
cKG09	GFP and copper-inducible Kat60-K339A + FLAG-Kat80
cKG10	GFP and copper-inducible Kat60 + Myc-Kat80
cKG11	GFP and copper-inducible FLAG-Kat80
cKG12	RFP-alpha-tubulin and copper-inducible GFP-Kat60-K339A
cKG13	RFP-alpha-tubulin and copper-inducible GFP-Kat60-ΔMIT-K339A
cKG14	RFP-alpha-tubulin and copper-inducible GFP-Kat60-AAA-K339A
cKG15	RFP-alpha-tubulin and copper-inducible GFP-Kat60-AAA-K339A + Myc-Kat80

Table 3.S5. List of the stable *Drosophila* S2 cell lines generated in this study. [a]Two independent *Drosophila* S2 cell lines stably expressing GFP and copper-inducible Kat60 were generated and used in this study. The first was used to acquire the data shown in Figures 3.3 and 3.S1 and the second was used to acquire the data shown in Figures 3.4, 3.5, and 3.6.

Table 3.S6. List of the DNA templates and gene-specific primer sequences used in this study for dsRNA synthesis.

dsRNA	DNA template	Forward primer[a]	Reverse primer[a]
Control	pFastBacHT-CAT expression plasmid	ATCCCAATGGCATCGTAAAG AACATTTTGAGGC	GGGCGAAGAAGTTGTCCATATTGGCCA
Kat60 CDS	BDGP cDNA clone RE17942	ATCCATCTGCCTGGTTCAAG	GTGGTTGTTGGGCTGAAACT
Kat60 UTR	S2 cell genomic DNA	GAATGGCTAGCGATTGTAGG	ATCTCTGCCTGCACTAAACTATG
Kat80 CDS	BDGP cDNA clone LD44201	GTCGTATATGGCGGAGCAAT	TTCGTTGTCCTCTTGTGCAG
Kat80 UTR	S2 cell genomic DNA	GGGCAACGCATATCCAGCTGTAGATGC	GTATGTTTTCTTTTATATATTTTCAAATTT TGGACTTAGGTATAGG

Table 3.S6. List of the DNA templates and gene-specific primer sequences used in this study for dsRNA synthesis. [a]Primer sequences are listed as 5' to 3' and each is preceded with the T7 promoter sequence 5'-TAATACGACTCACTATAGGG-3'.

CHAPTER 4: FUTURE DIRECTIONS

The overarching goal of our most recent study was to define the molecular determinants for regulation of microtubule severing by katanin. Although our findings identified the non-catalytic domains of katanin as the major determinants for regulation of its abundance and activity in living cells, there are many important questions that remain unanswered. Do the non-catalytic domains of katanin function cooperatively or redundantly in the context of the heterodimeric complex? Can the non-catalytic domains of katanin recognize unique structural features or post-translational modifications of microtubules? Is there cross-talk between the regulation of katanin's abundance and microtubule-severing activity? In this chapter, we outline future experiments that are designed to address each of these outstanding questions and thus advance our understanding of the molecular regulation of microtubule severing by katanin.

One of the biggest limitations of our structure-function analysis of the microtubule-severing activity of *Drosophila* katanin was that we were unable to determine whether the microtubule-binding domains of Kat60 and Kat80 function cooperatively or redundantly in the context of the heterodimeric complex. In order to overcome this limitation, we need separation-of-function mutants of Kat60 and Kat80 that exhibit defects in their microtubule-binding activity but not in their ability to associate with the other subunit. We envision that determining the three-dimensional structure of the Kat60 and Kat80 heterodimeric complex – a feat that has not been accomplished to date - would permit the rational design of such separation-of-function

mutants and that once generated, biochemical approaches would be necessary to fully validate each separation-of-function mutant of Kat60 and Kat80. Future studies could then use these separation-of-function mutants of Kat60 and Kat80 to dissect the functional importance of the microtubule-binding activity of each non-catalytic domain of *Drosophila* katanin in the context of the heterodimeric complex. Since katanin is the only microtubule-severing enzyme that exists as a heterodimeric complex, a detailed examination of how the individual microtubule-binding domains of each katanin subunit function together would likely reveal unique aspects of its ability to sever and disassemble microtubules.

One of the most interesting observations of our recent study was that not all microtubules were disassembled in cells expressing Kat60 alone or together with Kat80. Multiple lines of evidence support a model in which katanin preferentially severs microtubules that exhibit certain structural defects (Davis et al., 2002; Diaz-Valencia et al., 2011) or chemical modifications (Sharma et al., 2007; Sudo and Baas; 2010), but the structural and functional basis for this phenomenon remains poorly understood. A logical extension of our current work would thus be to explore possible roles for the non-catalytic domains of *Drosophila* katanin in recognizing unique structural features or post-translational modifications of microtubules. In order to conduct such studies, we need microtubules that display the desired physical and chemical properties in cells. We anticipate that microtubules with structural defects could be generated using microtubule-binding drugs or non-hydrolyzable analogs of GTP whose effects on purified microtubules are well established. Likewise, we imagine that depleting or overexpressing the enzymes that catalyze specific post-translational modifications of

tubulin would enable the generation of microtubules with particular chemical modifications. Once protocols for the generation of physically and chemically altered microtubules have been established, future studies could then use the separation-of-function mutants of Kat60 and Kat80 described above to determine whether the non-catalytic domains of *Drosophila* katanin confer specificity to the interaction with these microtubules. A comprehensive analysis of how katanin recognizes distinct microtubule substrates would likely provide crucial insight into its ability to selectively sever and disassemble certain microtubule subsets in cells.

One of the most important findings of our recent study was that the MIT domain and linker region of Kat60 cooperate to regulate its abundance and microtubule-disassembly activity. Considerable evidence supports the notion that the microtubule-binding region of the katanin catalytic subunit serves as a proteasomal degradation signal (Pintard et al., 2003; Xu et al., 2003; Stitzel et al., 2006; Maddika and Chen, 2009), but whether microtubule binding and/or severing by katanin influences its degradation remains unknown. Thus, an exciting next step would be to investigate potential mechanisms of cross-talk between the regulation of *Drosophila* katanin's abundance and microtubule-disassembly activity. In order to carry out such studies, we need separation-of-function mutants of Kat60 and Kat80 that exhibit defects in their microtubule-binding activity but not in their ability to be degraded by the proteasome. Although we expect that the generation of such mutants would be feasible, it is possible that the residues involved in interactions with microtubules and ubiquitin ligase complexes are not mutually exclusive. If this proves to be the case, we anticipate that alternative strategies using microtubule-destabilizing drugs to eliminate microtubules

would also be effective. By employing either of these two approaches, future studies could then elucidate the functional consequences of the integration of multiple regulatory inputs by the non-catalytic domains of *Drosophila* katanin. A careful inspection of how the regulation of katanin's abundance and activity are coordinated would likely shed light on the principal regulatory mechanisms controlling microtubule severing by katanin.

REFERENCES

Davis LJ, Odde DJ, Block SM, Gross SP. The importance of lattice defects in katanin-mediated microtubule severing in vitro. Biophys J. 2002; 82:2916–27.

Diaz-Valencia JD, Morelli MM, Bailey M, Zhang D, Sharp DJ, Ross JL. Drosophila Katanin-60 Depolymerizes and Severs at Microtubule Defects. Biophys J. 2011; 100:2440–9.

Maddika S, Chen J. Protein kinase DYRK2 is a scaffold that facilitates assembly of an E3 ligase. Nat Cell Biol. 2009; 11:409–19.

Pintard L, Willis JH, Willems A, Johnson J-LF, Srayko M, Kurz T, et al. The BTB protein MEL-26 is a substrate-specific adaptor of the CUL-3 ubiquitin-ligase. Nature. 2003; 425:311–6.

Sharma N, Bryant J, Wloga D, Donaldson R, Davis RC, Jerka-Dziadosz M, et al. Katanin regulates dynamics of microtubules and biogenesis of motile cilia. J Cell Biol. 2007; 178:1065–79.

Stitzel ML, Pellettieri J, Seydoux G. The C. elegans DYRK Kinase MBK-2 Marks Oocyte Proteins for Degradation in Response to Meiotic Maturation. Curr Biol. 2006; 16:56–62.

Sudo H, Baas PW. Acetylation of microtubules influences their sensitivity to severing by katanin in neurons and fibroblasts. J Neurosci. 2010; 30:7215–26.

Xu L, Wei Y, Reboul J, Vaglio P, Shin T-H, Vidal M, et al. BTB proteins are substrate-specific adaptors in an SCF-like modular ubiquitin ligase containing CUL-3. Nature. 2003; 425:316–21.